Supramolecular Assembly of Redox Proteins for Ultralong-Range Biological Electron Transfer

by

Justus Nmaduka Nwachukwu

A Dissertation Presented in Partial Fulfillment
of the Requirements for the Degree
Doctor of Philosophy

Approved June 2023 by the
Graduate Supervisory Committee:

Anne K. Jones, Chair
Jeremy Mills
Nicholas Stephanopoulos

ARIZONA STATE UNIVERSITY

August 2023

ABSTRACT

Exoelectrogenic organisms transfer electrons from their quinone pool to extracellular acceptors over μm-scale distances through appendages known as “biological nanowires”. These structures have been described as cytochrome-rich membrane extensions or pili. However, the components and mechanisms of this long-range electron transfer remain largely unknown. This dissertation describes supramolecular assembly of a tetraheme cytochrome into well-defined models of microbial nanowires and uses those structures to explore the mechanisms of ultra-long-range electron transfer. Chiral-induced-spin-selectivity through the cytochrome is also demonstrated.

Nanowire extensions in *Shewanella oneidensis* have been hypothesized to transfer electrons via electron tunneling through proteinaceous structures that reinforce π-π stacking or through electron hopping via redox cofactors found along their lengths. To provide a model to evaluate the possibility of electron hopping along micron-scale distances, the first part of this dissertation describes the construction of a two-component, supramolecular nanostructure comprised of a small tetraheme cytochrome (STC) from *Shewanella oneidensis* fused to a peptide domain that self-assembles with a β-fibrillizing peptide. Structural and electrical characterization shows that the self-assembled protein fibers have dimensions relevant to understanding ultralong-range electron transfer and conduct electrons along their length via a cytochrome-mediated mechanism of electron transfer. The second part of this dissertations shows that a model three-component fiber construct based on charge complementary peptides and the redox protein can also be assembled. Structural and electrical characterization of the three-component structure

also demonstrates desirable dimensions and electron conductivity along the length via a cytochrome-mediated mechanism.

In vivo, it has been hypothesized that cytochromes in the outer surface conduit are spin-selective. However, cytochromes in the periplasm of *Shewanella oneidensis* have not been shown to be spin selective, and the physiological impact of the chiral-induced-spin-selectivity (CISS) effect on microbial electron transport remains unclear. In the third part of this dissertation, investigations via spin polarization and a spin-dependent conduction study show that STC is spin selective, suggesting that spin selectivity may be an important factor in the electron transport efficiency of exoelectrogens.

In conclusion, this dissertation enables a better understanding of long-range electron transfer in bacterial nanowires and bioelectronic circuitry and offers suggestions for how to construct enhanced biosensors.

DEDICATION

To God, for His Love, Enduring mercies and Great faithfulness through the years.

To Lilian, my Love and Life Partner, you are God's gift to me, and I will continue to cherish you every day of my life.

To the memories of my Late Father Chief Reuben Nwachukwu, words are not enough to describe your eternal impact. To my mum, Mrs. Kate Nwachukwu, thank you for being so present, for all the worries I put you through, I will do better I promise.

ACKNOWLEDGMENTS

I will always be grateful to Prof. Anne Jones for taking a chance on me. For being such a great Supervisor in every way possible. Graduate school would have been unbearable without you. Prof. Jones helped me learn and grow, and I'm certain I would not be in this position now without her constant guidance, support and faith in me.

I want to acknowledge my lovely wife Lilian, for all her care and support, for finding ways to hold our home together through the busy life of Graduate School and to my little daughter Chinemelum Olivia, whose arrival filled our hearts with so much joy. I hope you grow up in love and good health and live a very fulfilled life.

My Late Dad, Chief Reuben Nwachukwu, I finally did it! Thank you for all the trust and hope you put in me, you believed so much in my capacity to be adventurous and do well academically, I can only hope I have made you proud. To my sweet Mum, Mrs. Kate Nwachukwu, thank you for all your prayers and love and support. Thank you for the loving family you and Daddy made for me and my siblings. To my siblings, Chukwudi, Chinonye, Chimezie, Nmachukwu and Chiamaka thank you for all the roles you played throughout the years.

To my friends who have supported my transition to the United States of America and helped me through every situation: Dr. Emmanuel Ogbonna and Dr. Chidozie Agu, Thank you.

To everyone in the Jones Lab who have been such wonderful colleagues, providing help where possible and just making research a little more fun along the way:

Dr. Miyuki Thirmurthy, Dr. Garrett Williams, Dr. Christina Forbes, Kelsea, Gaurav, Thao, Thank you.

I want to acknowledge our collaborators at University of Southern California: Prof. Moh El-Naggar, Dr. Joshua Atkinson and Christina Cole, thank you for all your help in discussing our projects and helping run complex electrochemical gating experiments. To my PhD committee members: Dr. Jeremy Mills and Dr. Nicholas Stephanopoulos, thank you for helping with my yearly reviews and giving insights of what I could do better. Thank you to the Office of Naval Research Multidisciplinary University Research (Initiative Number N00014-18-1-2632) for funding my research throughout the years and finally to Arizona State University for being such a calm and serene citadel of learning.

The research described in Chapter 4 has been submitted for publication to the Journal of Chemical Physics. My contribution to the work is the purification and characterization of the STC protein. The other protein, MtrA, was evaluated by collaborators at the other institutions.

TABLE OF CONTENTS

Page

CHAPTER Page

APPENDIX Page

LIST OF TABLES

Table Page

LIST OF FIGURES

Figure Page

Figure Page

Figure Page

Figure Page

Chapter 1

1. Introduction, Scope and Summary of this Thesis

J. N. Nwachukwu[1]

[1]School of Molecular Sciences, Arizona State University, Tempe, AZ, USA

1.1 Electron Transfer in Biology

Energy transduction occurs in living organisms through a coupling of electron transfer reactions to building of a proton (or other ion) gradient, the dissipation of which is coupled to phosphorylation of ADP to produce ATP, the energy currency of living things.[1]

Compartmentalization creates an inside and an outside of cells and organelles within them, creating defined locations for establishing ion gradients. Life has evolved to exploit virtually any redox niche that can support it. Although respiration using oxygen as a terminal electron acceptor might be the most well-known approach, there exist organisms employing myriad alternative terminal electron acceptors from soluble, organic molecules like fumarate to insoluble metal oxide surfaces. The latter presents a unique problem: insoluble inorganic substrates cannot be transferred to the inside of a cell. Thus, some organisms have developed the ability to transfer reducing equivalents from internal metabolism to extracellular substrates. This functionality is referred to as extracellular electron transfer (EET).[2]

1.2 Exoelectrogens and Extracellular Electron Transfer

Exoelectrogens are microorganisms that have unique capacity of transferring electrons from their inner quinone pool to their external surfaces.[3] Exoelectrogens, like *Shewanella oneidensis* and *Geobacter sulfurreducens,* are thought to have evolved to form a distinct feature that enables external electron transfer.[4] These distinct features include outer membrane extensions, pili and redox proteins found in electrogenic organisms that are believed to be essential to the transfer of electrons over lengths on the

micron scale.[5,6]

As a result of their unique functionality, exoelectrogens have found wide applications. For example, they transferr electrons for electricity generation in microbial fuel cells.[7] In bioelectronics, they are used to manufacture patterned biofilms.[8] They serve as redox active sensors or transducers in bionsensors.[9] Some can clean up nuclear waste by reducing soluble uranium (VI) to insoluble Uranium (IV) salts making them less available in the environment, or even reducing soluble mercury (II) to insoluble mercury (I) metals.[10] Because of their ability to anaerobically degrade monoaromatic hydrocarbons, exoelectrogens like *Geobacter* and *Desulfitobacterium* have also been used to mop up oil spills in waterbodies. This anaerobic decay is also crucial in waste water treatment especially in biohydrogen production where the decay of organic materials produces protons and electrons which can then be converted into hydrogen gas through "addition of small voltage to circuit".[11] Exoelectrogens have also found application in desalination where movement of charged species from salt water could lower the salt content of water while generating electricity.[12] These applications make exoelectrogens and EET an important research interest.

1.3 Modes of Electron Transfer in Exoelectrogens

There are three modes of EET in exoelectrogens (Fig. 1.1): (i) transfer "directly" from the cell membrane to external surfaces by virtue of the redox proteins in the cell membrane;[13] (ii) through redox-active, soluble shuttles which serve as an intervening medium between the cells and external surface;[14] and (iii) through hair-like conductive appendages often called microbial nanowires.[15] The last is believed to be the most

significant contributor to long-range electron transfer, i.e. on the micron-scale.

1.4 Mechanisms of EET through Microbial Nanowire

Two mechanism have been proposed to explain μm-scale electron conductivity through microbial nanowires (Fig. 1.2): i) electron hopping (governed by Marcus Theory) between regular or closely-spaced redox cofactors; and ii) electron tunneling through proteinaceous structures that enforce π-π stacking of aromatic amino acids along the lengths of bacterial nanowires.[16,17] The latter is often linked to the idea that bacterial nanowire are pili and that aromatic residues are structural components of pili. The hypothesis, however does not require this connection.[18] El-Naggar and coworkers have described *S. oneidensis* nanowires as cytochrome-rich membrane extensions of the periplasm distinct from pili.[19]

The mechanism of electron transfer along *Geobacter* nanowires remains disputed. Studies from Lovely and coworkers posit that electronic conduction in *Geobacter* nanowires is not as a result of cytochromes but occurs due to electron tunneling through proteinaceous structure that enforce the overlapping of π-π orbitals of the aromatic amino acid residues within the pili.[20] However, cryo-electron microscopy of *Geobacter* nanowires revealed structures consisting of OmcS, a multiheme cytochrome, in which the hemes are closely stacked, suggesting conductivity by electron hopping via the redox-active cofactors.[21] Using cryo-electron micrographs, Lovley and coworkers have argued that OmcS wires are thick filaments and pili are thin filaments, different anatomical structures with perhaps distinct expression and functionality.[22] However, this explanation has been disputed by Malvankar and coworkers, who have argued that the thin filaments

are DNA rather than pili.[23] *Geobacter* is known to express a multitude of different multi-heme cytochromes, and studies have shown that, at a fixed set of conditions, OmcZ is 1000 times more conductive than OmcS.[24] Perhaps surprisingly, OmcZs has also been shown to bind and reduce riboflavin, implying that soluble intervening medium might play a role in extracellular electron transfer.[25]

1.5 Natural and Synthetic Models of Microbial Nanowires

A dearth of adequate models to explain electron transfer on the scale of microns have made studying long-range electron transfer along bacterial nanowires challenging. Tunability and functionality of a defined model nanowire on a μm-scale is essential in distinguishing between the two prevailing relevant but conflicting hypothesis.[26]

Supramolecular structures fabricated from fibril assembling domains exist but structures with redox-active cofactors are rare. Basak and coworkers self-assembled fibers from polyalanine peptides based on changes in pH of assembling solutions.[27] Stupp and coworkers assembled fibrils using peptide amphiphiles that have small hydrophobic compartment that covalently bind to peptides/[28] Supramolecular glycosylated peptide nanofibers have also been reported by Hudalla and coworkers.[29] These fibrils are biomaterial with probable bioactive functions, but have, to date, not been exploited to understand nanofibril conductivity in exoelectrogens.

There are only a few notable examples of efforts to create conductive fibers relevant to understanding long-range electron transfer. In an effort to demonstrate the efficacy of transfer through aromatic systems, Creasey and coworkers assembled

structures from aromatic-rich peptides, but the structures are poorly formed and the conductivity clearly too low to function as models for microbial nanowire.[30] Xu and coworkers self-assembled peptide nanotubes using enzymes but also achieved minimal conductivity.[31] Similarly, Hochbaum and coworkers also assembled α-helical peptides into gels but obtained minimal conductivity.[32] Another approach has been to use biological components of functional systems from exoelectrogens. For example, Reguera and coworkers fabricated a hydrophobe-controlled self-assembling structure using recombinant *Geobacter* pilins, and the resistance was similar to the native pili.[33]

To understand the possibility of transferring electrons over long distances via hopping through redox-active cofactors, Altamura and coworkers assembled a redox-synthetic biofilm constructed from self-assembly of a prion backbone and rubredoxin, a redox-active iron-sulfur protein. These assemblies transfer electrons over a few microns, and the resulting biofilm can be used as a shuttle between electrodes and laccase for oxygen reduction.[34] Similarly, Glover and coworkers assembled gamma-prefoldin and a *c*-type cytochrome generating a structure with some conduction current.[35]

1.6 Chiral-induced Spin Selectivity in Exoelectrogenic Proteins

Chiral-induced spin selectivity (CISS) has been demonstrated in biomolecules such as nucleic acids and proteins and may contribute to long range electron transport. Most biomolecules are chiral. In a chiral medium like a protein, CISS couples electron spin to its linear momentum and enables efficient electron flux with reduced backscattering.[36] Exoelectrogens are often hypothesized to contain electron conduits of multiheme cytochromes.[1937] Along these ordered structures, CISS may reinforce the flow of

electrons with the same spin. However, this has not yet been demonstrated since it has not be possible to make CISS measurements through this type of supramolecular structure, and the possibly physiological impact of CISS remains unclear.

1.7 Summary and Scope of the Dissertation

This dissertation describes assembly of redox proteins into conductive fibers to serve as a model system to explore mechanisms of long-range electron transfer. Chapter 2 describes a two-component supramolecular assembly of the small tetraheme cytochrome (STC) from *Shewanella oneidensis* using Q11 fibrillizing peptide. Fibers are conductive, and electrochemical experiments demonstrate a redox-mediated mechanism of electron transfer. Chapter 3 presents a three-component supramolecular assembly of STC using CATCH peptides. Again, fibers conduct electrons with a redox-mediated mechanism of electron transfer, and the fibers offer the possibility of tuning composition to vary spacing between protein monomers. Chapter 4 demonstrates that electron transport through STC is spin-selective. Chapter 5 discusses the implications of this research and possible future directions including introduction of electrogenic proteins into host cells to develop living circuits, pioneer the idea of self-repair in bielectronic circuitry, and enhance biosensing.

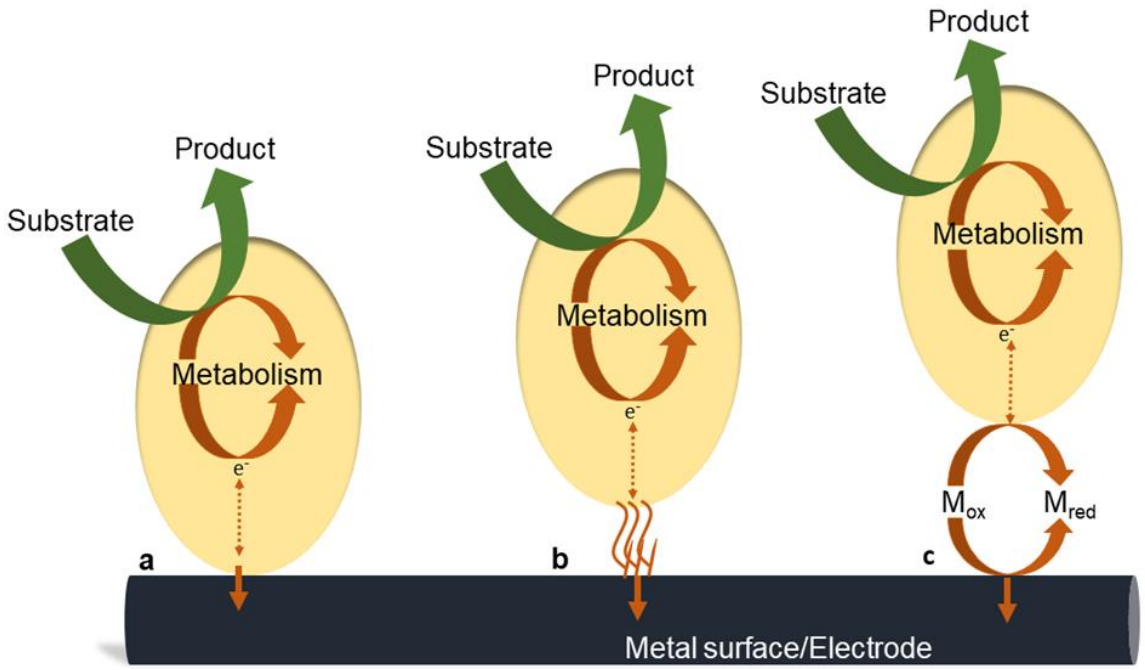

Figure 1.1. Schematic representation of the three modes of electron transfer in exoelectrogens. (a) Direct electron transfer through redox protein in the cell membranes (b) Electron transfer through hair-like structures or conductive appendages (c) Indirect electron transfer through shuttles that act as intervening medium between the cell and the metal surface.

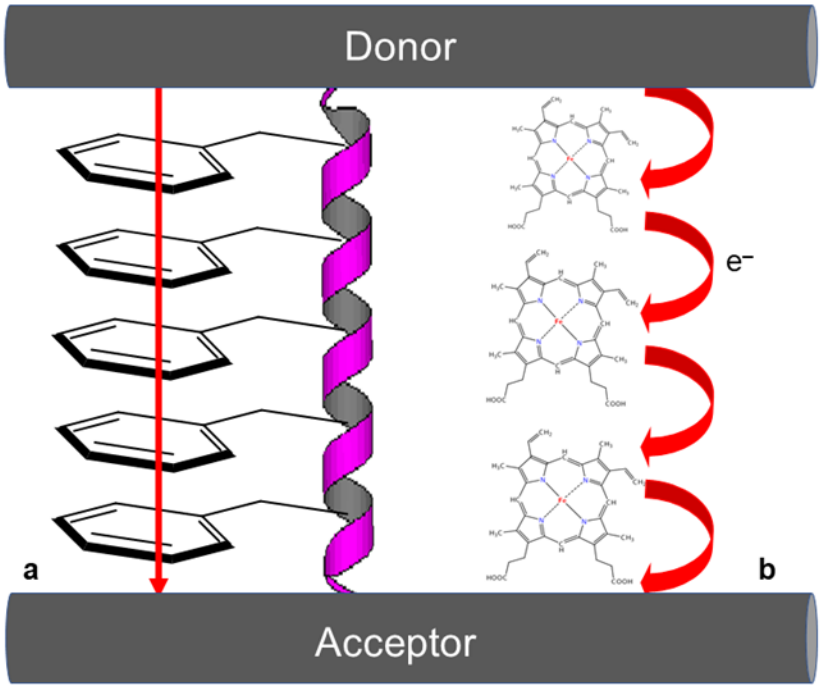

Figure 1.2. Schematic representation of the proposed mechanisms of electron transfer via microbial nanowires. a) Electron tunneling through proteinaceous structures that reinforce π-π stacking b) Electron hopping through redox cofactors.

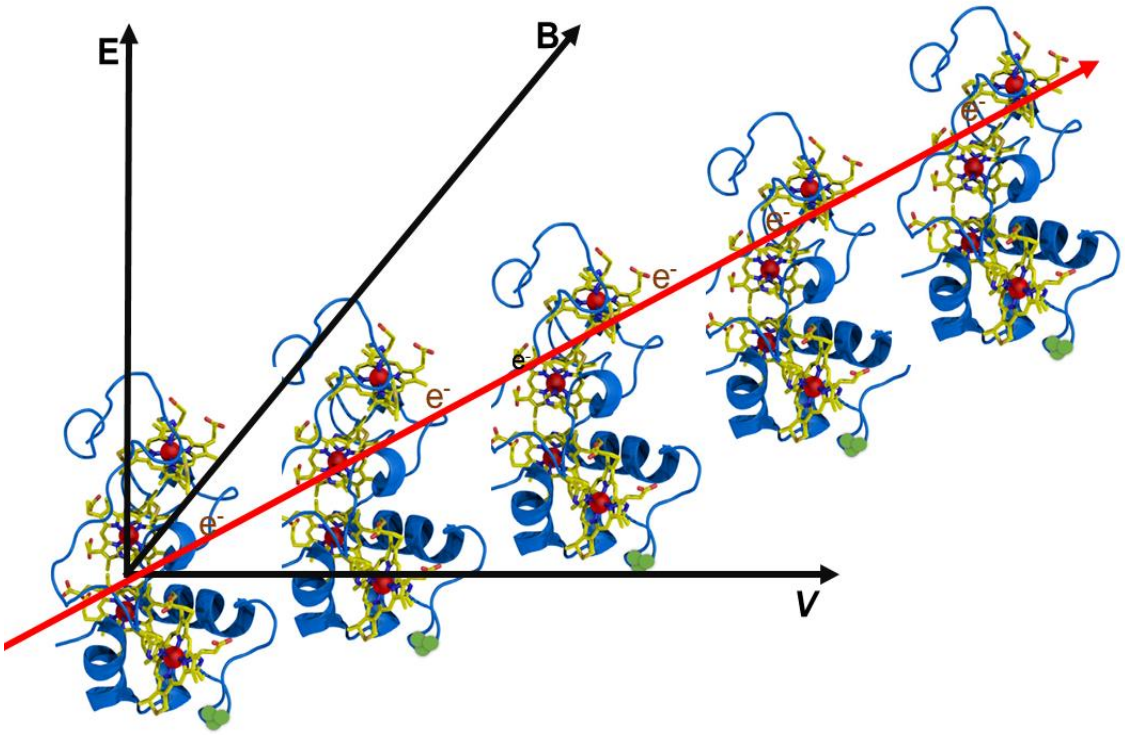

Figure 1.3. Schematic representation of chiral-induced spin selectivity in small tetraheme cytochrome (STC). If the redox cofactors (hemes) which are embedded in STC (chiral biomolecule) transfer electrons from one to another, then the magnetic field (B) generated is directly proportional to the velocity (V) of moving electrons given a specific spin direction and both functions impact the magnitude of electric field induced in a bio-chiral system (STC PDB ID: RCSB016488).

1.8 References

(1) Ragan, C. I.; Reed, J. S. Regulation of electron transfer by the quinone pool. *Journal of Bioenergetics and Biomembranes* **1986**, *18* (5), 403–418.

(2) Feist, A. M.; Nagarajan, H.; Rotaru, A. E.; Tremblay, P. L.; Zhang, T.; Nevin, K. P.; Lovley, D. R.; Zengler, K. Constraint-Based Modeling of Carbon Fixation and the Energetics of Electron Transfer in Geobacter metallireducens. *PLoS Computational Biology* **2014**, *10* (4), 1–10.

(3) Logan, B. E. Exoelectrogenic bacteria that power microbial fuel cells. *Nature Reviews Microbiology* **2009**, *7* (5), 375–381.

(4) Kumar, R.; Singh, L.; Zularisam, A. W. Exoelectrogens: Recent Advances in Molecular Driver Involved in Extracellular Electron Transfer and Strategies used to Improve it for Microbial Fuel Cell Applications. *Renewable and Sustainable Energy Reviews* **2016**, *56* (18), 1322–1336.

(5) Reguera, G. Harnessing the power of microbial nanowires. *Microbial Biotechnology* **2018**, *11* (6), 979–994.

(6) Lovley, D. R.; Walker, D. J. F. Geobacter Protein Nanowires. *Frontiers in Microbiology* **2019**, *10* (September).

(7) Cui, Y.; Lai, B.; Tang, X. Microbial Fuel Cell-Based Biosensors. *Biosensors* **2019**, *9* (3), 92.

(8) Lovley, D. R.; Yao, J. Intrinsically Conductive Microbial Nanowires for 'Green' Electronics with Novel Functions. *Trends in Biotechnology* **2021**, *39* (9), 940–952.

(9) Shi, M.; Jiang, Y.; Shi, L. Electromicrobiology and biotechnological applications of the exoelectrogens *Geobacter* and *Shewanella* spp. *Science China Technological Sciences* **2019**, *62* (10), 1670–1678.

(10) Newsome, L.; Morris, K.; Lloyd, J. R. The biogeochemistry and bioremediation of uranium and other priority radionuclides. *Chemical Geology* **2014**, *363*, 164–184.

(11) Logan, B. E. Extracting Hydrogen. *Environmental Science and Technology* **2004**, No. January 2004.

(12) Mehanna, M.; Kiely, P. D.; Call, D. F.; Logan, B. E. Microbial electrodialysis cell for simultaneous water desalination and hydrogen gas production. *Environmental Science and Technology* **2010**, *44* (24), 9578–9583.

(13) Clarke, T. A.; Edwards, M. J.; Gates, A. J.; Hall, A.; White, G. F.; Bradley, J.; Reardon, C. L.; Shi, L.; Beliaev, A. S.; Marshall, M. J.; Wang, Z.; Watmough, N.

J.; Fredrickson, J. K.; Zachara, J. M.; Butt, J. N.; Richardson, D. J. Structure of a bacterial cell surface decaheme electron conduit. *Proceedings of the National Academy of Sciences of the United States of America* **2011**, *108* (23), 9384–9389.

(14) Gross, B. J.; El-Naggar, M. Y. A combined electrochemical and optical trapping platform for measuring single cell respiration rates at electrode interfaces. *Review of Scientific Instruments* **2015**, *86* (064301), 1–8.

(15) El-Naggar, M. Y.; Wanger, G.; Leung, K. M.; Yuzvinsky, T. D.; Southam, G.; Yang, J.; Lau, W. M.; Nealson, K. H.; Gorby, Y. A. Electrical transport along bacterial nanowires from Shewanella oneidensis MR-1. *Proceedings of the National Academy of Sciences of the United States of America* **2010**, *107* (42), 18127–18131.

(16) Gilbert Gatty, M.; Kahnt, A.; Esdaile, L. J.; Hutin, M.; Anderson, H. L.; Albinsson, B. Hopping versus Tunneling Mechanism for Long-Range Electron Transfer in Porphyrin Oligomer Bridged Donor-Acceptor Systems. *Journal of Physical Chemistry B* **2015**, *119* (24), 7598–7611.

(17) Creasey, R. C. G.; Mostert, A. B.; Nguyen, T. A. H.; Virdis, B.; Freguia, S.; Laycock, B. Microbial nanowires – Electron transport and the role of synthetic analogues. *Acta Biomaterialia* **2018**, *69*, 1–30.

(18) Lovley, D. R. Electrically conductive pili: Biological function and potential applications in electronics. *Current Opinion in Electrochemistry* **2017**, *4* (1), 190–198.

(19) Subramanian, P.; Pirbadian, S.; El-Naggar, M. Y.; Jensen, G. J. Ultrastructure of *Shewanella oneidensis* MR-1 nanowires revealed by electron cryotomography. *Proceedings of the National Academy of Sciences of the United States of America* **2018**, *115* (14), E3246–E3255.

(20) Malvankar, N. S.; Tuominen, M. T.; Lovley, D. R. Lack of cytochrome involvement in long-range electron transport through conductive biofilms and nanowires of *Geobacter sulfurreducens*. *Energy and Environmental Science* **2012**, *5* (9), 8651–8659.

(21) Wang, F.; Gu, Y.; O'Brien, J. P.; Yi, S. M.; Yalcin, S. E.; Srikanth, V.; Shen, C.; Vu, D.; Ing, N. L.; Hochbaum, A. I.; Egelman, E. H.; Malvankar, N. S. Structure of Microbial Nanowires Reveals Stacked Hemes that Transport Electrons over Micrometers. *Cell.* **2019**, *177*, 361–369.

(22) Filman, D. J.; Marino, S. F.; Ward, J. E.; Yang, L.; Mester, Z.; Bullitt, E.; Lovley, D. R.; Strauss, M. Cryo-EM reveals the structural basis of long-range electron

transport in a cytochrome-based bacterial nanowire. *Communications Biology* **2019**, *2* (1), 19–24.

(23) Gu, Y.; Srikanth, V.; Salazar-Morales, A. I.; Jain, R.; O'Brien, J. P.; Yi, S. M.; Soni, R. K.; Samatey, F. A.; Yalcin, S. E.; Malvankar, N. S. Structure of Geobacter pili reveals secretory rather than nanowire behaviour. *Nature* **2021**, *597* (7876), 430–434.

(24) Yalcin, S. E.; O'Brien, J. P.; Gu, Y.; Reiss, K.; Yi, S. M.; Jain, R.; Srikanth, V.; Dahl, P. J.; Huynh, W.; Vu, D.; Acharya, A.; Chaudhuri, S.; Varga, T.; Batista, V. S.; Malvankar, N. S. Electric field stimulates production of highly conductive microbial OmcZ nanowires. *Nature Chemical Biology* **2020**, *16* (10), 1136–1142.

(25) Thirumurthy, M. A.; Jones, A. K. Geobacter cytochrome OmcZs binds riboflavin: Implications for extracellular electron transfer. *Nanotechnology* **2020**, *31* (12).

(26) Lovley, D. R. Untangling Geobacter sulfurreducens Nanowires. *mBio* **2022**, No. June, 1–3.

(27) Giri, K.; Bhattacharyya, N. P.; Basak, S. pH-dependent self-assembly of polyalanine peptides. *Biophysical Journal* **2007**, *92* (1), 293–302.

(28) Hendricks, M. P.; Sato, K.; Palmer, L. C.; Stupp, S. I. Supramolecular Assembly of Peptide Amphiphiles. *Accounts of Chemical Research* **2017**, *50* (10), 2440–2448.

(29) Restuccia, A.; Seroski, D. T.; Kelley, K. L.; O'Bryan, C. S.; Kurian, J. J.; Knox, K. R.; Farhadi, S. A.; Angelini, T. E.; Hudalla, G. A. Hierarchical self-assembly and emergent function of densely glycosylated peptide nanofibers. *Communications Chemistry* **2019**, *2* (1).

(30) Creasey, R. C. G.; Mostert, A. B.; Solemanifar, A.; Nguyen, T. A. H.; Virdis, B.; Freguia, S.; Laycock, B. Biomimetic Peptide Nanowires Designed for Conductivity. *ACS Omega* **2019**, *4* (1), 1748–1756.

(31) Xu, H.; Das, A. K.; Horie, M.; Shaik, M. S.; Smith, A. M.; Luo, Y.; Lu, X.; Collins, R.; Liem, S. Y.; Song, A.; Popelier, P. L. A.; Turner, M. L.; Xiao, P.; Kinloch, I. A.; Ulijn, R. V. An investigation of the conductivity of peptide nanotube networks prepared by enzyme-triggered self-assembly. *Nanoscale* **2010**, *2* (6), 960–966.

(32) Ing, N. L.; Spencer, R. K.; Luong, S. H.; Nguyen, H. D.; Hochbaum, A. I. Electronic Conductivity in Biomimetic α-Helical Peptide Nanofibers and Gels. *ACS Nano* **2018**, *12* (3), 2652–2661.

(33) Cosert, K. M.; Castro-Forero, A.; Steidl, R. J.; Worden, R. M.; Reguera, G.

Bottom-up fabrication of protein nanowires via controlled self-assembly of recombinant *Geobacter* pilins. *mBio* **2019**, *10* (6), 1–15.

(34) Altamura, L.; Horvath, C.; Rengaraj, S.; Rongier, A.; Elouarzaki, K.; Gondran, C.; Maçon, A. L. B.; Vendrely, C.; Bouchiat, V.; Fontecave, M.; Mariolle, D.; Rannou, P.; Le Goff, A.; Duraffourg, N.; Holzinger, M.; Forge, V. A synthetic redox biofilm made from metalloprotein-prion domain chimera nanowires. *Nature Chemistry* **2017**, *9* (2), 157–163.

(35) Chen, Y. X.; Ing, N. L.; Wang, F.; Xu, D.; Sloan, N. B.; Lam, N. T.; Winter, D. L.; Egelman, E. H.; Hochbaum, A. I.; Hochbaum, A. I.; Hochbaum, A. I.; Clark, D. S.; Clark, D. S.; Glover, D. J. Structural Determination of a Filamentous Chaperone to Fabricate Electronically Conductive Metalloprotein Nanowires. *ACS Nano* **2020**, *14* (6), 6559–6569.

(36) Naaman, R.; Waldeck, D. H. Chiral-Induced Spin Selectivity Effect. *The Journal of Physical Chemistry* **2012**, *1021* (3), 2178–2187.

(37) Naaman, R.; Paltiel, Y.; Waldeck, D. H. Chiral Induced Spin Selectivity and Its Implications for Biological Functions. *Annual Review of Biophysics* **2022**, *51* (1).

Chapter 2

2. Supramolecular Assembly of Redox Proteins to form Nanowires for Ultra Long-Range Biological Electron Transfer

J. N. Nwachukwu[1], M. A. Thirumurthy[1], J. T. Atkinson[2], M. Y. El-Naggar[2] and A. K. Jones[1]

[1]School of Molecular Sciences, Arizona State University, Tempe, AZ, USA

[2]Department of Physics and Astronomy, University of Southern California, Los Angeles, CA, USA

2.1 Abstract

Exoelectrogenic organisms transfer electrons from their internal quinone pool to extracellular acceptors over μm-scale distances through appendages known as "biological nanowires". These structures have been variously described as cytochrome-rich membrane extensions or pili, and the components and mechanisms of this long-range electron transfer remain largely unknown. In fact, current physical understanding of biological electron transfer is only sufficient to describe electron movement on the nm scale. Here, we describe a proteinaceous, supramolecular model for ultralong-range biological electron transfer consisting of fibers built from a self-assembling peptide together with a small tetraheme cytochrome (STC) from *Shewanella oneidensis*. Assembled fibers have average dimensions of 500 nm x 15 nm x 9 nm. Electrochemical measurements show the fibers retain the native reduction potential of their constituent STC, and electrochemical gating experiments show electrical conductivity occurs along the fiber length in a process likely mediated by electron transfer between cytochromes. Temperature-dependent studies suggest a thermally-activated process with an activation energy of 0.28 eV. Our work elucidates serves as the first synthetic, functional model of electron transfer in bacterial nanowires.

2.2 Introduction

Electron transfer is essential to the metabolism of all organisms.[1] Biological electron transfer is exploited in such technologies as biosensors, bioremediation, wastewater treatment, microbial fuel cells, bioelectronics and bioelectricity.[2] Exoelectrogens are a unique group of organisms that can transfer electrons from their

quinone pool to the external environment. Although a number of different microbial structures and components have been hypothesized to be involved in this process, the mechanisms of extracellular electron transfer remain unknown.[3] Exoelectrogens have been shows to employ three distinct modes of electron transfer from internal metabolism to external surfaces: direct electron transfer via redox proteins present on the surface of the cell membrane;[4] indirect electron transfer in which redox mediators act as shuttles between the exoelectrogen and the external surface;[5] and through hair-like appendages referred to as microbial nanowires.[6] While the mechanisms of direct transfer and indirect transfer through shuttles are relatively well understood, the mechanism of electron transfer via microbial nanowires is largely unknown.

Two conflicting mechanisms have been proposed to explain electron transfer along the lengths of a microbial nanowires: electron tunneling via proteinaceous structures that force π-π stacking of aromatic amino acids residues along the lengths of the nanowires and electron hopping between close-spaced redox cofactors along the length of the bacterial nanowire.[2] Evidence for the first hypothesis comes from Lovely and coworkers, who showed that *Geobacter* pili are highly conductive even in the absence of *c*-type cytochromes, the redox carriers believed to be responsible for a hopping mechanism.[7] On the other hand, cryo-electron microscopy of *Geobacter* pili revealed closely stacked hemes within distances of 3-6 Å, which suggests an electron hopping mechanism.[8] Additionally, electron cryomotography revealed that the extended conductive filaments of *Shewanella onediensis* contains redox proteins that are extensions of the periplasm.[9] Using structural models as a starting point, Monte Carlo simulations have shown that

hopping of electrons through cytochromes in the conductive filaments of *S. oneidensis* could plausibly occur on a timescale sufficient to support metabolism.[10]

Beyond the single protein scale, there are few biologically based models relevant to describing the mechanism of long-range electron transfer in microbial nanowires. Supramolecular structures containing proteins can be constructed using fibril assembling domains,[11] but structures involving redox-active or conductive components remain rare. Altamura and coworkers assembled a fiber comprised of prion backbone and rubredoxin, an FeS protein. While it is structurally well defined and possibly relevant to long-range extracellular electron transfer, it showed poor conductivity (3.1 μS cm^{-1}) compared to natural conductive structures (5 mS cm^{-1}).[12] Structures from biomimetic peptides assembled using aromatic amino acid residues also show poor conductivity that is insufficient for studying long range electron transfer.[13]

As shown schematically in Fig. 2.1, to evaluate the possibility of long-range (approximately μm) electron transfer via hopping along closely placed hemes, in this work we report assembly of the small tetraheme cytochrome (STC) from *Shewanella oneidensis* into supramolecular fibrillar structures via a self-assembling peptide. STC has the highest heme:protein ratio of any known *c*-type cytochrome, reflective of the close spacing between the four hemes and their largely solvent-exposed positions. We have used a β-tag peptide called Q11 to assemble STC in the first generation. The Q11 peptide is comprised of 11 amino acid residues (Ac-QQKFQFQFEQQ-NH_2) that have been previously employed by Hudalla and coworkers in molecular assembly of GFP owning to its ability to conformationally change to fibrilizing β-sheets.[14] Herein we will show that

STC can be assembled into fibrous structures using Q11, that is maintains its native redox properties within the fiber, and that the fibers are highly conductive along their lengths. This suggests that the STC fibers may be the first functional model relevant to explaining long-range extracellular electron transfer in exoelectrogens.

2.3 Methods

2.3.1 Heterologous Expression and Purification of Beta-tagged Small Tetraheme Cytochrome β-STCM in *E. coli*

A pD431-MR vector coding for *S. onediensis*[1] STC with a single surface serine residue exchanged for a cysteine (S87C), a twin-strep tag sequence on the C-terminus, and the sequence encoding the β-tail peptide appended to the N-terminus (β-STCM) and a kanamycin resistance gene was produced by DNA 2.0 (Table 2.1). The pD431 plasmid was transformed with a plasmid encoding the *ccm* (Cytochrome *c* maturation) operon (with chloramphenicol resistance gene) into *E. coli* using the heat shock method.[2] Cells were aerobically grown in LB (Luria-Bertani) media at 37 °C with shaking at 7 x g. Kanamycin and chloramphenicol were added to a final concentration of 50 mg ml^{-1} and 35 mg ml^{-1}, respectively. Cells were induced at an optical density (OD_{600}) of 0.6 with 0.2 mM isopropyl β-D-1-thiogalactopyranoside (IPTG) in the culture. After induction, cells were grown for 18 h and harvested by centrifugation at 4 °C, 16,128 x g for 1 h. Periplasmic extracts were obtained by adding 28 μM lysozyme in 20 mM PBS buffer at pH 7.2 with 100 mM EDTA, 0.0002 U/μL DNase I (Thermo Fisher Scientific), and 2 tablets of Pierce protease inhibitor and gently stirring for 90 min at 4 °C. The resulting extract was cleared by centrifugation (16,128 x g) for 1 h, and the supernatant collected. The supernatant was dialyzed against

20 mM PBS (Phosphate Buffer Saline) pH 7.2 at 4 °C overnight. Dialyzed supernatant containing the protein of interest was applied to a 40 mL DEAE column equilibrated at 20 mM PBS pH 7.2 at room temperature. The column was washed with increasingly concentrated PBS (50 mM – 350 mM, 5 column volume for each concentration) at pH 7.2. The STC mutant eluted at 400 mM PBS at pH 7.2. Fractions containing STC mutant were pooled and concentrated with amicon ultra-centrifugal filters (2 kDa molecular weight cut-off) before applying to a 30 ml S*trep*-Tactin column equilibrated with 20 mM PBS at pH 7.2 at room temperature. The column was washed with 100 ml of 20 mM PBS at pH 7.2, and then the β-STCM was eluted with 20 mM PBS containing 5 mM desthiobiotin.

2.3.2 Protein Characterization

Protein concentrations were determined via Bradford assay with a Thermo Scientific Varioskan Lux Mode multimode microplate reader using Bovine serum albumin (BSA) as standard.[15] Sodium Dodecyl Sulphate Polyacrylamide Gel Electrophoresis (SDS-PAGE) was used to evaluate protein purity which was visualized in Coomassie blue.

2.3.3 Enzyme-linked Immunosorbent Assay

Aliquots of purified β-STCM fusion protein (100 µL, 0.78 mg/ml) were placed on a 96-well maxi-sorp ELISA plate and incubated for 2 h at room temperature. After which β-STCM was removed and the plate washed using deionized water. Aliquots of the three peptide antibodies raised against the antigenic determinants of β-STCM (SELHKLKSELGSGGGGSGGGGSGGGGSA, ESGGCESCHKDGTP, and GKLSEMDAVHKPHD) were added to different wells, incubated for another 1 h at room temperature and then rinsed repeatedly. Aliquots of 100 µL of horseradish peroxidase

conjugate were applied to each well, incubated for 30 min and washed before subsequent addition of chromogenic substrate (HRP) solution. Plates were then incubated in the dark for 30 min before addition of a stop solution (100 µL of 0.16 M H_2SO_4) with observed color change from blue to yellow noted. Absorbance for each well was read at 450 nm using a Thermo Scientific Varioskan Lux Plate reader.

2.3.4 Q11 Peptide synthesis and purification

Q11 (Ac-QQKFQFQFEQQ-NH_2) was synthesized on a PS3 peptide synthesizer on a 0.1 mmol scale using the standard Fmoc/tBu (Fmoc, 9-fluoromethoxycarbonyl) protection strategy on Rink amide resin (100-150 mesh, 149 mg) with HTCU (O-(1H-6-chlorobenzotriazole-1-yl)-1,1,3,3-tetramethyluronium hexafluorophosphate) (165 mg) as the activator.[16] Following synthesis, the N-terminus was acetylated using acetic anhydride and pyridine after which peptide was simultaneously deprotected and cleaved from the resin using the TFA cleavage cocktail (10 % of Trifluoracetic acid in Dichloromethane) described by Amblard and co-workers.[17] Following concentration, the crude peptide was precipitated with cold diethyl ether and then dissolved in water. The resin was filtered off using spin columns (60 µm pore size, 1 mL column volume) and centrifugation for 10 min at 3,500 x g. Crude peptide was lyophilized before purification or storage. Crude peptide was purified using High Performance Liquid Chromatography (HPLC) on a C18 column. The column was washed with solvent A (5% acetonitrile, 95% water and 0.1% TFA) for 10 min followed by gradient elution with solvent A mixed with increasing concentrations of solvent B (5% water, 95% acetonitrile and 0.1% TFA) from 10%-70% over 50 min. Crude peptide was dissolved in water and TFA before injection

into the HPLC. Fractions collected from several injections were pooled and lyophilized. Purity and molecular weight of the peptide were verified using Matrix Assisted Laser Desorption/Ionization-Time of flight (MALDI-TOF) mass spectrometry (20 Hz and linear mode at 25,000 V) using sinapinic acid as the matrix.

2.3.5 β-STCM-Q11 fiber preparation

Purified Q11 peptide and β-STCM were mixed at a ratio of 1000:1 at concentration of 6.6 mM: 6.6 μM. Each component was dissolved in PBS before mixing overnight at room temperature.

2.3.6 Transmission Electron Microscopy (TEM) of β-STCM-Q11 Nanowire

Glow discharged 400 Mesh copper grids (FCF-400) were first floated on top of 20 μl of PBS containing β-STCM-Q11 fibers and wiped on the sides with chemwipes after each float. These grids were further floated in water and 2% uranyl acetate as negative stain. Samples on mesh grids were analyzed using the TEM Philip CM 200.

2.3.7 Atomic Force Microscopy

β-STCM-Q11 fibers solution (5 μL) was absorbed on mica (1.5 cm x 1.5 cm, Ted Pella, Inc.) and placed in a humidifier for 30 min after which surface was cleaved and cleaned with ultrapure water. After evaporation, samples were immediately imaged using the tapping mode Tap300Al-G probes (with 40 N/m force constant, 300 kHz resonant frequency, Budget Sensors). Images were processed using Gwyddion software.

2.3.8 Fluorescence Microscopy

β-STCM-Q11 fibers (5 μL) were spotted on poly-lysine coated slides. Primary monoclonal mouse anti-STC antibody was incubated on to the slide surface overnight at

night at 4 °C. Primary monoclonal mouse anti-STC antibody was filtered off and washed (3 times) using PBS at 7.2 and 0.1% tween 20 (PBST). Secondary antibody alexa-fluor 647 was incubated for 1 h at room temperature followed by washed and rinsing using PBST and PBS, respectively. Samples were imaged with Leica TCS SP5 AOBS Spectral Confocal System after covering the sample with a coverslip.

2.3.9 Electrochemical studies of purified β-STCM and β-STCM-Q11 Fibers

Electrochemical experiments were conducted in a glovebox under nitrogen in a three-electrode electrochemical cell using a PGSTAT 12 Autolab Potentiostat. The electrodes consist of a custom-made 1.2 mm diameter graphite (Minteq International pyrogenic group) working electrode, Ag/AgCl reference, and a platinum wire counter electrode. The working electrode was polished with 120 grit sandpaper and alumina (5μm size followed by 0.3 μm and 0.05 μm sizes of BASi Polishing Alumina Powder) before each use. Protein films were formed by spotting β-STCM or β-STCM-Q11 fibers (10 μl, 250 mM for both β-STCM or β-STCM-Q11 fibers) on graphite electrode surface and allowing them to dry. The electrode potential was cycled between +0.2 V and –0.4 V vs SHE at a scan rate of 25 mV s^{-1} in 20 mM sodium phosphate buffer at pH 7.2 with 100 mM NaCl as supporting electrolyte. All potentials are corrected to the standard hydrogen electrode (SHE) according to the equation $E_{SHE} = E_{Ag/AgCl}$ +197 mV at 25 °C.[18]

2.3.10 Charge transport measurement of β-STCM-Q11 Fibers

Electrochemical gating measurements were made using a bipotentiostat configuration consisting of two Reference 600 potentiostats (Gamry Inc.) connected with a communication cable and using in a MultEchem configuration. Linked cyclic

voltammetry scans were performed using a custom script provided by the manufacturer. Interdigitated electrodes consisting of interdigitated 5 µM wide Au bands with 5 µM gaps (ED-IDE3-Au, Micrux Technologies) were washed by sonication in isopropanol for 15 min, followed by milliQ water for 15 min, and were dried in a stream of N_2 gas. Immediately following washing, IDEs were transferred into an anerobic chamber with a 5% H_2/95% N_2 atmosphere (Bactron). An electrochemical cell was constructed by placing the IDE at the bottom of the cell using an AIO-cell (ED-AIO-CELL, Micrux Technologies) IDE interface with a 400 µL well placed on top of the IDE using a batch PEEK cell (BC-PEEK-5,0, Micrux Technologies). 400 µL of buffer (20 mM PBS, 50 mM NaCl, pH 7.2) was added to the cell and a platinum counter electrode and a reference electrode (3M KCl Ag/AgCl) were inserted into the top of the well. The potentiostats were connected to shared reference and counter electrodes and each of the two interdigitated electrodes were connected to individual potentiostats using the AIO wiring harness. All potentials are reported relative to the Standard Hydrogen Electrode (+0.210 V vs Ag/AgCl in 3M KCl).

Gating measurements were performed by simultaneously scanning the potential (from 230 V_{SHE} to -0.38 V_{SHE}) of both the source (E_S) and drain (E_D) at the same scan rate (5 mV s^{-1}) while maintaining a fixed potential offset ($V_{SD} = E_S - E_D = 0.02$ V) and individually measuring the currents from the source and drain electrodes. As previously described by El-Naggar and coworkers,[3] conduction currents were calculated as $I_{cond} = (I_{Drain} - I_{Source}) / 2$ and reported relative to the average potential of the two electrodes ($E_{Gating} = (E_D\text{-}E_S)/2$). For each electrode, gating measurements were also made in buffer

alone. The electrochemical cell was deconstructed and 10 µL of peptide or protein solution was spotted onto the IDE and allowed to incubate at 25 ºC for 30 min. Excess protein was removed and the cell washed three times with 10 uL of buffer. The cell was reconstructed and 400 µL of buffer was added and gating measurements were repeated. Protein solutions contained the either 6.6 mM Q11 peptide or 6.6 µM β-STCM fibers assembled at a ratio of 6.6mM Q11:6.6 µM β-STCM.

2.4 Results

2.4.1 Heterologous expression, purification and characterization of β-STCM fusion protein

Fig. 2.1 shows a schematic version of the aspirational supramolecular conductive fiber consisting of alternating conductive STC cytochrome and self-assembling Q11 peptide. To assemble this structure, a variant form of STC was expressed in *E. coli*, the sequence of which is shown in Fig. 2.2. The protein is functionalized at the N-terminus with the β-tail tag that self-assembles with the Q11 peptide to form fibers. Two other changes have been made to the wild-type protein sequence. At the C-terminus, the signal peptide OmpA and a *strep*-tag were attached to facilitate periplasmic expression and subsequent purification. Additionally, the serine at position 87 was exchange for a cysteine to provide an attachment point to anchor the protein onto gold surfaces via Au-S bonds. The modified protein is referred to hereafter as β-STCM.

The β-STCM protein was expressed in *E. coli* and purified as described in the methods section. Fig. 2.3 shows via Coomassie-stained SDS-PAGE that the procedure results in high purity protein of the desired molecular weight. UV-vis spectroscopy was

used to characterize the fusion protein and estimate its purity. As expected for a multi-heme containing *c*-type cytochrome, Fig. 2.4 shows that the UV-vis spectrum of β-STCM features a Soret peak at 408 nm and a corresponding broad β-band at 534 nm.[19] Both of these peaks are characteristics of *c*-type cytochromes. The A_{408}/A_{280} ratio, representing the ratio of heme to aromatic amino acid absorbance, is often used to estimate purity of heme-containing proteins with values above 0.5 generally considered pure for proteins with a single heme.[20] Preparations of β-STCM have a ratio of 4.05, indicating highly pure protein.

2.4.2 Synthesis and purification of Q11 peptides

Q11 peptide was synthesized via FMOC solid-phase synthesis and purified via the HPLC as described in the methods.[17] Fig. 2.5 shows that Q11 elutes from the HPLC around 30 min, and its identity was verified as shown in Fig. 2.6 using MALDI. The observed m/z of 1527.4120 Da corresponds to the parent ion with hydrogen.

2.4.3 Assembly and Structural characterization of β-STCM-Q11 nanowires

Fibers containing both β-STCM and Q11, henceforth referred to as β-STCM-Q11, were assembled by combining β-STCM fusion protein and Q11 peptide at a molar ratio of 1:1000 (6.6 μM: 6.6 mM) and incubating overnight at 4 ºC (Fig. 2.1). TEM, AFM, and fluorescence microscopy were used to structurally characterize the dimensions of the resulting fibers. TEM images of fibers in Fig. 2.7 confirm assembly of β-STCM-Q11 fibers with an average length x width of 500 nm x 14.6 nm. Fig. 2.8 shows that AFM images of β-STCM-Q11fibers have an average height of 9 nm with strip-like wire morphology and semi-rough surfaces.

As mentioned previously, in PBS Q11 can self-assemble without an additional protein into fibers. Thus, fluorescence microscopy was used to determine whether β-STCM was incorporated into the fiber. Three monoclonal antibodies were raised against STC antigens, and Fig. 2.9 shows via ELISA assay that all three react with β-STCM. Assembled β-STCM-Q11 fibers were incubated with primary monoclonal mouse anti-STC antibody and then anti-mouse antibody conjugated with Alexa Fluoro 647. Following extensive washings, Fig. 2.10 shows fluorescence images confirming the presence of β-STCM along the entire lengths of the assembled fibers. Note that the resolution of this technique is not sufficient to determine the distance between β-STCM monomers.

2.4.4 Redox characterization of β-STCM fusion protein and β-STCM-Q11 nanowires

Protein film electrochemistry was used to determine whether incorporation of β-STCM into fibers modifies its redox properties. Fig. 2.11 shows cyclic voltammograms from β-STCM and β-STCM-Q11 fibers, each separately immobilized on pyrolytic graphite electrode. Each sample yields voltammograms featuring reversible redox events, with oxidative peaks at -98 mV vs. SHE and reductive peaks at 245 mV vs. SHE (henceforth, all potentials will be quoted relative to the Standard Hydrogen Electrode [SHE]); with an average reduction potential at -171 mV and a peak separation of -147 mV. This demonstrates that β-STCM maintains its native redox properties when incorporated into the fiber with Q11.

2.4.5 Charge transport measurements of β-STCM-Q11 nanowires

Electrochemical gating measurements were used to evaluate the charge transport properties of the β-STCM-Q11 fibers. Electrochemical gating measurements have previously been used to determine whether charge transport mechanisms are redox-mediated.[21,22,23]. In these experiments, samples are deposited onto Au interdigitated electrodes with a 5 μm gap. A fixed bias voltage is applied between source and drain electrodes relative to a global gate electrode (Ag/AgCl reference electrode), Mathematically, $E_{SD} = E_D - E_S$ in which E_{SD} is source-to-drain bias voltage; E_D is the potential of the drain electrode relative to the global reference; and E_S is the potential of the source electrode relative to the global reference. If the material spanning the gaps between the electrodes is conductive, signals are observed, and the source-drain current, I_{cond}, can be calculated by $(I_D - I_S)/2$.[3]

Figure 2.12 shows cyclic voltammograms measured at each of the source and drain electrodes for Q11, β-STCM, and β-STCM-Q11 fibers. Peaks attributable to the redox cycling of the cyctochromes are observed in the samples containing protein. Fig. 2.13 shows conduction currents between the source and drain electrodes derived from these voltammetry experiments which can be compared to data for the same electrodes in buffer before exposure to samples that are shown in Fig. 2.14. The results show that only β-STCM-Q11 fiber films conduct current between the source and the drain at a similar potential to the reduction potential of -171 mV of STC and show no current at blank This contrasts with films of the Q11 fibers without β-STCM or the β-STCM fusion protein without Q11 for which limited conduction in the same potential region is observed.

These results indicate that supramolecular assembly of β-STCM into fibers enhances charge transport relative to β-STCM fusion protein alone and that charge transport is dependent on the presence of STC in the fibers. Figures 2.18-2.23 show that repeated experiments over a range of different source-drain bias voltages affirm charge transport along the β-STCM-Q11 fibers, and, as expected, the magnitude of conductive scales directly with the bias voltage (Fig. 2.15).

2.4.6 Temperature-dependent conduction studies of β-STCM-Q11 nanowire

Electrochemical gating measurements have previously been used by El-Naggar and coworkers to determine the temperature-dependence of nanowire conductivity, and electrochemical gating measurements of β-STCM-Q11 fibers were made at 25 ºC, 30 ºC, 35 ºC, and 40 ºC.[3] Fig. 2.16 shows that β-STCM-Q11 fiber conduction current at the potential of the hemes increases with increasing temperature, as expected for a thermally activated redox process. Fig. 2.17 shows that the conduction current can be fit to an Arrhenius plot with an activation energy of 0.29 eV.

2.5 Discussion

Previous models for biological long-range electron transfer have largely been based on repeating peptide units of with predictable placement of aromatic amino acids. Although the goal has been to create functional bioelectronic components in which π-π stacking leads to electronic conductivity, these structures have had limited conductivity. For example, super bundling of nanowires from so-called e-pili yielded structures with little to no conductivity.[24] Similarly, Creasey and coworkers designed structures with repeat units of aromatic amino acids residues with semi-conductive to non-conductive

properties. Additionally, Cosert and coworkers also produced structures that did not yield the desired conductivity, these structures were engineered *Geobacter* pilins with improved helicity of the constituting amino acid residues differing from Creasey's repeating units of aromatic amino acid residues and Lovley's super-bundling of pili as opposed .[25] Perhaps most significantly, no synthetic structure has been reported with a conductivity comparable to naturally occurring systems.[26]

On the other hand, there is promising evidence that c-type cytochromes are involved in long-range electron conduction in natural systems. For example, Malvankar and coworkers reported a 300-fold increase in conductivity of OmcS nanowires with changes in temperature,[27] suggesting that changes in heme ruffling displacement, planarity and temperature can increase nanowire conductivity significantly. They also reported a 1000-fold increase in the conductivity of OmcZ nanowires with stimulation by an electric field.[28]

Few redox proteins have been assembled into supramolecular structures with maintenance of their functionality. Altamura and coworkers assembled rubredoxin into fibers using a prion domain, but the resulting structures were not conductive.[12] On the other hand, Stevens and coworker reported that incorporation of hemin into serum albumin mats on a cm-length scale increased conductivity 40-fold between adjacent hemin molecules.[29]

Herein, we have successfully assembled β-STCM-Q11 fibers containing protein throughout the structure and maintaining the protein's native redox characteristics. Structural analysis reveals dimensions of 500-700 nm x 10-15 nm x 8-10 nm, ideal for

applications in bioelectronics and in patterned biofilms. Additionally, the dimensions are comparable to those of conductive structures found in exoelectrogenic bacteria, making these fibers first generation models of this ultra-long range electron transport. Electrochemical gating experiments demonstrate functional conductivity along the lengths of the assembled fibers. The potential dependence of fiber current matches that of the STC embedded in it implying that the mechanism of electron transfer along the fiber is redox-mediated by STC. Additionally, the temperature dependence of conductivity along the fibers also suggests a hopping mechanism mediated by hemes. Cryo-EM of the extensions of *Geobacter* has revealed closely stacked hemes, suggesting that natural systems may employ mechanisms similar to those of the β-STCM-Q11 fibers.[8]

Table 2.1 *E. coli* Strains and Plasmid used in the β-STCM-Q11 Study

Strain or Plasmid	Relevant characteristics or sequence	Source or reference
Plasmids		
pEC86 (p*ccm*)[a]	6.5 kb PCR fragment including *ccmABCDEFGH* with Cat^r	[30]
pD431 (p*bstcm*)[b]	*bstcm* with a N or C terminal OmpA signal peptide[31], kan^r. Beta-tail tag fused to STC gene	This study
E. coli strains		
BL21(DE3)	fhuA2 [lon] ompT gal (λDE3) [dcm] ΔhsdS λDE3 = λ sBamHIo ΔEcoRI-B int::(lacI::PlacUV5::T7 gene1) i21 Δnin5	New England Biolabs[32]

[a]The pEC86 plasmid was provided by D. Kramer's lab (Michigan State University); [b]The pD431 plasmid was prepared by DNA 2.0.

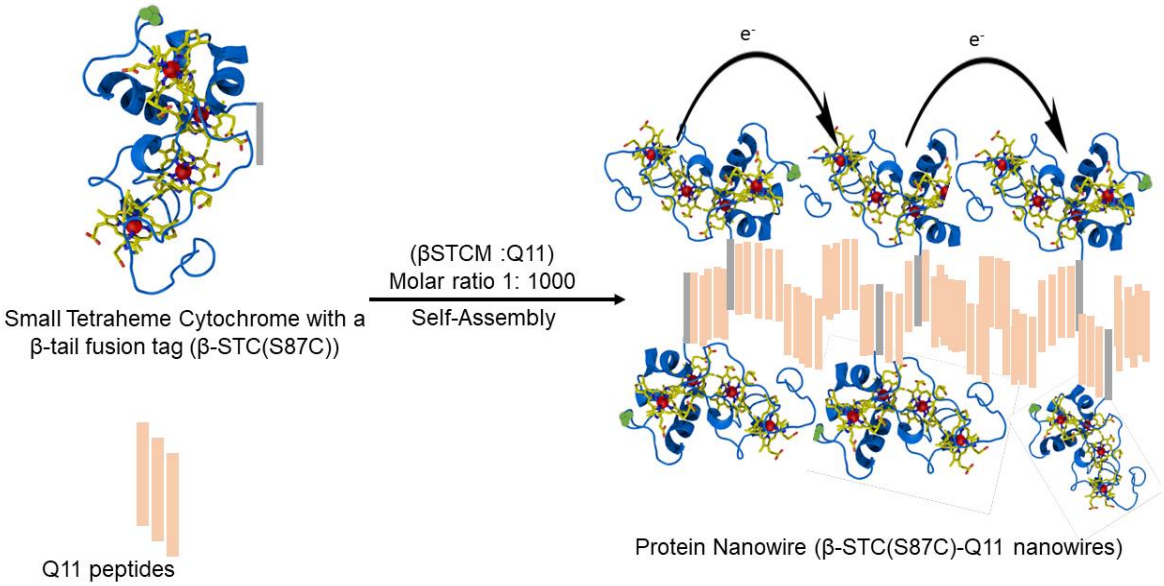

Fig. 2.1. Schematic representation of supramolecular assembly of β-STCM-Q11 nanowire. The β-STCM-Q11 nanowire is made of a beta-tagged STCM fusion protein which self-assembles into fibers on addition of Q11 peptide in optimal conditions (STC PDB ID: RCSB016488).

Fig. 2.2. β-STCM sequence expressed in this work. The OmpA leader sequence (gold) followed by the β-tail tag (purple) and an arrow (black) showing the site for cleavage of the signal peptide. The twin strep tag (green) is attached to the STCM (red) by the glycine-serine linker (blue). The 87th amino acid of the STCM have been mutated from serine to cysteine (black).

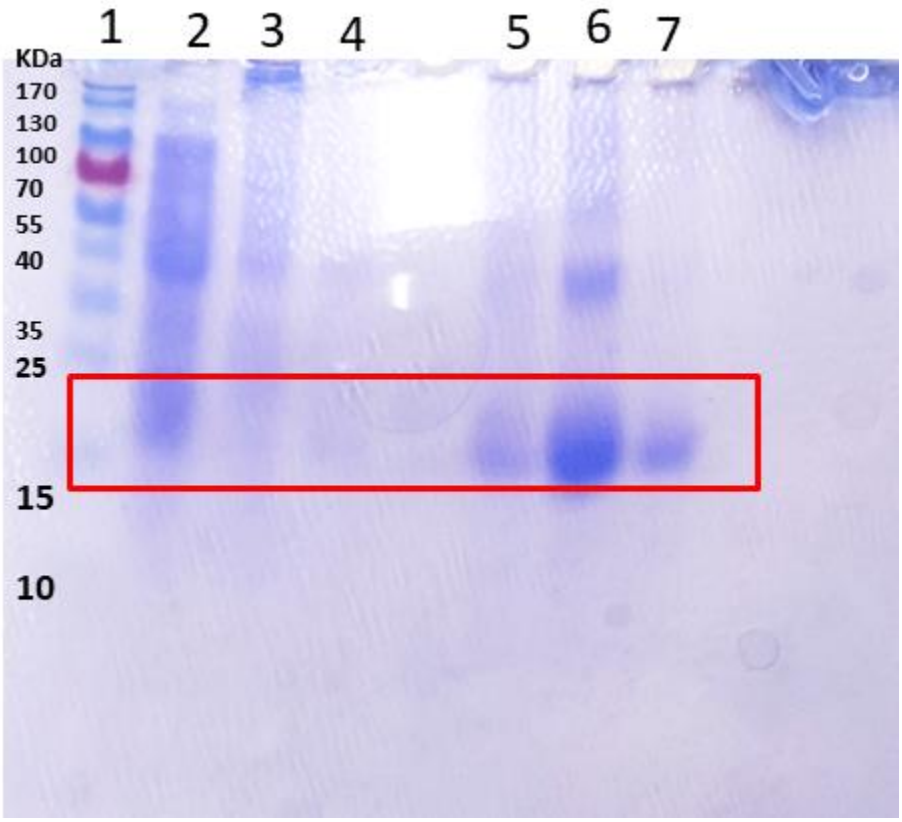

Fig. 2.3. SDS-PAGE gel visualized with Coomassie blue staining of various stages of β-STCM fusion protein purification. Lane 1: Protein standard (10 to 180 kDa); Lane 2: crude cell lysate; Lane 3: 200 mM Eluate from ion exchange chromatography; Lane 4: 300 mM Eluate from ion exchange chromatography; Lane 5: 400 mM Eluate from ion exchange chromatography; Lane 6: Recombinant Eluate from ion exchange chromatography Eluate from Streptactin Column; Lane 7: Purified β-STCM fusion protein from Streptactin column. β-STCM fusion protein is present as a prominent 21 kDa band in all lanes as shown in the red box. In each lane, 10 µl (600 µg/ml) of the designated sample was applied to the gel.

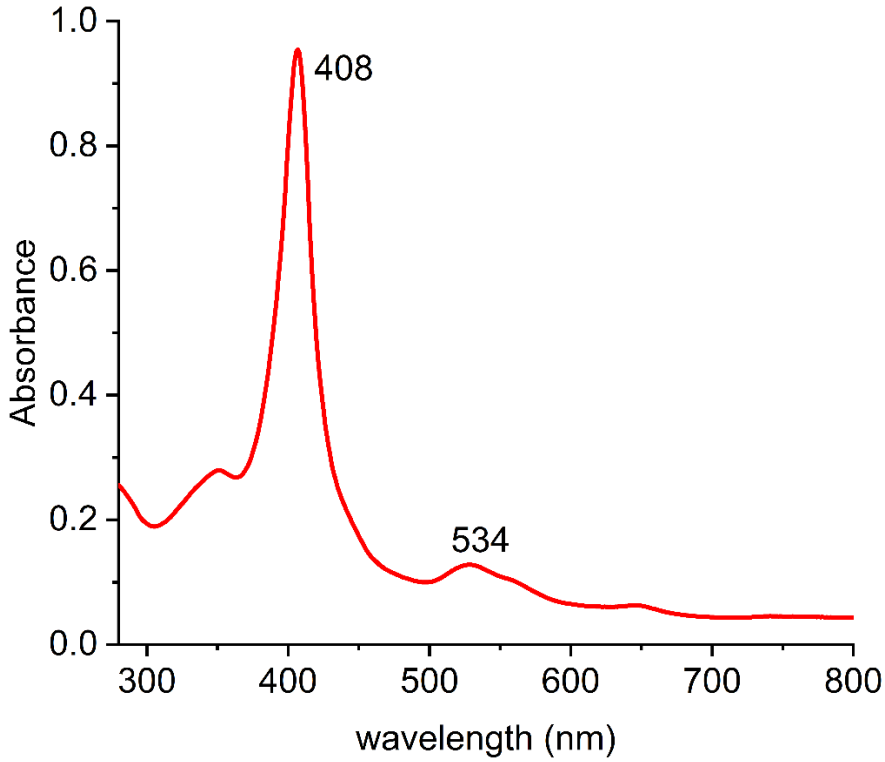

Fig. 2.4. UV-vis Spectrum of purified β-STCM fusion protein showing a Soret peak at 408 nm and a broad β-band peak at 534 nm characteristic of multiheme cytochromes.

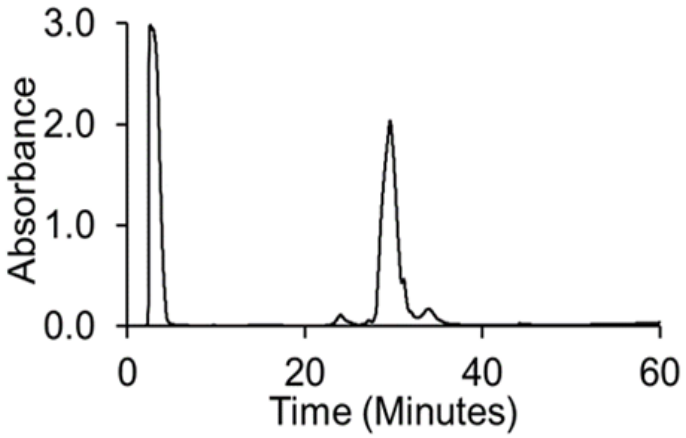

Fig. 2.5. HPLC chromatogram of Q11 peptide at 220 nm. Both peaks at 5 and 30 minutes were collected and lyophilized.

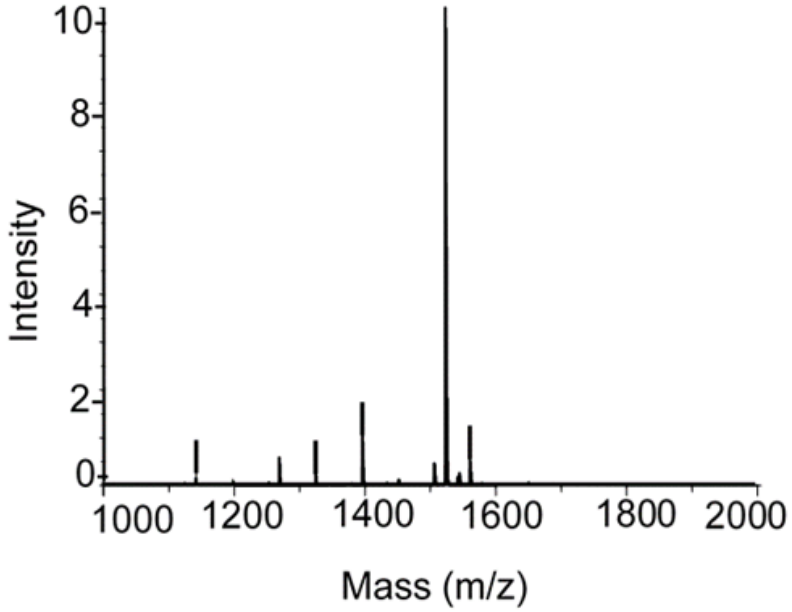

Fig. 2.6. MALDI-TOF mass spectrometry of purified Q11 peptide. Calculated m/z for Q11 peptide is 1526.652 Da, observed $[M + H]^+$ is 1527.4120 with the. The 30 minutes HPLC eluent contained our purified Q11. Scans were averaged over 150 shots.

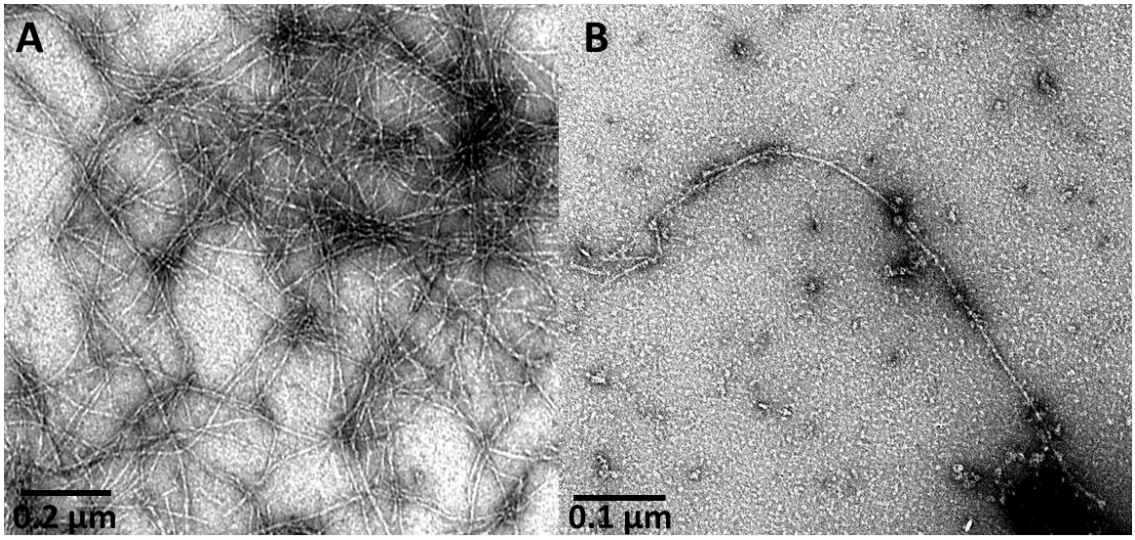

Fig. 2.7. Transmission electron micrograph of β-STCM-Q11 nanowires assembled at a concentration of 6.6 µM: 6.6 mM. (A) Image of assembled nanowires in clusters (B) Image of a single nanowire fibril. Nanowires were stained with 1% uranyl acetate.

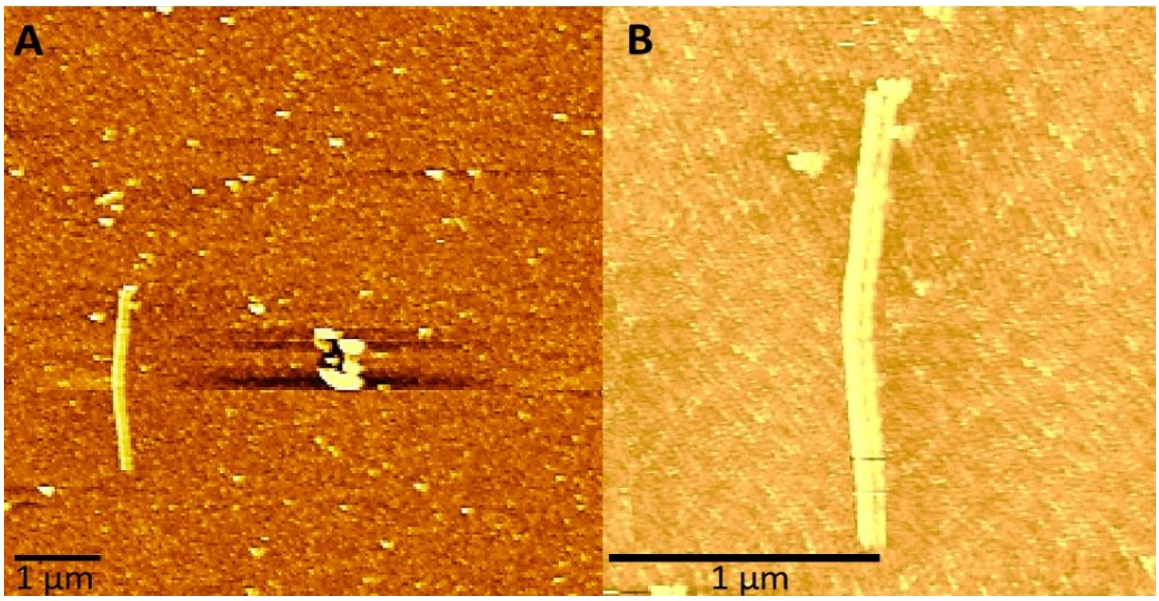

Fig. 2.8. Atomic force micrograph of β-STCM-Q11 nanowires on mica. Nanowires were assembled in ratio 1:1000 for Q11 peptide and β-STCM fusion protein, respectively.

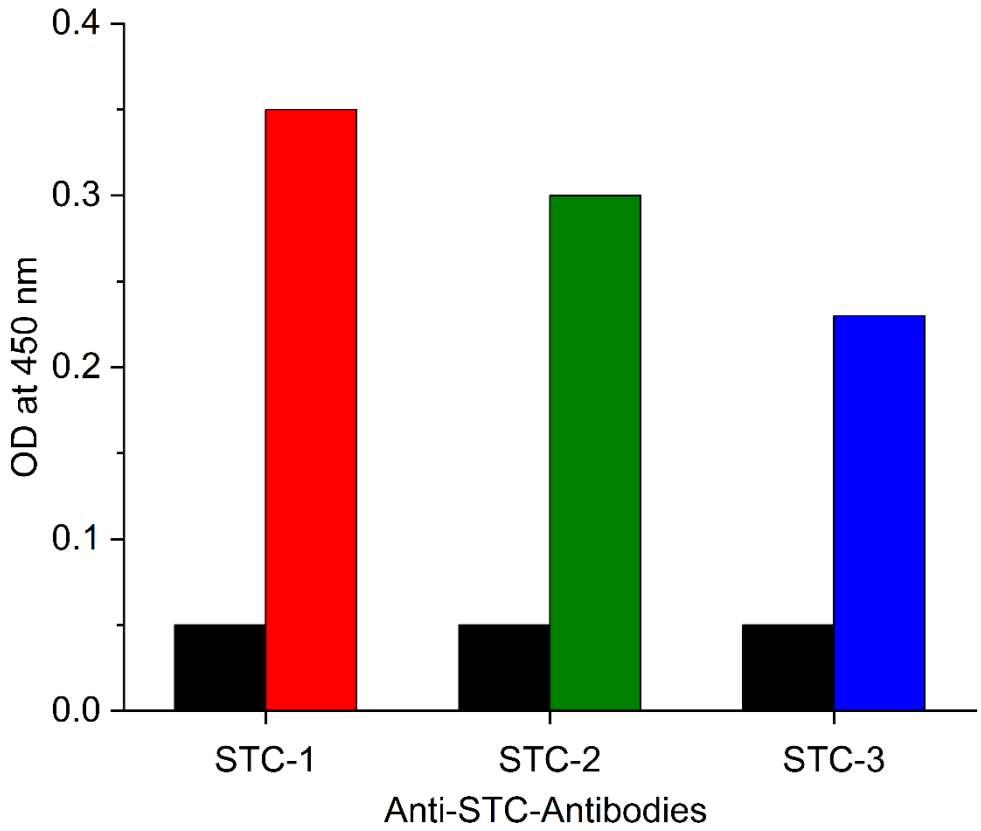

Fig. 2.9. ELISA of three different peptide antibodies against β-STCM. Black bars show each peptide antibody tested against bovine serum albumin.

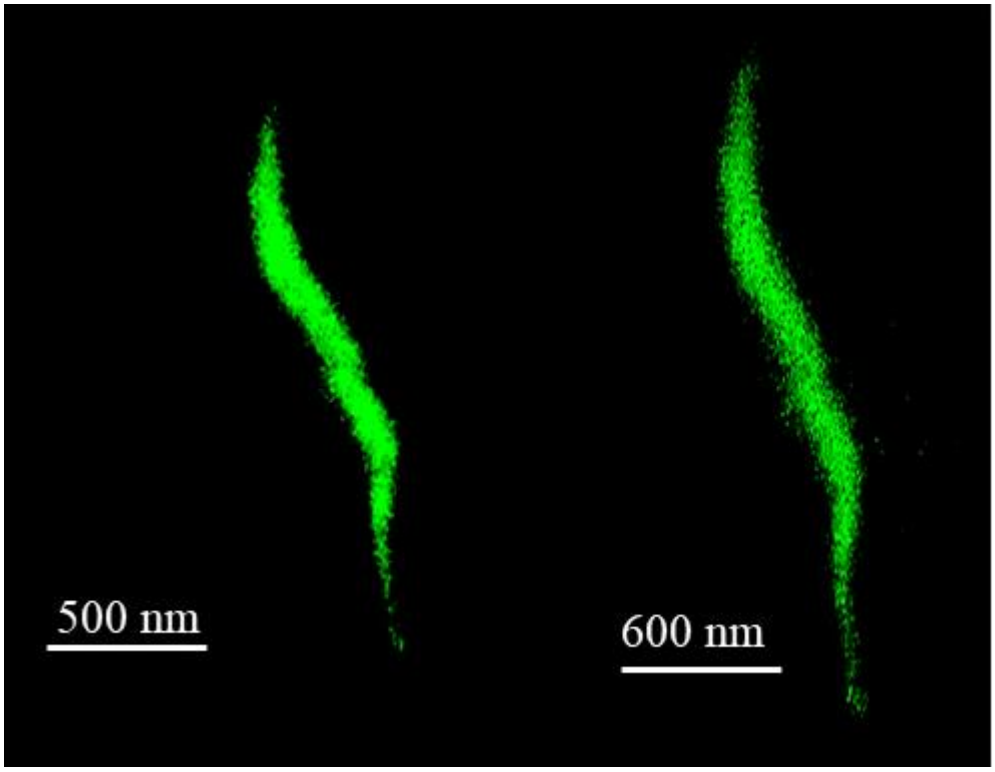

Fig. 2.10. Fluorescence micrograph of a single fibril of β-STCM-Q11. Nanowires show the presence of fluorescent antibodies bound to the β-STCM through the entire length of the nanowire.

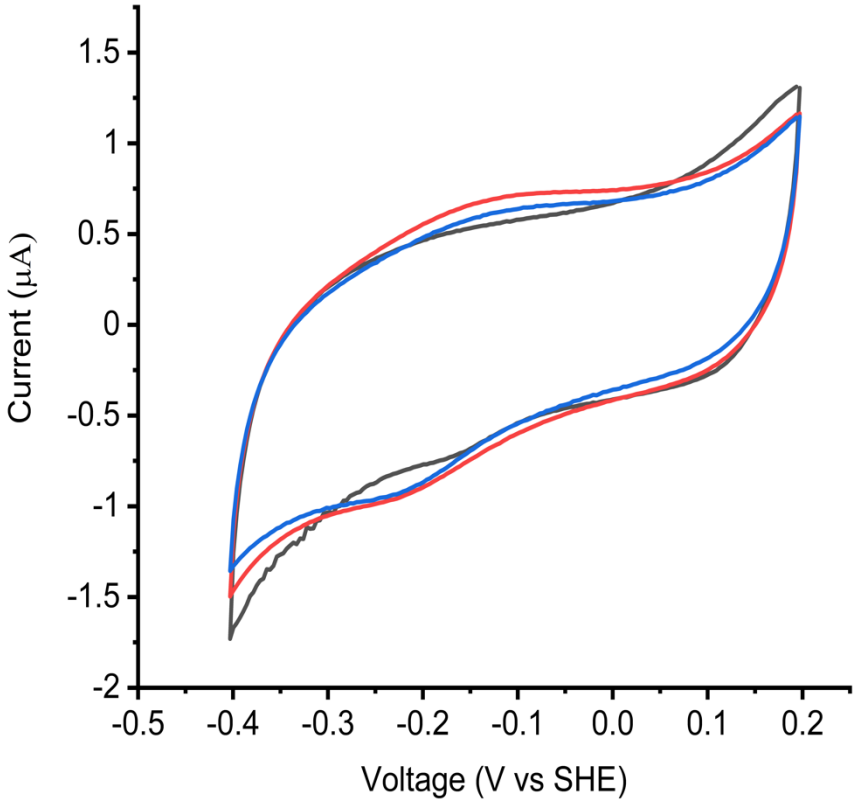

Fig. 2.11. Cyclic voltammograms from β-STCM (red) and β-STCM-Q11 fibers (blue) absorbed on graphite electrode. Experimental conditions are a scan rate of 25 mV s^{-1}, room temperature, 50 mM PBS at pH 7.2, and a potential window of -0.4 V to 0.2 V starting from the reducing side. The black line is buffer measured under the same conditions.

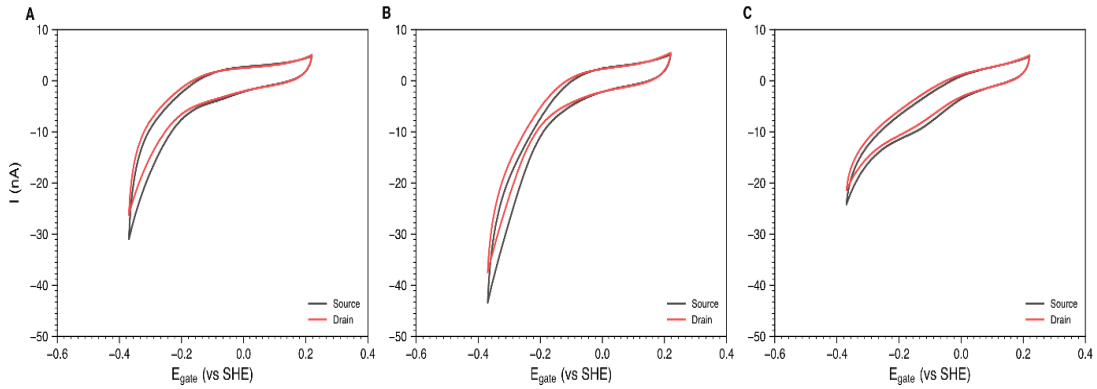

Fig. 2.12. Cyclic voltammograms from electrochemical gating measurement**.** Raw cyclic voltammograms from electrochemical gating measurements with an V_{SD} = 0.02 V of electrodes coated with (A) Q11, (B) β-STCM, and (C), β-STCM-Q11. Black lines represent source electrode, while red lines represent drain electrodes.

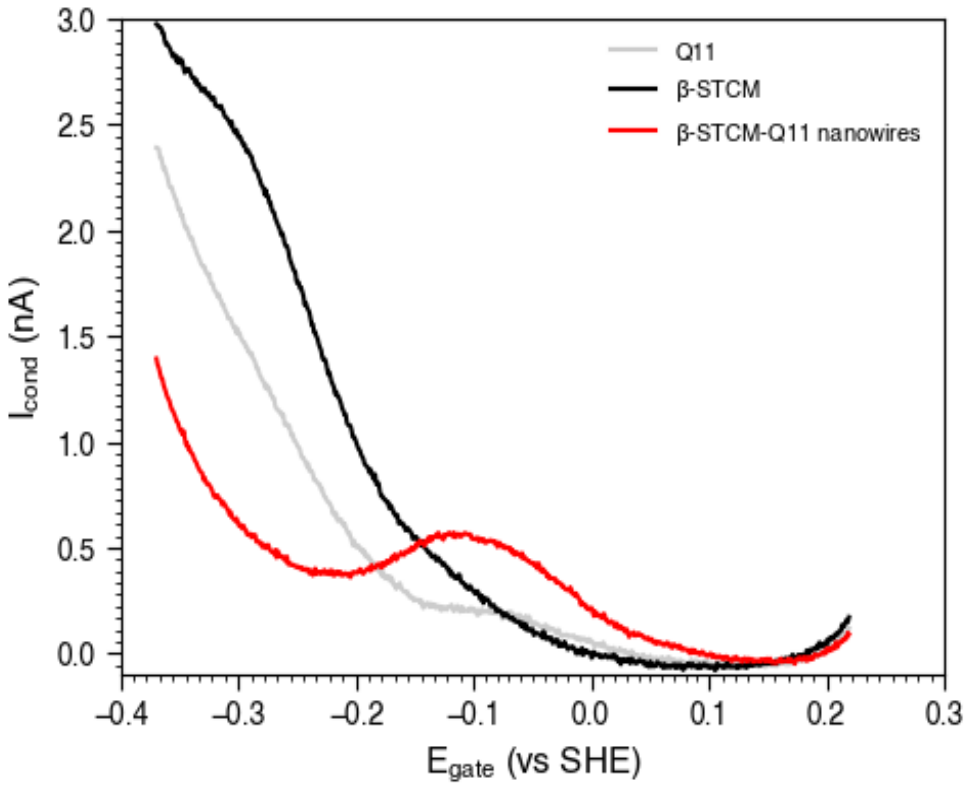

Fig. 2.13. Conduction current (I_{cond}) from electrochemical gating measurements using interdigitated electrodes (IDE) coated with Q11 peptide (grey), β-STCM (black) and β-STCM-Q11 fibers (red). Experimental conditions are a scan rate of 5 mV s^{-1}, room temperature, 50 mM PBS at pH 7.2, and a potential window of scanning the potential (from 230 V_{SHE} to -0.38 V_{SHE}) of both the source (E_S) and drain (E_D) at the same scan rate (5 mV s^{-1}) while maintaining a fixed potential offset ($V_{SD} = E_S - E_D = 0.02$ V) and individually measuring the currents from the source and drain electrodes. Conduction currents were calculated as $I_{cond} = (I_{Drain} - I_{Source}) / 2$ and are reported relative to the average potential of the two electrodes ($E_{Gating} = (E_D\text{-}E_S)/2$).

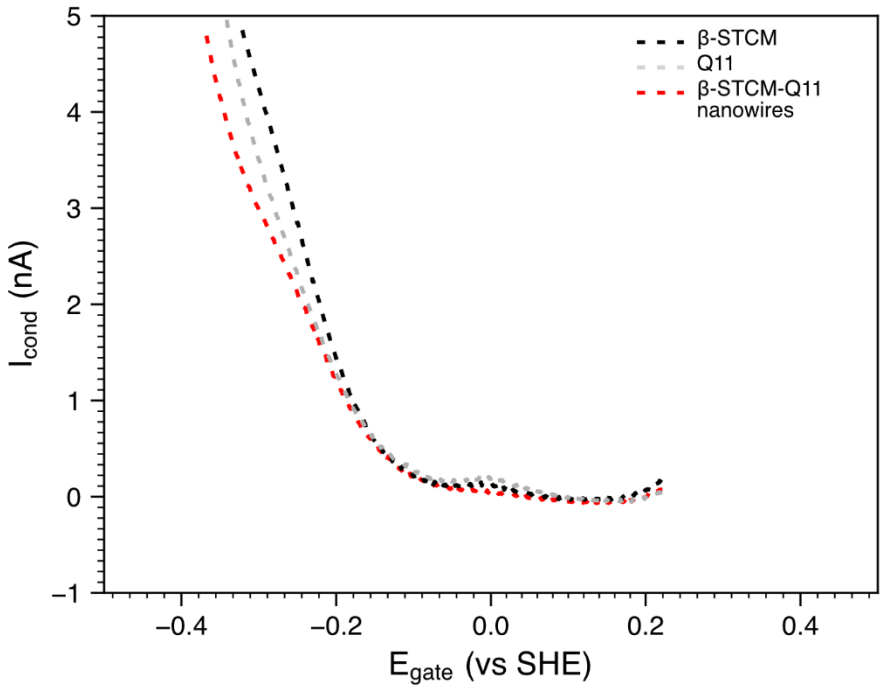

Fig. 2.14. Conduction current (I_{cond}) from electrochemical gating measurements of blank Interdigitated electrodes (IDE) before coating with Q11 peptide, β-STCM and β-STCM-Q11 nanowires. Experimental conditions are a scan rate of 5 mV s^{-1}, room temperature, 50 mM PBS at pH 7.2, and a potential window of scanning the potential (from 230 V_{SHE} to -0.38 V_{SHE}) of both the source (E_S) and drain (E_D) at the same scan rate (5 mV s^{-1}) while maintaining a fixed potential offset ($V_{SD} = E_S - E_D = 0.02$ V) and individually measuring the currents from the source and drain electrodes. Conduction currents were calculated as $I_{cond} = (I_{Drain} - I_{Source}) / 2$ and are reported relative to the average potential of the two electrodes ($E_{Gating} = (E_D\text{-}E_S)/2$)

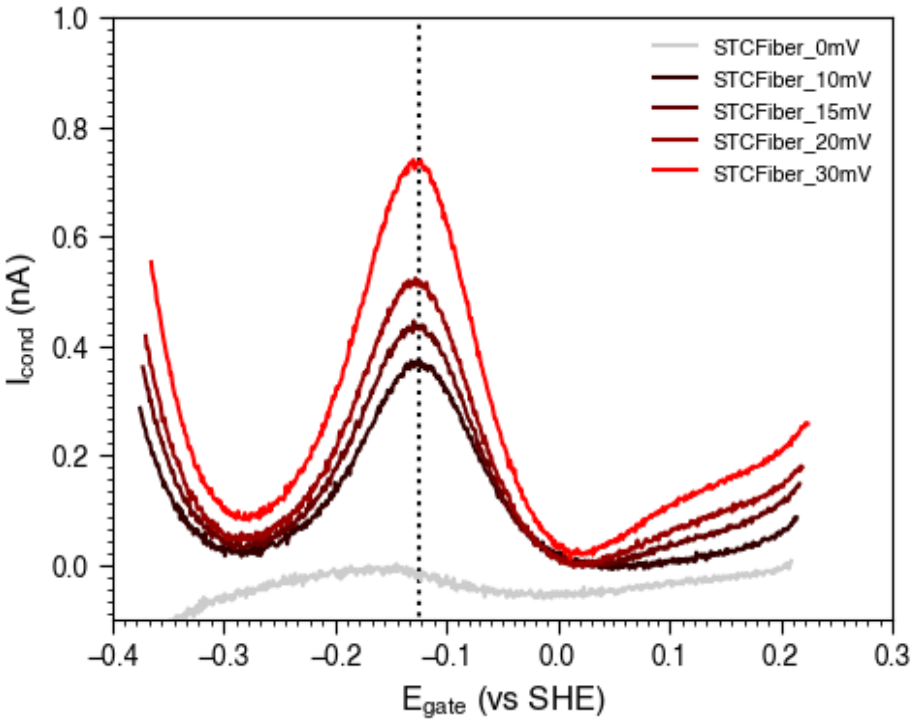

Fig. 2.15. Dependence of β-STCM-Q11 fiber conduction current on gate potential for offset voltages shown in the legend. Experimental conditions are a scan rate of 5 mV s^{-1}, room temperature, 50 mM PBS at pH 7.2, and varying potential window of scanning the potential (from 230 V_{SHE} to -0.38 V_{SHE}) of both the source (E_S) and drain (E_D) at the same scan rate (5 mV s^{-1}) while maintaining a fixed potential offset ($V_{SD} = E_S – E_D = 0.02$ V) and individually measuring the currents from the source and drain electrodes. Conduction currents were calculated as $I_{cond} = (I_{Drain} – I_{Source}) / 2$ and are reported relative to the average potential of the two electrodes ($E_{Gating} = (E_D\text{-}E_S)/2$)

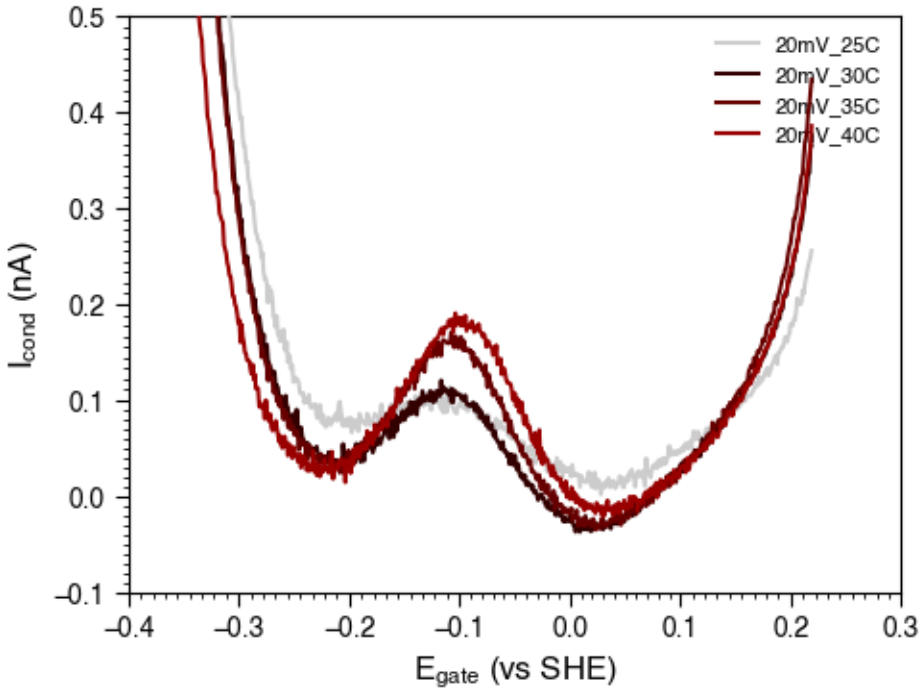

Fig. 2.16. Conduction current of β-STCM-Q11 fibers as a function of gate potential over a range of temperatures from 25 °C to 40 °C. Experimental conditions are a scan rate of 5 mV s^{-1}, room temperature, 50 mM PBS at pH 7.2, and a potential window of scanning the potential (from 230 V_{SHE} to -0.38 V_{SHE}) of both the source (E_S) and drain (E_D) at the same scan rate (5 mV s^{-1}) while maintaining a fixed potential offset ($V_{SD} = E_S – E_D = 0.02$ V) and individually measuring the currents from the source and drain electrodes. Conduction currents were calculated as $I_{cond} = (I_{Drain} – I_{Source}) / 2$ and are reported relative to the average potential of the two electrodes ($E_{Gating} = (E_D\text{-}E_S)/2$)

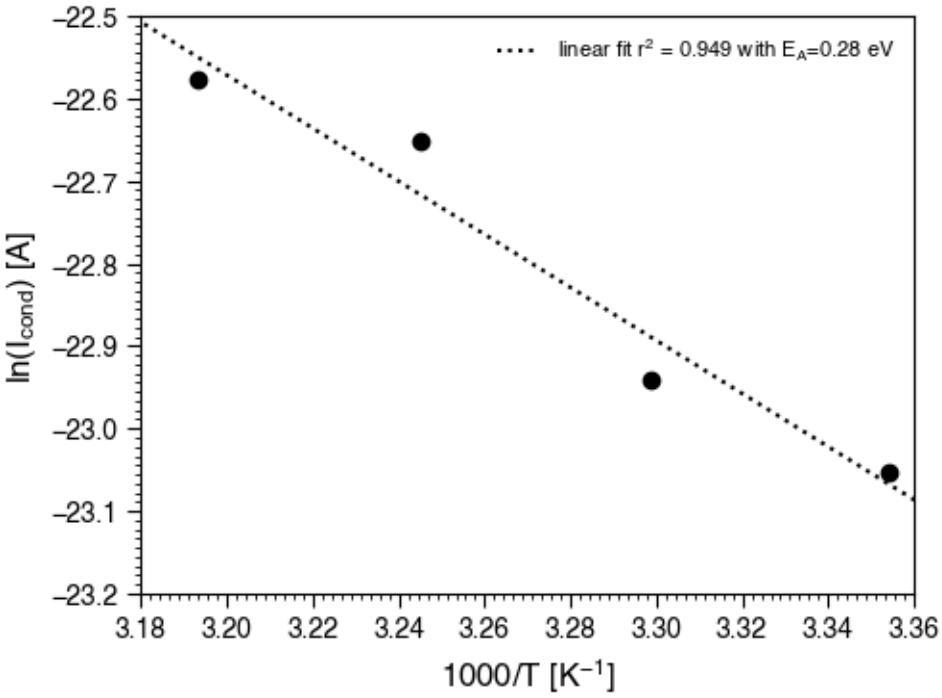

Fig. 2.17. Arrehnius-style plot and line of best fit using peak I_{cond} at $E_{Gate} = E^{0'}$. Analysis yields an activation energy of 0.28 eV.

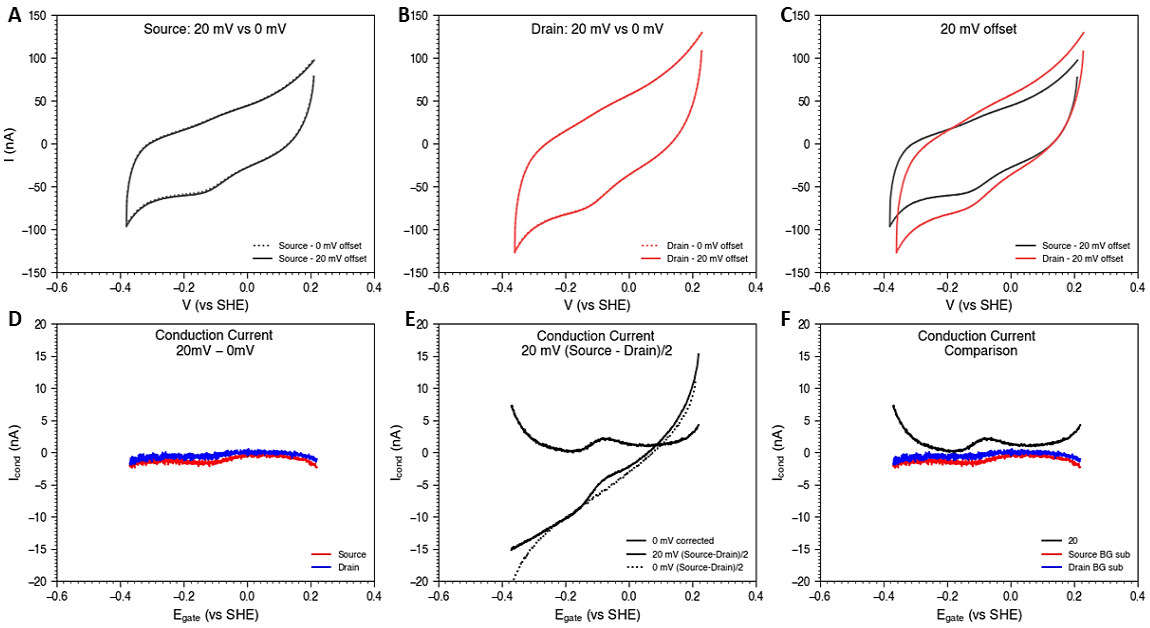

Fig. 2.18. Electrochemical gating measurements of β-STCM-Q11 fibers at 20 mV offset voltage. (A) Cyclic voltammogram of β-STCM-Q11 fibers using the source electrode at 0 mV and 20 mV offset. (B) Cyclic voltammogram of β-STCM-Q11 fibers using the drain electrode at 0 mV and 20 mV offset. (C) An overlay of redox signal of β-STCM-Q11 fibers using source (A) and drain (B) electrodes. (D) Conduction current signal of β-STCM-Q11 fibers plotted against gate potential; conduction current is calculated in terms of 0 mV subtraction from higher offset (20 mV) used. (E) Conduction current signal of β-STCM-Q11 fibers plotted against gate potential; conduction current is calculated in terms of (source-drain)/2 at 20 mV offset. (F) An overlay of conduction current signal of β-STCM-Q11 fibers versus gate potential of (D) and (E). Experimental conditions are a scan rate of 50 mV s^{-1}, room temperature, 50 mM PBS at pH 7.2, and a potential window of -0.4 V to 0.2 V starting from the reducing side.

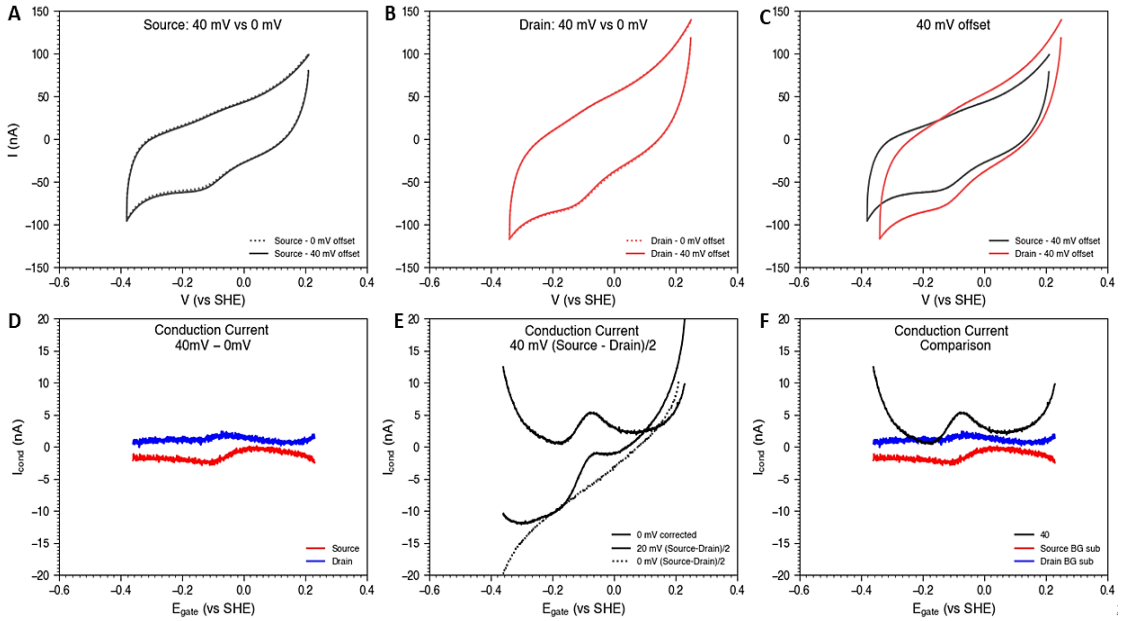

Fig. 2.19. Electrochemical gating measurements of β-STCM-Q11 fibers at 40 mV offset voltage. (A) Cyclic voltammogram of β-STCM-Q11 fibers using the source electrode at 0 mV and 40 mV offset. (B) Cyclic voltammogram of β-STCM-Q11 fibers using the drain electrode at 0 mV and 40 mV offset. (C) An overlay of redox signal of β-STCM-Q11 fibers using source (A) and drain (B) electrodes. (D) Conduction current signal of β-STCM-Q11 fibers plotted against gate potential; conduction current is calculated in terms of 0 mV subtraction from higher offset (40 mV) used. (E) Conduction current signal of β-STCM-Q11 fibers plotted against gate potential; conduction current is calculated in terms of (source-drain)/2 at 40 mV offset. (F) An overlay of conduction current signal of β-STCM-Q11 fibers versus gate potential of (D) and (E). Experimental conditions are a scan rate of 50 mV s^{-1}, room temperature, 50 mM PBS at pH 7.2, and a potential window of -0.4 V to 0.2 V starting from the reducing side.

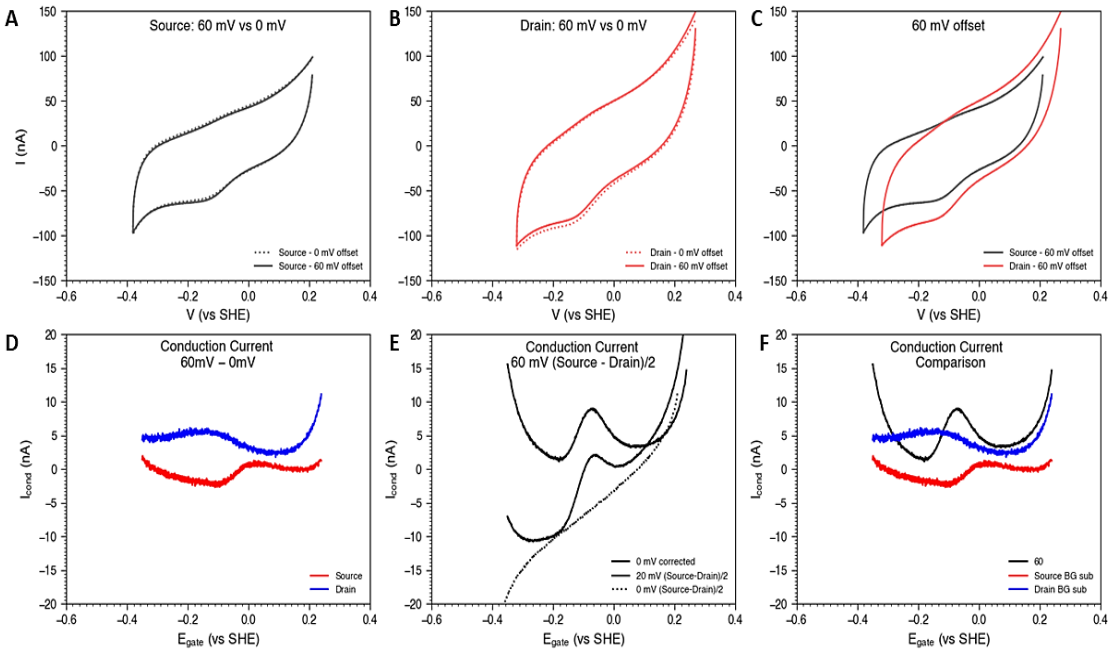

Fig. 2.20. Electrochemical gating measurements of β-STCM-Q11 fibers at 60 mV offset voltage. (A) Cyclic voltammogram of β-STCM-Q11 fibers using the source electrode at 0 mV and 60 mV offset. (B) Cyclic voltammogram of β-STCM-Q11 fibers using the drain electrode at 0 mV and 60 mV offset. (C) An overlay of redox signal of β-STCM-Q11 fibers using source (A) and drain (B) electrodes. (D) Conduction current signal of β-STCM-Q11 fibers plotted against gate potential; conduction current is calculated in terms of 0 mV subtraction from higher offset (60 mV) used. (E) Conduction current signal of β-STCM-Q11 fibers plotted against gate potential; conduction current is calculated in terms of (source-drain)/2 at 60 mV offset. (F) An overlay of conduction current signal of β-STCM-Q11 fiberss versus gate potential of (D) and (E). Experimental conditions are a scan rate of 50 mV s^{-1}, room temperature, 50 mM PBS at pH 7.2, and a potential window of -0.4 V to 0.2 V starting from the reducing side.

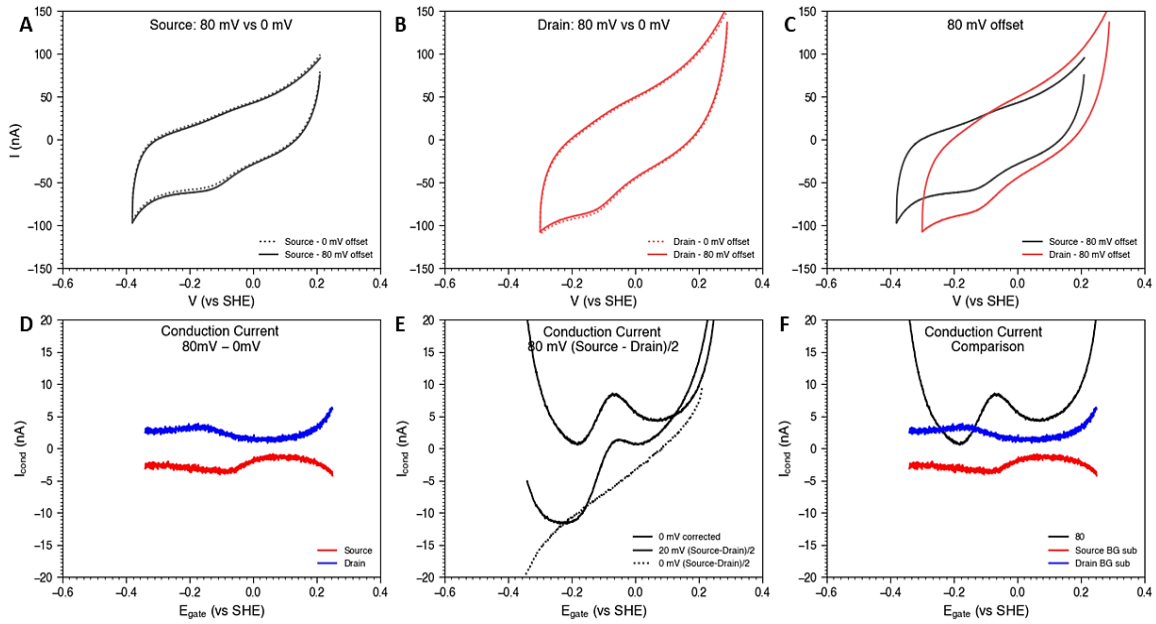

Fig. 2.21. Electrochemical gating measurements of β-STCM-Q11 fibers at 80 mV offset voltage. (A) Cyclic voltammogram of β-STCM-Q11 fibers using the source electrode at 0 mV and 80 mV offset. (B) Cyclic voltammogram of β-STCM-Q11 fibers using the drain electrode at 0 mV and 80 mV offset. (C) An overlay of redox signal of β-STCM-Q11 fibers using source (A) and drain (B) electrodes. (D) Conduction current signal of β-STCM-Q11 fibers plotted against gate potential; conduction current is calculated in terms of 0 mV subtraction from higher offset (80 mV) used. (E) Conduction current signal of β-STCM-Q11 fibers plotted against gate potential; conduction current is calculated in terms of (source-drain)/2 at 80 mV offset. (F) An overlay of conduction current signal of β-STCM-Q11 fibers versus gate potential of (D) and (E). Experimental conditions are a scan rate of 50 mV s^{-1}, room temperature, 50 mM PBS at pH 7.2, and a potential window of -0.4 V to 0.2 V starting from the reducing side.

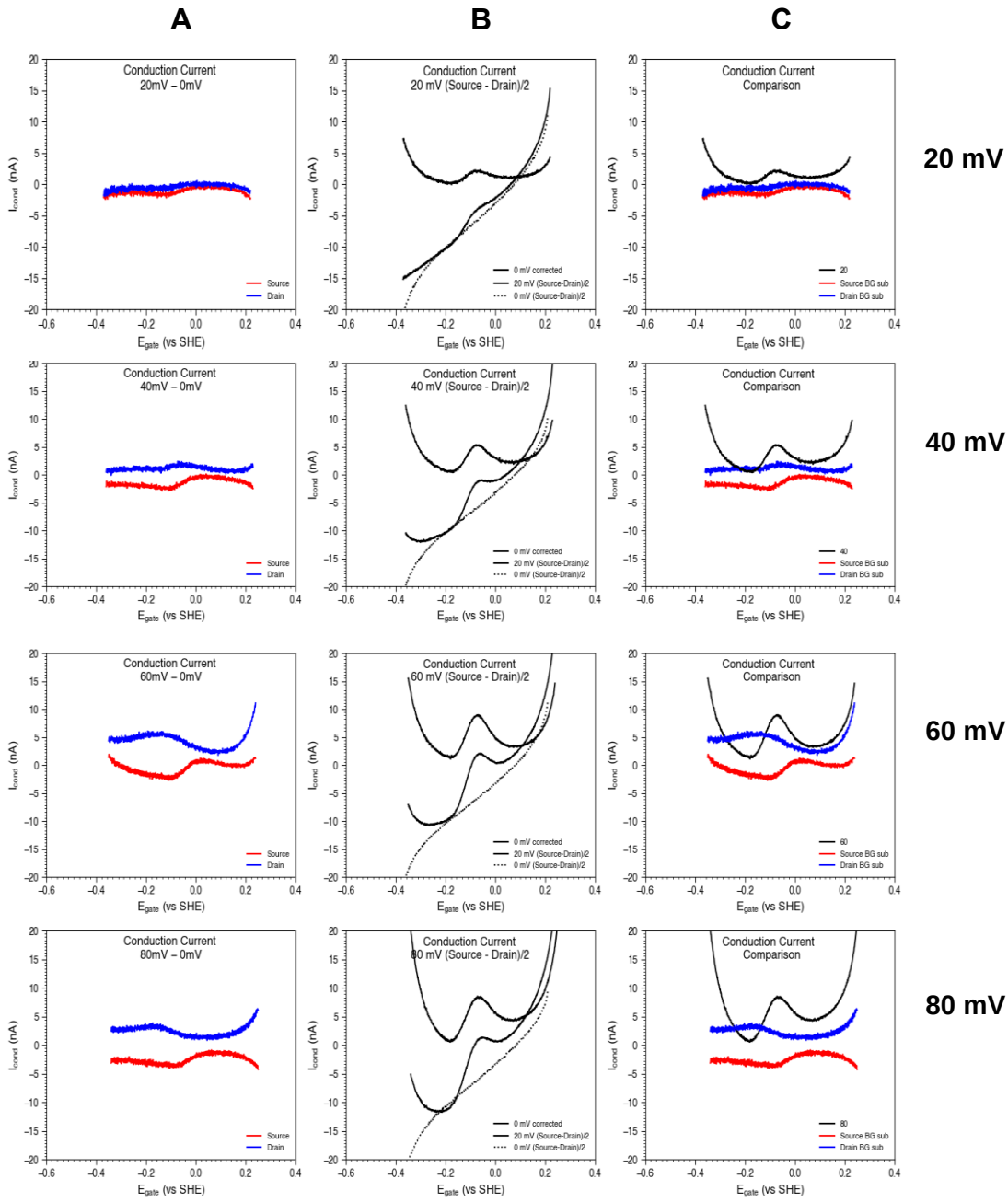

Fig. 2.22. Electrochemical gating measurements of β-STCM-Q11 fibers showing conduction current signal plotted against gate potential at various offset voltages. (A) Conduction current signal of β-STCM-Q11 fibers plotted against gate potential; conduction current is calculated in terms of 0 mV subtraction from higher offset (i.e 20 mV, 40 mV, 60 mV and 80 mV) used. (B) Conduction current signal of β-STCM-Q11 fibers plotted against gate potential; conduction current is calculated in terms of (source-drain)/2 at varying offsets. (C) An overlay of conduction current signal of β-STCM-Q11 nanowires versus gate potential of (A) and (B). Experimental conditions are a scan rate of

50 mV s^{-1}, room temperature, 50 mM PBS at pH 7.2, and a potential window of -0.4 V to 0.2 V starting from the reducing side.

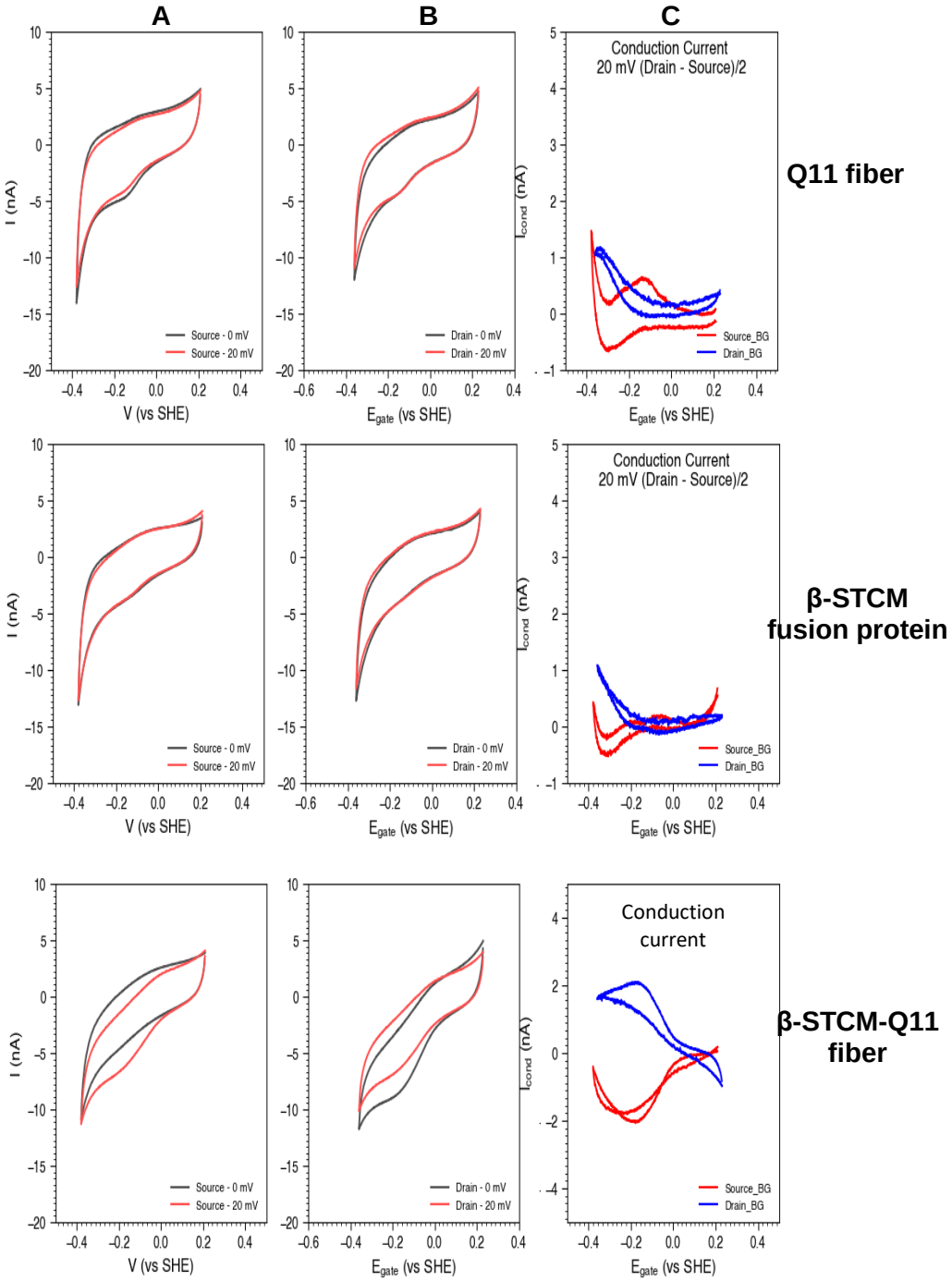

Fig. 2.23. Electrochemical gating measurements of β-STCM-Q11 fibers of source and drain electrode. (A) Cyclic voltammograms of Q11 fibers, β-STCM and β-STCM-Q11 fibers using the source electrode at 0 mV and 20 mV offset. (B) Cyclic voltammograms of Q11 fiber, β-STCM and β-STCM-Q11 fibers using the drain electrode at 0 mV and 20 mV offset (C) Conduction current signal of β-STCM-Q11 fibers plotted against gate

potential; conduction current is calculated in terms of (source-drain)/2 at 20 mV offset. Experimental conditions are a scan rate of 50 mV s^{-1}, room temperature, 50 mM PBS at pH 7.2, and a potential window of -0.4 V to 0.2 V starting from the reducing side.

2.6 References

(1) Reguera, G. Harnessing the power of microbial nanowires. *Microbial Biotechnology* **2018**, *11* (6), 979–994.

(2) Creasey, R. C. G.; Mostert, A. B.; Nguyen, T. A. H.; Virdis, B.; Freguia, S.; Laycock, B. Microbial nanowires – Electron transport and the role of synthetic analogues. *Acta Biomaterialia* **2018**, *69*, 1–30.

(3) Xu, S.; Barrozo, A.; Tender, L. M.; Krylov, A. I.; El-Naggar, M. Y. Multiheme Cytochrome Mediated Redox Conduction through Shewanella oneidensis MR-1 Cells. *Journal of the American Chemical Society* **2018**, *140* (32), 10085–10089.

(4) Clarke, T. A.; Edwards, M. J.; Gates, A. J.; Hall, A.; White, G. F.; Bradley, J.; Reardon, C. L.; Shi, L.; Beliaev, A. S.; Marshall, M. J.; Wang, Z.; Watmough, N. J.; Fredrickson, J. K.; Zachara, J. M.; Butt, J. N.; Richardson, D. J. Structure of a bacterial cell surface decaheme electron conduit. *Proceedings of the National Academy of Sciences of the United States of America* **2011**, *108* (23), 9384–9389.

(5) Gross, B. J.; El-Naggar, M. Y. A combined electrochemical and optical trapping platform for measuring single cell respiration rates at electrode interfaces. *Review of Scientific Instruments* **2015**, *86* (064301), 1–8.

(6) El-Naggar, M. Y.; Wanger, G.; Leung, K. M.; Yuzvinsky, T. D.; Southam, G.; Yang, J.; Lau, W. M.; Nealson, K. H.; Gorby, Y. A. Electrical transport along bacterial nanowires from *Shewanella oneidensis* MR-1. *Proceedings of the National Academy of Sciences of the United States of America* **2010**, *107* (42), 18127–18131.

(7) Malvankar, N. S.; Lovley, D. R. Microbial nanowires: A new paradigm for biological electron transfer and bioelectronics. *ChemSusChem* **2012**, *5* (6), 1039–1046.

(8) Wang, F.; Gu, Y.; O'Brien, J. P.; Yi, S. M.; Yalcin, S. E.; Srikanth, V.; Shen, C.; Vu, D.; Ing, N. L.; Hochbaum, A. I.; Egelman, E. H.; Malvankar, N. S. Structure of Microbial Nanowires Reveals Stacked Hemes that Transport Electrons over Micrometers. *Cell.* **2019**, *177*, 361–369.

(9) Subramanian, P.; Pirbadian, S.; El-Naggar, M. Y.; Jensen, G. J. Ultrastructure of *Shewanella oneidensis* MR-1 nanowires revealed by electron cryotomography. *Proceedings of the National Academy of Sciences of the United States of America* **2018**, *115* (14), E3246–E3255.

(10) Terao, T. Hopping electron model with geometrical frustration: Kinetic Monte Carlo simulations. *European Physical Journal B* **2016**, *89* (10), 209–216.

(11) Otter, R.; Besenius, P. Supramolecular assembly of functional peptide–polymer conjugates. *Organic & Biomolecular Chemistry* **2019**, *17* (28), 6719–6734.

(12) Altamura, L.; Horvath, C.; Rengaraj, S.; Rongier, A.; Elouarzaki, K.; Gondran, C.;

Maçon, A. L. B.; Vendrely, C.; Bouchiat, V.; Fontecave, M.; Mariolle, D.; Rannou, P.; Le Goff, A.; Duraffourg, N.; Holzinger, M.; Forge, V. A synthetic redox biofilm made from metalloprotein-prion domain chimera nanowires. *Nature Chemistry* **2017**, *9* (2), 157–163.

(13) Creasey, R. C. G.; Mostert, A. B.; Solemanifar, A.; Nguyen, T. A. H.; Virdis, B.; Freguia, S.; Laycock, B. Biomimetic Peptide Nanowires Designed for Conductivity. *ACS Omega* **2019**, *4* (1), 1748–1756.

(14) Hudalla, G. A.; Sun, T.; Gasiorowski, J. Z.; Han, H.; Tian, Y. F.; Chong, A. S.; Collier, J. H. Gradated assembly of multiple proteins into supramolecular nanomaterials. *Nature Materials* **2014**, *13* (8), 829–836.

(15) Bradford, M. M. A rapid and sensitive method for the quantitation of microgram quantities of protein utilizing the principle of protein-dye binding. *Analytical Biochemistry* **1976**, *72*, 248–254.

(16) Chantell, C. A.; Onaiyekan, M. A.; Menakuru, M. Fast conventional Fmoc solid-phase peptide synthesis: A comparative study of different activators. *Journal of Peptide Science* **2012**, *18* (2), 88–91.

(17) Amblard, M.; Fehrentz, J.; Martinez, J.; Subra, G. Modern Solid Phase Peptide Synthesis: Methods and Protocols of Modern Solid Phase Peptide Synthesis. *Molecular Biotechnology* **2006**, *33*, 240–255.

(18) Bard, A. J.; Abruiia, H. D.; Chidsey, C. E.; Faulkner, L. R.; Feldberg, S. W.; Melroy, O.; Murray, R. W.; Hill, C.; Carolina, N.; Porter, M. D.; Soriaga, M. P.; White, H. S. The Electrode/Electrolyte Interface-A status Report. *Society* **1993**, *97*, 7147–7173.

(19) Tsapin, A. I.; Nealson, K. H.; Meyers, T.; Cusanovich, M. A.; Van Beuumen, J.; Crosby, L. D.; Feinberg, B. A.; Zhang, C. Purification and properties of a low-redox-potential tetraheme cytochrome c3 from Shewanella putrefaciens. *Journal of Bacteriology* **1996**, *178* (21), 6386–6388.

(20) Wada, K.; Hase, T.; Tokunaga, H.; Matsubara, H. Amino Acid Sequence of *Spirulina platensis* Ferredoxin: A Far Divergency of Blue-Green Algal Ferredoxins. *FEBS Letters* **1975**, *55* (1), 102–104.

(21) Blauch, D. N.; Savéant, J. M. Dynamics of Electron Hopping in Assemblies of Redox Centers. Percolation and Diffusion. *Journal of the American Chemical Society* **1992**, *114* (9), 3323–3332.

(22) Ing, N. L.; Spencer, R. K.; Luong, S. H.; Nguyen, H. D.; Hochbaum, A. I. Electronic Conductivity in Biomimetic α-Helical Peptide Nanofibers and Gels. *ACS Nano* **2018**, *12* (3), 2652–2661.

(23) Chen, Y. X.; Ing, N. L.; Wang, F.; Xu, D.; Sloan, N. B.; Lam, N. T.; Winter, D. L.; Egelman, E. H.; Hochbaum, A. I.; Hochbaum, A. I.; Hochbaum, A. I.; Clark, D.

S.; Clark, D. S.; Glover, D. J. Structural Determination of a Filamentous Chaperone to Fabricate Electronically Conductive Metalloprotein Nanowires. *ACS Nano* **2020**, *14* (6), 6559–6569.

(24) Sun, Y. L.; Montz, B. J.; Selhorst, R.; Tang, H. Y.; Zhu, J.; Nevin, K. P.; Woodard, T. L.; Ribbe, A. E.; Russell, T. P.; Nonnenmann, S. S.; Lovley, D. R.; Emrick, T.; Russell, T. P. Solvent-Induced Assembly of Microbial Protein Nanowires into Superstructured Bundles. *Biomacromolecules* **2021**, *22* (3), 1305–1311.

(25) Cosert, K. M.; Castro-Forero, A.; Steidl, R. J.; Worden, R. M.; Reguera, G. Bottom-up fabrication of protein nanowires via controlled self-assembly of recombinant *Geobacter* pilins. *mBio* **2019**, *10* (6), 1–15.

(26) Lovley, D. R. Electrically conductive pili: Biological function and potential applications in electronics. *Current Opinion in Electrochemistry* **2017**, *4* (1), 190–198.

(27) Dahl, P. J.; Yi, S. M.; Gu, Y.; Acharya, A.; Shipps, C.; Neu, J.; Patrick O'Brien, J.; Morzan, U. N.; Chaudhuri, S.; Guberman-Pfeffer, M. J.; Vu, D.; Yalcin, S. E.; Batista, V. S.; Malvankar, N. S. A 300-fold conductivity increase in microbial cytochrome nanowires due to temperature-induced restructuring of hydrogen bonding networks. *Science Advances* **2022**, *8* (19).

(28) Yalcin, S. E.; O'Brien, J. P.; Gu, Y.; Reiss, K.; Yi, S. M.; Jain, R.; Srikanth, V.; Dahl, P. J.; Huynh, W.; Vu, D.; Acharya, A.; Chaudhuri, S.; Varga, T.; Batista, V. S.; Malvankar, N. S. Electric field stimulates production of highly conductive microbial OmcZ nanowires. *Nature Chemical Biology* **2020**, *16* (10), 1136–1142.

(29) Amdursky, N.; Wang, X.; Meredith, P.; Riley, D. J.; Payne, D. J.; Bradley, D. D. C.; Stevens, M. M. Electron Hopping Across Hemin-Doped Serum Albumin Mats on Centimeter-Length Scales. *Advanced Materials* **2017**, *29* (27).

(30) Arslan, E.; Schulz, H.; Zufferey, R.; Künzler, P.; Thöny-Meyer, L. Overproduction of the Bradyrhizobium japonicum c-type cytochrome subunits of the cbb3 oxidase in Escherichia coli. *Biochemical and Biophysical Research Communications* **1998**, *251* (3), 744–747.

(31) Pechsrichuang, P.; Songsiriritthigul, C.; Haltrich, D.; Roytrakul, S.; Namvijtr, P.; Bonaparte, N.; Yamabhai, M. OmpA signal peptide leads to heterogenous secretion of B. subtilis chitosanase enzyme from E. coli expression system. *SpringerPlus* **2016**, *5* (1).

(32) Studier, F. W.; Moffat, B. A. Selective expression of cloned genes directed by T7 RNA polymerase. *J. Mol. Biol.* **1986**, *189*, 113–130.

Chapter 3

3. CATCH Protein Nanowires: Second Generation Assembly of Small Tetraheme Cytochrome from *Shewanella oneidensis*

J. N. Nwachukwu[1], M. A. Thirumurthy[1], G. Galiyan[1], J. T. Atkinson[2], M. Y. El-Naggar[2] and A. K. Jones[1]

[1]School of Molecular Sciences, Arizona State University, Tempe, AZ, USA
[2]Department of Physics and Astronomy, University of Southern California, Los Angeles, CA, USA

3.1 Abstract

Exoelectrogenic organisms transfer electrons from their internal quinone pool to extracellular acceptors over μm-scale distances through appendages known as "biological nanowires". These structures have been variously described as cytochrome-rich membrane extensions or pili, and the components and mechanisms of this long-range electron transfer remain largely unknown. In fact, current physical understanding of biological electron transfer is only sufficient to describe electron movement on the nm scale. Here, we describe a proteinaceous, supramolecular model for ultralong-range biological electron transfer. This supramolecular structure is based on a pair of charge complementary, self-assembling peptides. A small redox protein from *Shewanella oneidensis*, a model exoelectrogen, is fused to one of the peptide components, and the other carries an N-terminal modification facilitating interaction with electrodes and electrical characterization. Assembled nanowires have dimensions of 530 nm x16.4 nm x 11 nm. Electrochemical measurements show the nanowires retain the native reduction potential of their constituent STC, and results from electrochemical gating suggest electrical conductivity occurs along the length of these structures.

3.2 Introduction

As a result of the ability to transfer electrons from metabolism to extracellular materials, exoelectrogens like *Shewanella oneidensis* and *Geobacter sulfurreducens* have been exploited in biosensors, bioelectronics, microbial fuel cells and wastewater treatment.[1] Extracellular electron transfer has been associated with hair-like appendages known as microbial nanowires whose mechanism and mode of electron transfer is largely unknown.[2] Two distinct mechanisms have been proposed: electron tunneling through

structures with extensive π-π stacking and electron hopping through closely stacked redox active centers.

Exoelectrogens often express significant numbers of multiheme cytochromes, lending credence to the idea that microbial nanowires consist of ordered chains of hemes. Cryo-electron microscopy of *Geobacter* nanowires has shown they contain OmcS cytochromes stacked within heme distances typically in the range 3Å-6Å[3]. Similarly, recent work by Malvankar and coworkers has suggested that nanowires containing OmcZs, another multiheme cytochrome, are 1000 times more conductive than OmcS nanowires.[4] Furthermore, work in the Jones group has shown that OmcZs binds and reduces riboflavin, suggesting that this soluble shuttle may play a role in extracellular electron transfer, i.e. transfer of electrons may rely on multiple mechanisms.[5] Part of the challenge of defining the mechanisms of long-range electron transfer in exoelectrogens is a dearth of model systems for biological electron transfer beyond the scale of one to two protein molecules. Tunable models with defined μm-scale structures built from biomolecules are essential to discriminating between the two conflicting conductivity hypotheses.

Several supramolecular systems have been described as models for long-range electron transfer. For example, Altamura and coworkers[6] have fused of a self-assembling prion domain with a rubredoxin, a small electron transferring [FeS] protein, creating films that transfer electrons over a μm and can be used as mediators between an electrode and the enzyme laccase for oxygen reduction. Inspired by the π-stacking hypothesis, Creasey and coworkers have reported assembly of an aromatic-rich peptide into a

hydrogel. However, the conductivity of their structure is very poor and clearly not high enough to be a functional model of microbial nanowires.[7] Xu and coworkers achieved minimal conductivity by assembling nanotube networks using an enzyme.[8] However, all these models leave open questions of conductivity or mechanism or fail to achieve conductivity on the scale observed in natural systems.

A number of self-assembling peptide systems, often based on prion domains, have been reported that can carry protein cargo into supramolecular structures via simple, covalent fusions.[6] Some offer systematic tunability of composition that will be essential in defining the minimum structural requirements for μm-scale biological electron transfer.[9] Previously, our lab constructed a two-component bacterial nanowire model based on the small tetraheme cytochrome (STC) from *Shewanella oneidensis* and a self-assembling peptide known as Q11 (Fig. 2.1). The protein was tagged with a β-tail peptide to allow incorporation into fibers and serve as a redox-active component in an otherwise insulating structure. STC was chosen for this work because it is small, i.e. has a high redox cofactor to protein ratio, and has been extensively characterized structurally, electrochemically and spectroscopically. Furthermore, it is one of the most common types of small electron transfer proteins in biology.[10] Although these fibers have length-wise conductivity that is likely a result of hopping through the STC, the interprotein distance is not tunable, limiting the ability to probe its effect on conductivity.

To create a more tunable structure, herein we describe construction of a second generation redox-active fiber using the CATCH (Co-assembly Tags based on Charge complementarity) system. As shown in Fig. 3.1., CATCH employs a pair of oppositely

charged peptides to form 600-1000 nm long supramolecular nanostructures. Importantly, it can incorporate precise amounts of proteins into nanofibers with fixed distances.[11] CATCH peptides form β-sheet nanofibers only when combined and, as a result of electrostatic repulsion, are not capable of independent assembly. In this work, the CATCH (-) (anionic peptide) sequence has been fused to the C-terminus of the small tetraheme cytochrome (STC) from *S. oneidensis*, and the fusion protein is microbially expressed. The CATCH(+) (cationic peptide) is synthesized by solid phase synthesis. The CATCH petides are combined *in vitro* to assemble nanostructures. Electrochemical gating experiments show that the fibers are conductive and the mechanism likely relies on hopping through the cytochromes.

3.3 Methods

3.3.1 Heterologous Expression and Purification of Small Tetraheme Cytochrome tagged with CATCH peptide fusion protein (STC-CATCH(-)) in *E. coli*

A plasmid coding for the S87C point mutant of *S. onediensis* STC[12] with a strep tag on the C-terminus and CATCH(-) tag on N-terminus (CATCH(-)-STC(S87C)) and a Ampicillin resistance gene was produced by DNA 2.0. The pD434-SR plasmid (Table 2) was transformed with a plasmid encoding the *ccm* (cytochrome c maturation) operon[13] (with chloramphenicol resistance gene) into *E. coli* using the heat shock method.[14] Cells were aerobically grown in LB (Luria-Bertani) media at 37 °C with shaking at 7 x g. Kanamycin and chloramphenicol were added to a final concentration of 50 mg ml^{-1} and 35 mg ml^{-1}, respectively. Cells were induced at an optical density (OD_{600}) of 0.6 with 0.2 mM isopropyl β-D-1-thiogalactopyranoside (IPTG) in the culture. After induction, cells were grown for

18 h and harvested by centrifugation at 4 °C, 16,128 x g for 1 h. Soluble extracts were obtained by sonication (4 cycles at 60% amplitude) in 20 mM PBS (1 L of Phosphate buffer solution contains 2.25 g of Na_2HPO_4, 0.88 g of NaH_2PO_4 and 2.92 g of NaCl) buffer at pH 6.2, before adding 28 μM lysozyme, 100 mM EDTA, 0.0002 U/μL DNase I (Thermo Fisher Scientific), and 2 tablets of Pierce protease inhibitor with gentle stirring for 90 min at 4 °C. The resulting extract was cleared by centrifugation (16,128 x g) for 1 h, and the supernatant collected. The supernatant was dialyzed (>10kDa MWCO) against 20 mM PBS (Phosphate Buffered Saline) pH 6.2 at 4 °C overnight. Dialyzed supernatant containing the fusion protein was applied to a 40 mL DEAE equilibrated with 20 mM PBS at pH 6.2 at room temperature. The column was washed with 5 column volumes each of increasingly concentrated PBS (50 mM, 100 mM, 150 mM, 200 mM, 250 mM, 300 mM, 350 mM and 400 mM) at pH 6.2. Fractions containing fusion protein were reddish brown and eluted at 400 mM; they were pooled and concentrated with amicon ultra-centrifugal filters (2 kDa MWCO) before applying to a 30 ml S*trep*-Tactin column equilibrated with 20 mM PBS at pH 6.2 at room temperature. The column was washed with 100 ml of 20 mM PBS at pH 6.2, and then the fusion protein eluted with 20 mM PBS containing 5 mM desthiobiotin. Partially purified protein was then re-purified over the S*trep*-Tactin column a second time.[15]

3.3.2 Protein Characterization

Protein concentrations were determined via Bradford assay with a Thermo Scientific Varioskan Lux Mode multimode microplate reader using Bovine serum albumin (BSA) as standard.[16] Sodium Dodecyl Sulphate Polyacrylamide Gel Electrophoresis (SDS-PAGE)

was used to evaluate protein purity which was visualized in Coomassie blue and confirmed using heme stain.[17]

3.3.3 CATCH(+) and CATCH(-) synthesis and purification

Two peptides, CATCH(+) and CATCH(-) (Ac-QQKFKFKFKQQ-NH_2 and Ac-EQEFEFEFEQE-NH_2) were synthesized on a PS3 peptide synthesizer using HCTU (O-(1H-6-chlorobenzotriazole-1-yl)-1,1,3,3-tetramethyluronium hexafluorophosphate) (165 mg) as activator on a 0.1 mmol scale on rink amide (100-150 mesh, 149 mg).[18] Peptides were N-acetylated with 5% acetic anhydride in pyridine and cleaved from the resin using 2.5% H_2O, 2.5% tri-isopropyl silane (TIPS) and 6% TFA. They were then dried under nitrogen, precipitated with cold diethyl ether, and left at -20 ˚C overnight.[19] The diethyl ether was filtered off and peptide redissolved in water after which the resin was removed using spin columns (60 μm pore size, 1 mL column volume) while peptides were lyophilized. The lyophilized impure peptides were purified using HPLC. Dissolved impure peptides were injected into the HPLC with initial gradient elution of solvent A (5% Acetonitrile, 95% water and 0.1% TFA) for 10 min and gradient elution of solvent B (5% water, 95% Acetonitrile and 0.1% TFA) from 0%-40% over 60 min while monitoring absorbance at 220 nm. The desired peptide elutes for CATCH(+) and CATCH(-) were collected. Fractions from several injections were pooled, frozen and lyophilized. The purity and molecular weight of each peptide (CATCH(+) at 1525.8720 Da and CATCH(-) at 1552.834 Da) was verified by MALDI-TOF (20 Hz and linear mode at 25,000 V) using sinapinic acid as the matrix.

3.3.4 Synthesis of [Py-CATCH(+)]

CATCH(+) was modified at the N-terminus by capping the synthesized CATCH(+) peptide with 0.1 mmol of 1-pyrene butyric acid (20 mg) on the peptide synthesizer with the same coupling reagents as for adding an amino acid. Synthesis proceeds as usual except with an additional vial containing pyrene-1-butyric acid with HCTU (O-(1H-6-chlorobenzotriazole-1-yl)-1,1,3,3-tetramethyluronium hexafluorophosphate) (165 mg) as activator on a 0.1 mmol scale on rink amide (100-150 mesh, 149 mg).[18] Modified peptide was cleaved directly from the resin (no acetylation) using 2.5% H_2O, 2.5% tri-isopropyl silane (TIPS) and 6% TFA. They were then dried under nitrogen, precipitated with cold diethyl ether, and left at -20 $^{\circ}$C overnight.[19] The diethyl ether was filtered off and peptide redissolved in water after which the resin was removed using spin columns (60 μm pore size, 1 mL column volume) while peptides were lyophilized. The lyophilized modified peptides were purified using HPLC. Dissolved impure peptides were injected into the HPLC with initial gradient elution of solvent A (5% Acetonitrile, 95% water and 0.1% TFA) for 10 min and gradient elution of solvent B (5% water, 95% Acetonitrile and 0.1% TFA) from 0%-40% over 60 min while monitoring absorbance at 220 nm. The desired peptide elutes at 47-51 min. Fractions from several injections were pooled, frozen and lyophilized. The purity and molecular weight of the peptide Py(CATCH(+) at 1754 was verified by MALDI-TOF (20 Hz and linear mode at 25,000 V) using sinapinic acid as the matrix.

3.3.5 Nanowire CATCH(+/-) preparation

CATCH(+/-) peptides were mixed at a 1:1 ratio at final concentration of 5 μg ml^{-1} in PBS (pH 7.2) for each component peptide. The mixture was allowed to stand overnight at room temperature.

3.3.6 Nanowire STC-CATCH preparation

Purified CATCH(+) peptide, CATCH(-) peptide and STC-CATCH(-) fusion protein were mixed at a ratio of 1000:500:1 at concentration of 10 mM: 5 mM: 10 μM. All components were dissolved in PBS (pH 7.2) before mixing overnight at room temperature.

3.3.7 Transmission Electron Microscopy (TEM)

Glow discharged 400 Mesh copper grids (FCF-400) were first floated on top of 30 μl of PBS containing CATCH peptides or STC-CATCH nanowires and wiped on the sides with chemwipes after each float. These grids were further floated in water and 2% uranyl acetate as negative stain. Samples on mesh grid were analyzed using the TEM Philip CM 200.

3.3.8 Atomic Force Microscopy

Nanowire solution (5 μL) were absorbed on mica (1.5 cm x 1.5 cm, Ted Pella, Inc.) and placed in a humidifier for 30 min after which surface was cleaved and cleaned with ultrapure water. After evaporation, samples were immediately imaged using the tapping mode Tap300Al-G probes (with 40 N/m force constant, 300 kHz resonant frequency, Budget Sensors). Images were processed using Gwyddion software.

3.3.9 Fluorescence Microscopy

STC-CATCH fibers (5 µL) were spotted on the poly-lysine coated slides. Primary monoclonal mouse anti-STC antibody were added to the slide surface and then incubated overnight at 4 °C. Primary monoclonal mouse anti-STC was filtered off and washed (3 times) using PBS at 7.2 and 0.1% tween 20 (PBST). Secondary antibody alexa-fluor 647 was added and incubated for 1 h at room temperature followed by washed and rinsing using PBST and PBS, respectively. Sample were imaged with Leica TCS SP5 AOBS Spectral Confocal System after covering the sample with a coverslip.

3.3.10 Electrochemical studies of purified STC-CATCH fusion protein and STC-CATCH Nanowire

Electrochemical experiments were conducted in a glovebox under nitrogen in a three-electrode electrochemical cell using an PGSTAT 12 Autolab Potentiostat. The electrodes consist of a custom-made 1.2 mm diameter graphite (Minteq International pyrogenic group) working electrode, Ag/AgCl reference, and a platinum wire counter electrode. The working electrode was polished with 120 grit sandpaper and alumina (5µm size followed by 0.3 µm and 0.05 µm sizes of BASi Polishing Alumina Powder) before each use. Protein films were formed by spotting STC-CATCH fusion protein or STC-CATCH fibers (10 µl, 250 mM) on the graphite electrode surface and allowing them to dry. The electrode potential was cycled between +0.2 V and –0.4 V vs SHE at a scan rate of 25 mV s^{-1} in 20 mM Phosphate buffer at pH 7.2 with 100 mM NaCl as supporting electrolyte. All potentials are corrected to the standard hydrogen electrode (SHE) according to the equation $E_{SHE} = E_{Ag/AgCl}$ +197 mV at 25 °C.[20]

3.3.11 Conductivity studies of STC-CATCH Nanowire

Electrochemical gating measurements were made using a bipotentiostat configuration consisting of two Reference 600 potentiostats (Gamry Inc.) connected with a communication cable and used in a MultEchem configuration. Linked cyclic voltammetry scans were performed using a custom script provided by the manufacturer. Interdigitated electrodes consisting of interdigitated 5 µM wide Au bands with 5 µM gaps (ED-IDE3-Au, Micrux Technologies) were washed by sonication in isopropanol for 15 min, followed by milliQ water for 15 min, and were dried in a stream of N_2 gas. Immediately following washing, IDEs were transferred into an anerobic chamber with a 5% H_2/95% N_2 atmosphere (Bactron). An electrochemical cell was constructed by placing the IDE at the bottom of the cell using an AIO-cell (ED-AIO-CELL, Micrux Technologies) IDE interface with a 400 µL well placed on top of the IDE using a batch PEEK cell (BC-PEEK-5,0, Micrux Technologies). 400 µL of buffer (20 mM PBS, 50 mM NaCl, pH 7.2) was added to the cell and a platinum counter electrode and a reference electrode (3M KCl Ag/AgCl) were inserted into the top of the well. The potentiostats were connected to shared reference and counter electrodes and the each of the two interdigitated electrodes were connected to individual potentiostat using the AIO wiring harness. All potentials are reported relative to the Standard Hydrogen Electrode (+0.210 V vs Ag/AgCl in 3M KCl).

Gating measurements were performed by simultaneously scanning the potential (from 230 mV to -0.38 mV) of both the source (E_S) and drain (E_D) at the same scan rate (5 mV s^{-1}) while maintaining a fixed potential offset ($V_{SD} = E_S - E_D = 0.02$ V) and

individually measuring the currents from the source and drain electrodes. As previously described El-Naggar and coworker,[21] conduction currents were calculated as $I_{cond} = (I_{Drain} – I_{Source}) / 2$ and reported relative to the average potential of the two electodes ($E_{Gating} = (E_D\text{-}E_S)/2$). For each electrode, gating measurements were made in buffer alone were made for each electrode. The electrochemical cell was deconstructed and 10 µL of protein solution was spotted onto the IDE and allowed to incubate at 25C for 30 min. Excess protein was removed and washed three times with 10 uL of buffer. The cell was reconstructed and 400 µL of buffer was added and gating measurements were repeated. Protein solutions contained the following; 10 mM CATCH(+) peptide, 5 mM CATCH(-) peptide and 10 µM STC-CATCH fusion protein; nanowires assembled at a ratio of 10 mM CATCH(+): 5 mM 5 mM CATCH(-): 10 µM STC-CATCH nanowire.

3.4 Results

3.4.1 Heterologous expression, purification and characterization of STC(S87C)-CATCH(-) fusion protein

The STC(S87C)-CATCH sequence is a variant of STC (S87C) modified at the N-terminus with a sequence encoding the CATCH(-) component of the CATCH system to facilitate assembly of fibers in the presence of CATCH(+) (Fig. 3.1). Additionally, at the C-terminus, the protein contains an OmpA signal peptide which gets cleaved on site while facilitating periplasmic expression and a *strep*-tag (Fig. 3.2). These tags were added to facilitate purification. The STC(S87C)-CATCH protein, hereafter referred to as STC-CATCH, was purified to homogeneity as described in the method section. As shown in Fig. 3.3, SDS-PAGE was used to visualize and confirm the purity of the STC-CATCH

protein at various stages of the purification. A single prominent band (Fig. 3.3, lane 13) is observed at the expected 21 kDa molecular weight, confirming the purity of STC(S87C)-CATCH(-).

UV-vis spectroscopy was used to estimate the purity of STC(S87C)-CATCH. As shown in Fig. 3.4, UV-vis spectra from purified STC(S87C)-CATCH(-) have absorbance maxima at 408 nm and 534 nm characteristic of cytochromes.[12] The A_{408}/A_{280} ratio for purified STC(S87C)-CATCH(-) is 1.18, indicating an excellent preparation that is not as pure as the β-STC described in Chapter 2.

3.4.2 Synthesis and purification of CATCH peptides

The CATCH(-) and CATCH(+) peptides were synthesized using FMOC-based peptide synthesis and purified via reversed-phase HPLC as described in the methods, and Fig. 3.5 and 3.6 show MALDI mass spectra demonstrating their purity. To use pyrene to anchor assembled fibers onto carbon substrates, CATCH(+) modified with pyrene at the N-terminus [py-CATCH(+)] was also synthesized and purified in Fig. 3.7.

3.4.3 Assembly and Structural characterization of STC-CATCH fibers

Assembly of CATCH fibers was demonstrated by mixing CATCH(+) and CATCH(-) in a 1:1 ratio (3 μM each) at room temperature and incubating. Fig. 3.8 shows transmission electron microscopy images showing that the resulting fibers are 500 nm long and 15.2 nm wide.

While two-component mixtures of CATCH(+) peptide and STC-CATCH fusion protein do not form fibers, protein-containing STC(S87C)-CATCH fibers do form from the three component mixture containing CATCH(+) peptide, CATCH(-) peptide and

STC-CATCH fusion protein in the molar ratio of 1000:500:1 (10 mM: 5 mM: 10 μM) after overnight incubation at 4 ºC. As shown in Fig. 3.9a, TEM images show that STC(S87C)-CATCH fibers have average length and width dimensions of 530 nm and 16.4 nm, respectively. AFM images show an average height dimension of 11 nm with a strip-like wire morphology and a semi-rough surface (Fig. 3.9b). Since CATCH(+) and CATCH(-) peptides can assemble fibrous structures without protein, fluorescence microscopy was used to demonstrate the presence of STC protein in the fibers. Assembled fibers were specifically coated with primary monoclonal mouse anti-STC antibody followed by an anti-mouse antibody conjugated with Alexa Fluoro 647 (with several successive washing). The images shown in Fig. 3.9c confirm the presence of STC protein along the lengths of the assembled fiber.

3.4.4 Redox characterization of STC(S87C)-CATCH fusion protein and STC(S87C)-CATCH fibers

Fig. 3.10 shows cyclic voltammograms from STC(S87C)-CATCH fusion protein and STC(S87C)-CATCH fibers These redox signals have reversible peaks with oxidative peaks at -98 mV_{SHE} and reductive peak at 245 mV_{SHE}; with an average reduction potential at -173 mV_{SHE} and a peak separation of -149 mV_{SHE}. These values match those of wild-type STC protein indicating that assembly into the CATCH fiber does not affect the redox function of the protein.

3.4.5 Charge transport measurements of STC(S87C)-CATCH fibers

Electrochemical gating measurements were used to determine the charge transport properties of STC-CATCH fibers.[22,23,24] Assembled CATCH peptide fibers, STC-

CATCH fibers, or soluble STC-CATCH fusion protein were deposited onto Au interdigitated electrodes with a 5 μm gap and source-drain measurements were performed using a bipotentiostat as outlined in Chapter 2. In these experiments, samples are deposited onto Au interdigitated electrodes with a 5 μm gap. A fixed bias voltage is applied between source and drain electrodes relative to a global gate electrode (Ag/AgCl reference electrode), Mathematically, $E_{SD} = E_D - E_S$ in which E_{SD} is source-to-drain bias voltage; E_D is the potential of the drain electrode relative to the global reference; and E_S is the potential of the source electrode relative to the global reference. If the material spanning the gaps between the electrodes is conductive, signals are observed, and the source-drain current, I_{cond}, can be calculated by $(I_D - I_S)/2$.[21]

As shown in Fig. 3.11, cyclic voltammograms of STC-CATCH fibers show peaks corresponding to STC. Conduction current calculations show that STC-CATCH nanowire films conduct current between the source and the drain at a similar potential to the STC reduction potential of -171 mV_{SHE}. This contrasts with films of the CATCH peptide fibers without STC-CATCH or the STC-CATCH fusion protein without CATCH peptide for which limited conduction in the same potential region is observed. These results indicate that supramolecular assembly of STC-CATCH fusion proteins into fibers enhances charge transport relative to STC-CATCH fusion protein alone and that that charge transport is dependent on the presence of STC in the nanowires.

3.5 Discussion

Chapter 2 described assembly of conductive nanofibers based on STC and the Q11 self-assembling peptide system. Because β-tail/Q11 is basically self-assembly of a

single peptide, it offers limited opportunities for tuning supramolecular structures. As shown in Fig. 3.1, the CATCH system, on the other hand, relies on two distinct, charge complementary peptides for self-assembly, forcing an alternating structure. Thus, it offers the chance to tune the distance between protein monomers by varying the concentration of protein present in the fiber assembly mixture.

This work shows that a three component systems consisting of CATCH (-) (anionic peptide) sequence fused to the C-terminus of the small tetraheme cytochrome (STC) from *S. oneidensis*, and the CATCH (+) and CATCH (-) peptides assembles in vitro into conductive nanofibers. The redox properties of STC in these structures match those of soluble, wild-type protein, indicated that assembly into the fiber does not affect functionality of the protein. Electrochemical gating results suggest that the fiber conductivity is likely mediated by an electron hopping mechanism between the hemes of the STC monomers.

This work provides a starting point for synthetic engineers in the construction of living circuits or self-repairing circuitry.

Table 3.1 *E. coli* Strains and Plasmids used in this Study

Strain or Plasmid	Relevant characteristics or sequence	Source or reference
Plasmids		
pEC86 (p*ccm*)[a]	6.5 kb PCR fragment including *ccmABCDEFGH* with Cat^r	[25]
pD434 (p*stccatch*)[b]	*Stc-catch* with C terminal OmpA signal peptide[26], Amp^r, CATCH tag fused to STC gene	This study
E. coli strains		
BL21(DE3)	fhuA2 [lon] ompT gal (λDE3) [dcm] ΔhsdS λDE3 = λ sBamHIo ΔEcoRI-B int::(lacI::PlacUV5::T7 gene1) i21 Δnin5	New England Biolabs[27]

[a]The pEC86 plasmid was provided by D. Kramer's lab (Michigan State University); [b]The pD434 plasmid was prepared by DNA 2.0.

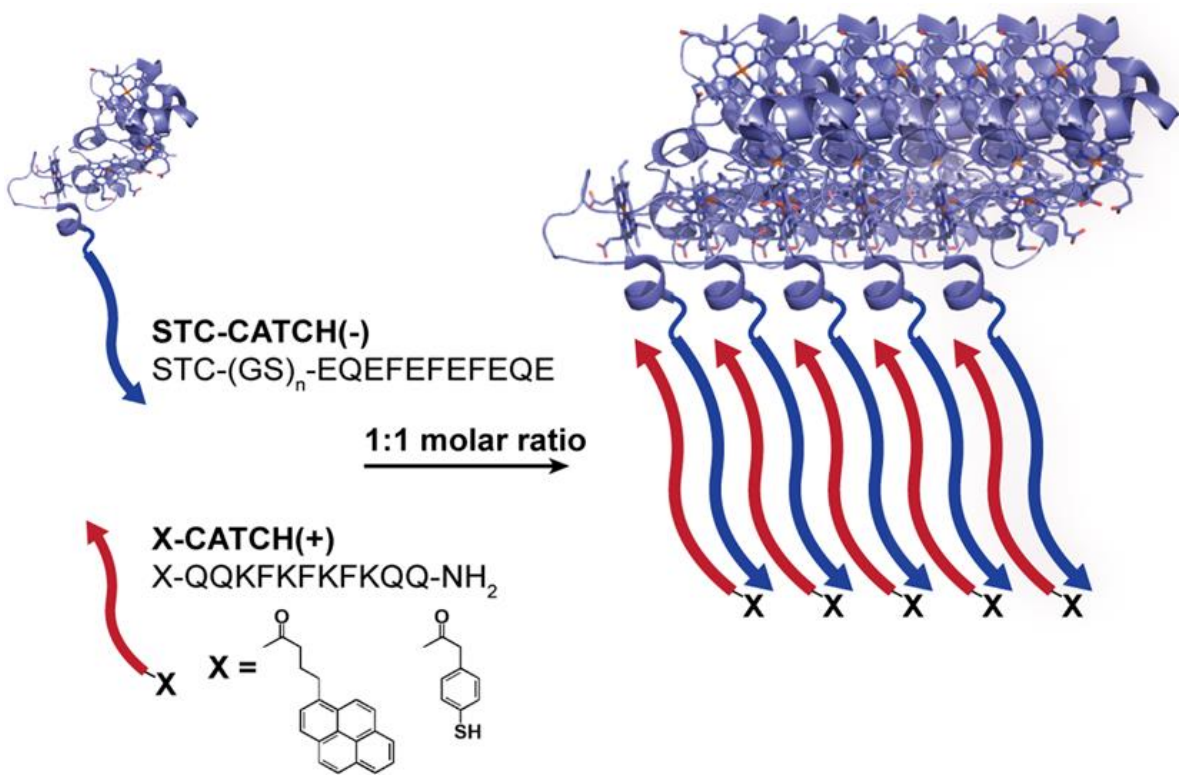

Fig. 3.1. Schematic representation showing ideal molecular-recognition based assembly of STC into protein fiber using CATCH peptides. The STC-CATCH fiber is made of a CATCH(-) peptide tagged with STCM fusion protein which self-assembles into fibers on addition of its CATCH(+) peptide in optimal conditions.

MSKKLLSVLFGASLAALALSPTAFAAWSHPQFEK
GGGSGGGSGGSAWSHPQFEKGSGGGGSGGGG
SGGG ADQKLSDFHAESGGCESCHKDGTPSADG
AFEFAQCQSCHGKLSEMDAVHKPHDGNLVCADC
HAVHDMNVGQKPTCESCHDDGRTSASVLKKGSG
GGGSGGGGSGGGEQEFEFEFEQE

Fig. 3.2. STC-CATCH sequence expressed in this work. The signal peptide (red) is followed by the *strep* tag (blue). The twin strep tag (blue) is attached to the STC (green) by the glycine-serine linker (black) which also links the CATCH(-) tag (gold). To facilitate interaction with gold, the 87th amino acid of the STC has been mutated from serine to cysteine.

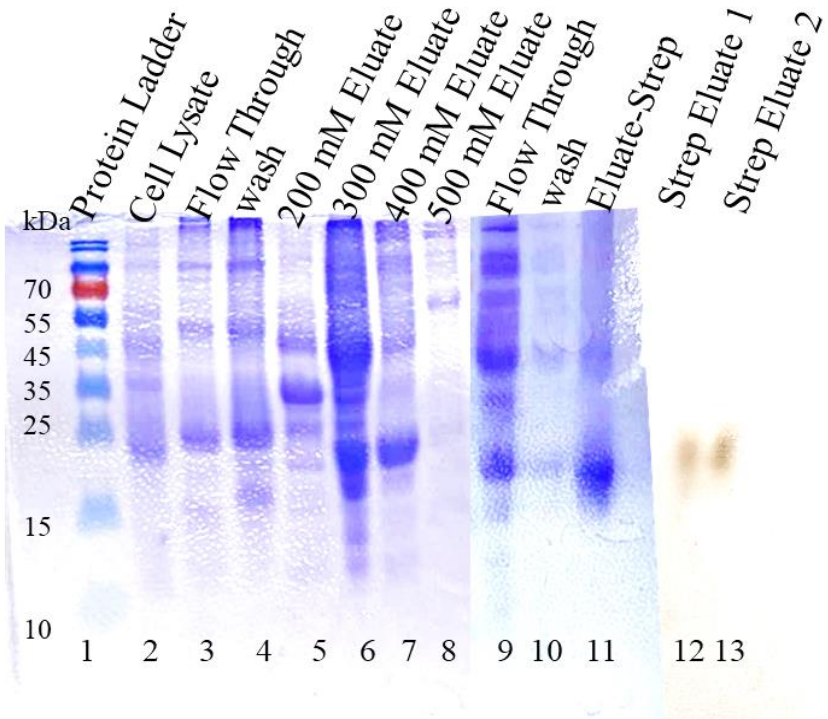

Fig. 3.3. SDS-PAGE visualized with Coomassie blue staining of various stages of STC-CATCH(-) purification. Lane 1: Protein standard (10 to 180 kDa); Lane 2: Crude cell lysate; Lane 3: Flow through from DEAE column; Lane 4: Wash from DEAE column; Lane 5: 200 mM NaCl eluate from DEAE column; Lane 6: 300 mM NaCl eluate from DEAE column; Lane 7: 400 mM NaCl eluate from DEAE column; Lane 8: 500 mM NaCl eluate from DEAE column; Lane 9: Flow through from Streptactin column; Lane 10: Wash from Streptactin column; Lane 11: Eluate from Streptactin column; Lane 12: Eluate from Streptactin column (Heme-stained); Lane 13: Eluate from Streptactin column (Heme-stained). STC-CATCH(-) is the prominent band at 21 kDa in lanes 6, 7, 9, 11, 12 and 13 (btw 15 and 25 kDa). In each lane, 10 µl (566 µg/ml) of the designated sample was applied to the gel.

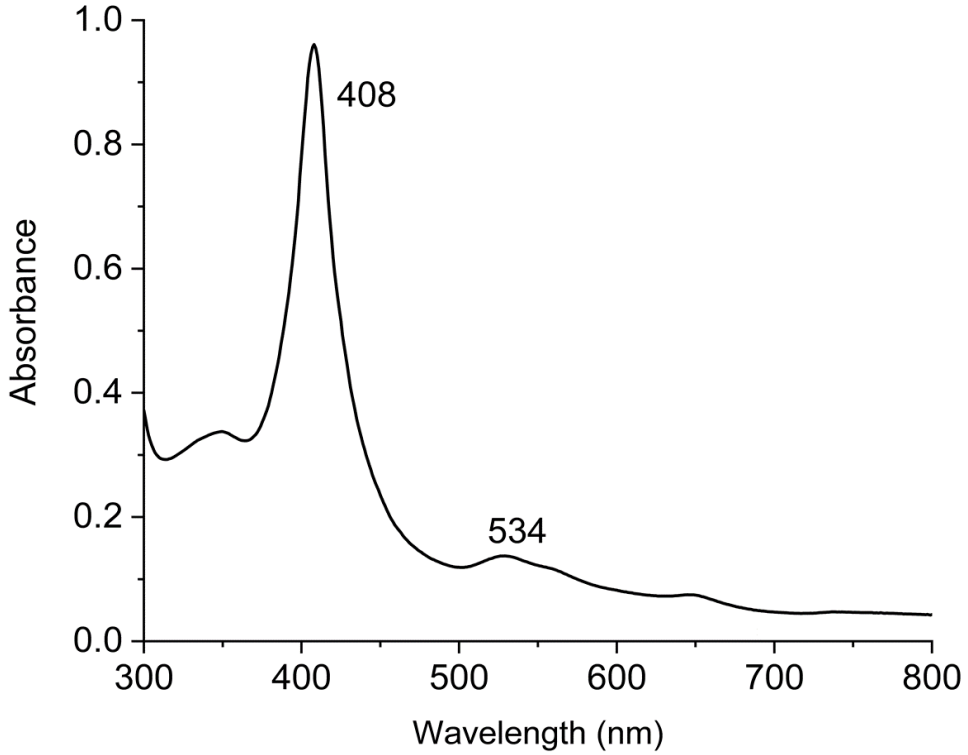

Fig. 3.4. UV-vis Spectrum of purified STC-CATCH(-) fusion protein. The UV-vis spectrum shows a Soret peak at 408 nm and a broad β-band peak at 534 nm which is characteristic of multiheme cytochrome.

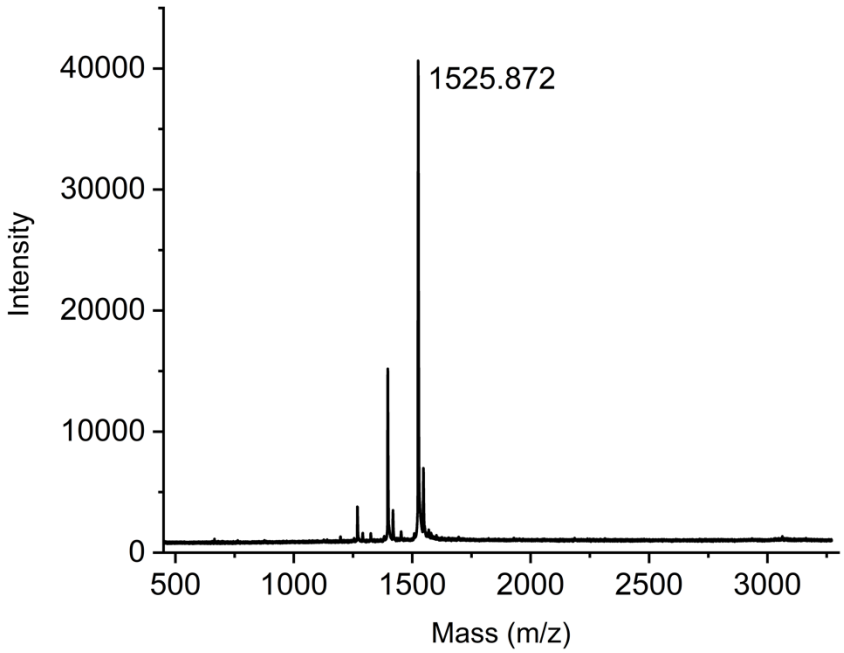

Fig. 3.5. MALDI-MS of purified CATCH(+) peptide. Scans were averaged over 25 shots. Observed m/z is 1525.8720 Da and calculated as 1524.846 Da.

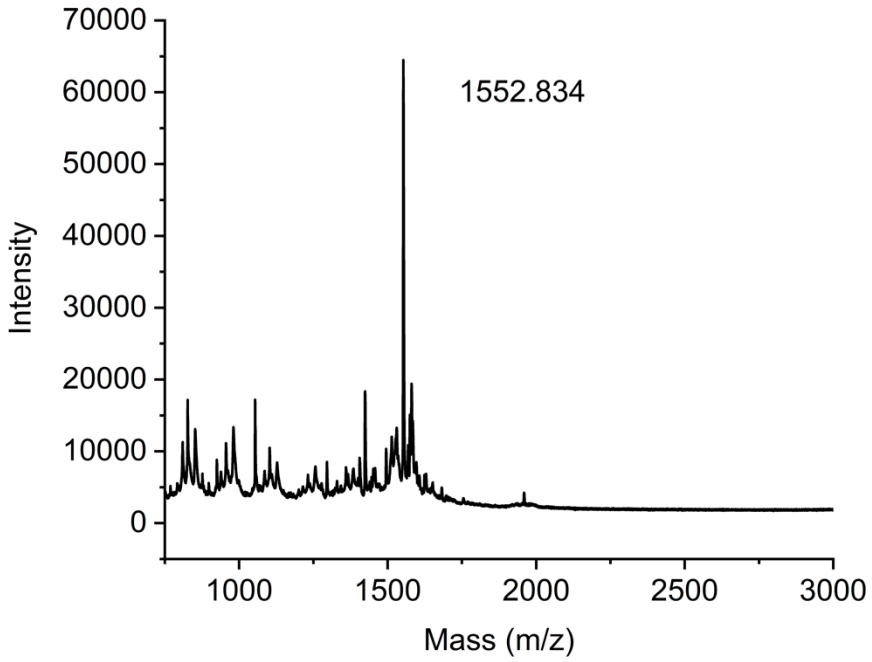

Fig. 3.6. MALDI-MS of purified CATCH(-) peptide. Scans were averaged over 25 shots. Observed m/z is 1552.834 Da and calculated as 1553 Da.

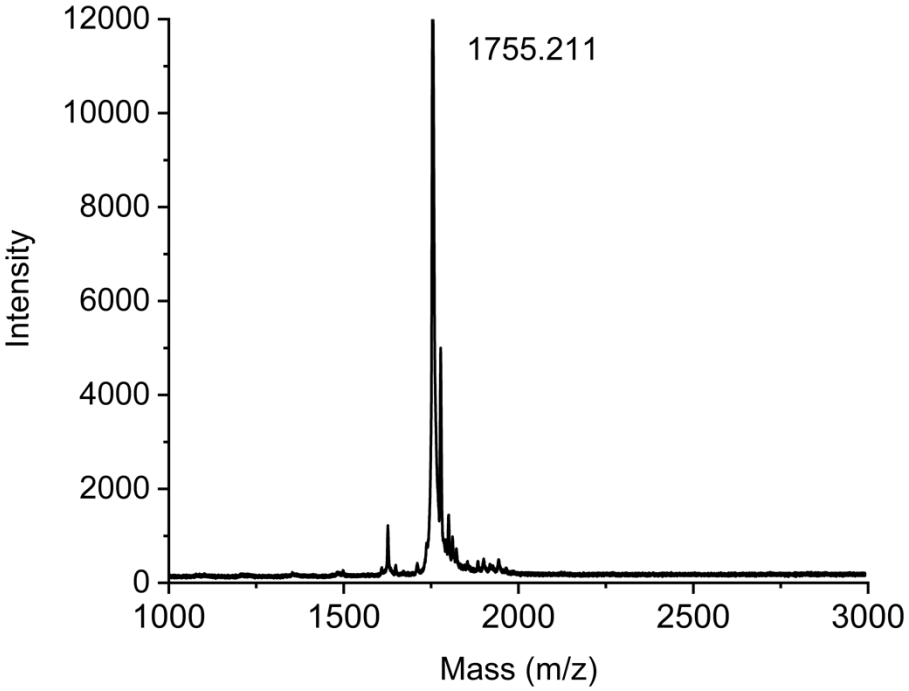

Fig. 3.7. MALDI-MS of purified [Py-CATCH (+)] peptide. Scans were averaged over 25 shots. Observed m/z is 1755.211 Da and calculated as 1754 Da.

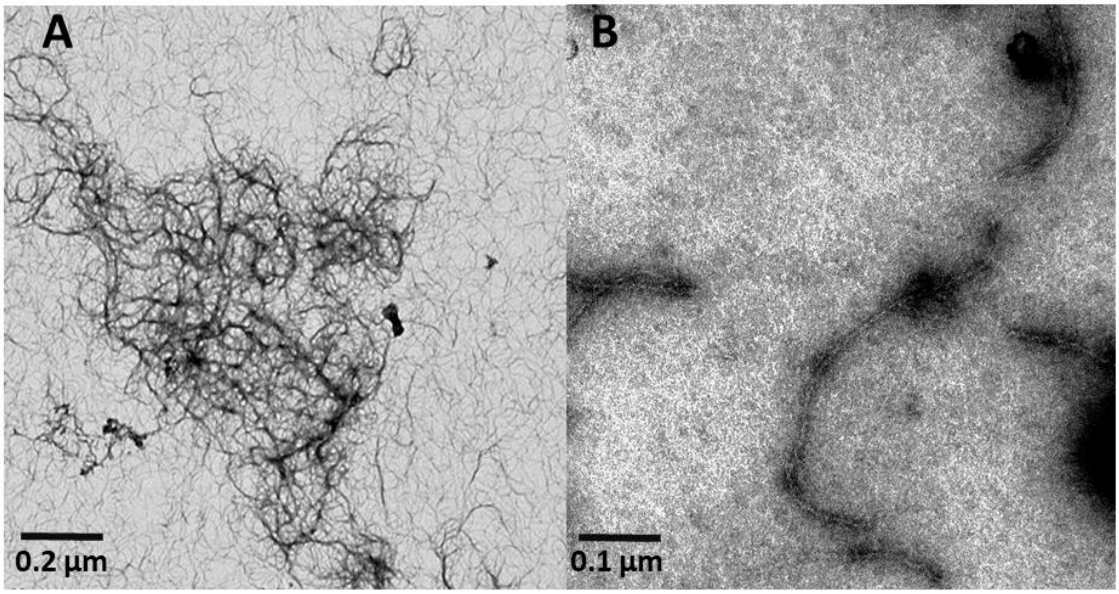

Fig. 3.8. TEM images of CATCH(+/-) peptides assembled at equimolar concentration (3 µM). (a) Image of assembled fibers in clusters; (b) Image of single fibril.

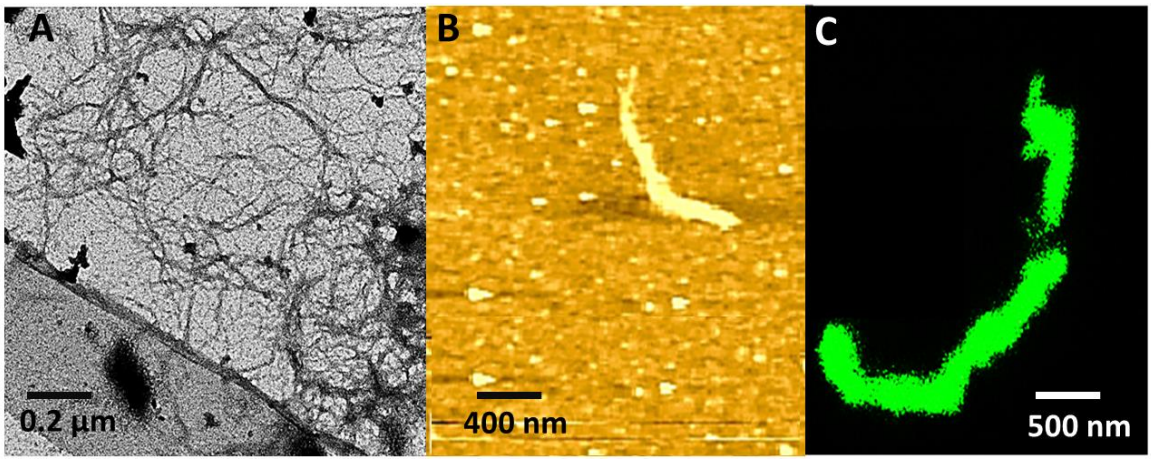

Fig. 3.9. Structural Characterization of STC-CATCH fibers. (A) TEM image showing self-assembled STC-CATCH fibers. Fibers were assembled in the ratio of 1000:500:1 for CATCH(+) peptide, CATCH(-) peptide and STC-CATCH fusion protein, respectively. (B) AFM of STC-CATCH fibers. (C) Fluorescence microscopy of STC-CATCH fiber.

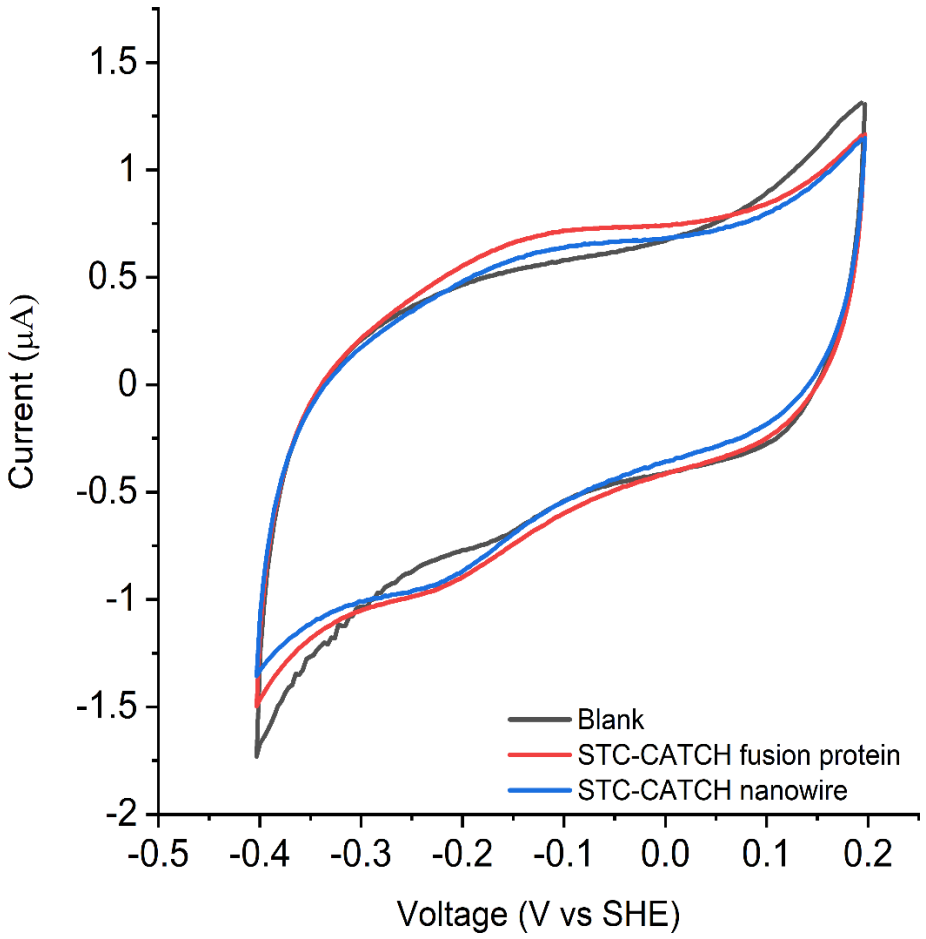

Fig. 3.10. Cyclic voltammograms from STC-CATCH fusion protein (red) and STC-CATCH fibers (blue) absorbed on graphite electrode. Experimental conditions are a scan rate of 25 mV s^{-1}, room temperature, 50 mM PBS at pH 7.2, and a potential window of -0.4 V to 0.2 V starting from the reducing side. The black line is the electrode without exposure to sample.

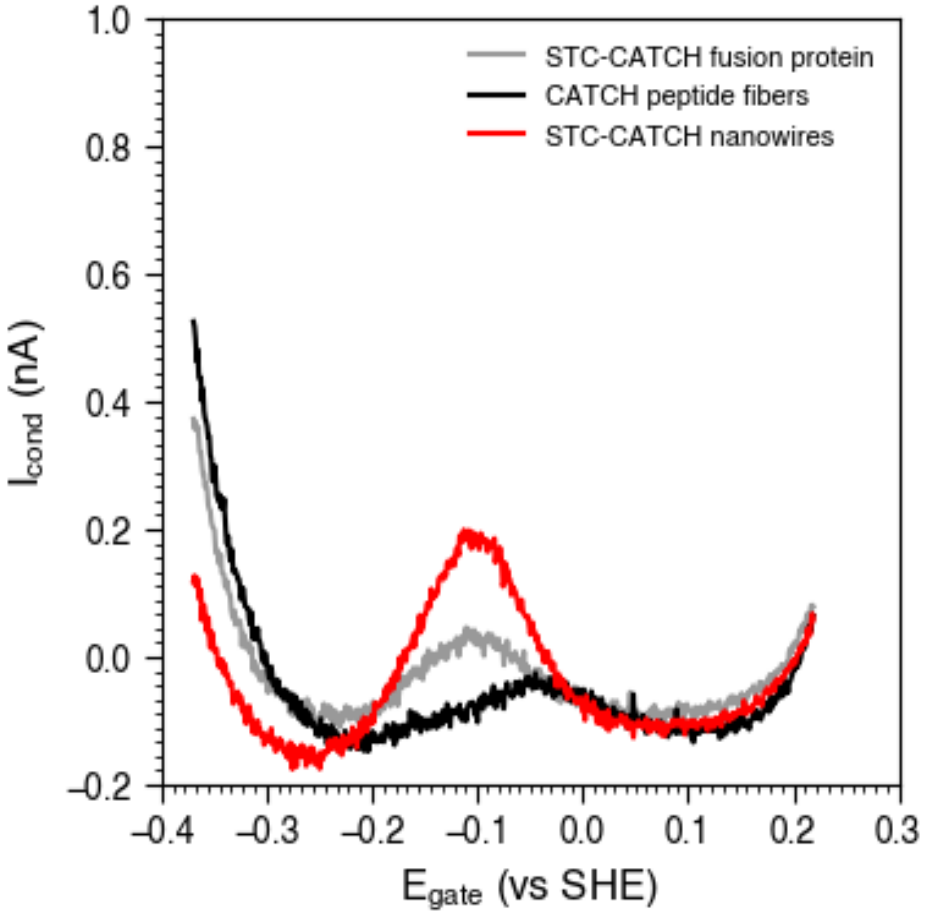

Fig. 3.11. Conduction current (I_{cond}) of electrochemical gating measurements of Interdigitated electrodes (IDE) coated with CATCH peptide fibers (black), STC-CATCH fusion protein (grey) and STC-CATCH fibers (red). Experimental conditions are a scan rate of 5 mV s^{-1}, room temperature, 50 mM PBS at pH 7.2, and a potential window of 230 mV to -0.38 mV of both the source (E_S) and drain (E_D) while maintaining a fixed potential offset ($V_{SD} = E_S – E_D = 0.02$ V) and individually measuring the currents from the source and drain electrodes. Conduction currents were calculated as $I_{cond} = (I_{Drain} – I_{Source}) / 2$ and reported relative to the average potential of the two electodes ($E_{Gating} = (E_D-E_S)/2$). All plots were obtained under the same experimental conditions.

3.6 References

(1) Kumar, R.; Singh, L.; Zularisam, A. W. Exoelectrogens: Recent Advances in Molecular Driver Involved in Extracellular Electron Transfer and Strategies used to Improve it for Microbial Fuel Cell Applications. *Renewable and Sustainable Energy Reviews* **2016**, *56* (18), 1322–1336.

(2) Clarke, T. A.; Edwards, M. J.; Gates, A. J.; Hall, A.; White, G. F.; Bradley, J.; Reardon, C. L.; Shi, L.; Beliaev, A. S.; Marshall, M. J.; Wang, Z.; Watmough, N. J.; Fredrickson, J. K.; Zachara, J. M.; Butt, J. N.; Richardson, D. J. Structure of a bacterial cell surface decaheme electron conduit. *Proceedings of the National Academy of Sciences of the United States of America* **2011**, *108* (23), 9384–9389.

(3) Wang, F.; Gu, Y.; O'Brien, J. P.; Yi, S. M.; Yalcin, S. E.; Srikanth, V.; Shen, C.; Vu, D.; Ing, N. L.; Hochbaum, A. I.; Egelman, E. H.; Malvankar, N. S. Structure of Microbial Nanowires Reveals Stacked Hemes that Transport Electrons over Micrometers. *Cell.* **2019**, *177*, 361–369.

(4) Yalcin, S. E.; O'Brien, J. P.; Gu, Y.; Reiss, K.; Yi, S. M.; Jain, R.; Srikanth, V.; Dahl, P. J.; Huynh, W.; Vu, D.; Acharya, A.; Chaudhuri, S.; Varga, T.; Batista, V. S.; Malvankar, N. S. Electric field stimulates production of highly conductive microbial OmcZ nanowires. *Nature Chemical Biology* **2020**, *16* (10), 1136–1142.

(5) Thirumurthy, M. A.; Jones, A. K. Geobacter cytochrome OmcZs binds riboflavin: Implications for extracellular electron transfer. *Nanotechnology* **2020**, *31* (12).

(6) Altamura, L.; Horvath, C.; Rengaraj, S.; Rongier, A.; Elouarzaki, K.; Gondran, C.; Maçon, A. L. B.; Vendrely, C.; Bouchiat, V.; Fontecave, M.; Mariolle, D.; Rannou, P.; Le Goff, A.; Duraffourg, N.; Holzinger, M.; Forge, V. A synthetic redox biofilm made from metalloprotein-prion domain chimera nanowires. *Nature Chemistry* **2017**, *9* (2), 157–163.

(7) Creasey, R. C. G.; Shingaya, Y.; Nakayama, T. Improved electrical conductance through self-assembly of bioinspired peptides into nanoscale fibers. *Materials Chemistry and Physics* **2015**, *158*, 52–59.

(8) Xu, H.; Das, A. K.; Horie, M.; Shaik, M. S.; Smith, A. M.; Luo, Y.; Lu, X.; Collins, R.; Liem, S. Y.; Song, A.; Popelier, P. L. A.; Turner, M. L.; Xiao, P.; Kinloch, I. A.; Ulijn, R. V. An investigation of the conductivity of peptide nanotube networks prepared by enzyme-triggered self-assembly. *Nanoscale* **2010**, *2* (6), 960–966.

(9) Hudalla, G. A.; Sun, T.; Gasiorowski, J. Z.; Han, H.; Tian, Y. F.; Chong, A. S.; Collier, J. H. Gradated assembly of multiple proteins into supramolecular nanomaterials. *Nature Materials* **2014**, *13* (8), 829–836.

(10) Hosseinzadeh, P.; Lu, Y. Design and fine-tuning redox potentials of metalloproteins involved in electron transfer in bioenergetics. *Biochimica et Biophysica Acta - Bioenergetics* **2016**, *1857* (5), 557–581.

(11) Seroski, D. T.; Restuccia, A.; Sorrentino, A. D.; Knox, K. R.; Hagen, S. J.; Hudalla, G. A. Co-Assembly Tags Based on Charge Complementarity (CATCH) for Installing Functional Protein Ligands into Supramolecular Biomaterials. *Cellular and Molecular Bioengineering* **2016**, *9* (3), 335–350.

(12) Tsapin, A. I.; Vandenberghe, I.; Nealson, K. H.; Scott, J. H.; Meyer, T. E.; Cusanovich, M. A.; Harada, E.; Kaizu, T.; Akutsu, H.; Leys, D.; Van Beeumen, J. J. Identification of a Small Tetraheme Cytochrome *c* and a Flavocytochrome *c* as Two of the Principal Soluble Cytochromes *c* in *Shewanella oneidensis* Strain MR1. *Applied and Environmental Microbiology* **2001**, *67* (7), 3236–3244.

(13) Simpósio, X. I. I.; Enzimática, D. E. H.; Rinaldi, B. G.; Santos, M. M.; Mello, C. M.; Marteleto, N. B.; Marques, T. O.; Linhares, D. C.; Piccoli, R. A. M.; Léo, P.; Rodrigues, F. A. Evaluation of Plasmid Stability in *E. coli* Cultivation in High Cell Density. *journal of bioprocessing* **2017**, *6*, 1–4.

(14) Bergmans, H.; Van, D.; Hoekstra, P. Transformation in *Escherichia coli*: Stages in the Process. *J. Bacteriol.* **1981**, *146* (2), 564–570.

(15) Feist, A. M.; Nagarajan, H.; Rotaru, A. E.; Tremblay, P. L.; Zhang, T.; Nevin, K. P.; Lovley, D. R.; Zengler, K. Constraint-Based Modeling of Carbon Fixation and the Energetics of Electron Transfer in Geobacter metallireducens. *PLoS Computational Biology* **2014**, *10* (4), 1–10.

(16) Bradford, M. M. A rapid and sensitive method for the quantitation of microgram quantities of protein utilizing the principle of protein-dye binding. *Analytical Biochemistry* **1976**, *72*, 248–254.

(17) Thomas, P. E.; Ryan, D.; Levin, W. An improved staining procedure for the detection of the peroxidase activity of cytochrome P-450 on sodium dodecyl sulfate polyacrylamide gels. *Analytical Biochemistry* **1976**, *75* (1), 168–176.

(18) Chantell, C. A.; Onaiyekan, M. A.; Menakuru, M. Fast conventional Fmoc solid-phase peptide synthesis: A comparative study of different activators. *Journal of Peptide Science* **2012**, *18* (2), 88–91.

(19) Amblard, M.; Fehrentz, J.; Martinez, J.; Subra, G. Modern Solid Phase Peptide Synthesis: Methods and Protocols of Modern Solid Phase Peptide Synthesis. *Molecular Biotechnology* **2006**, *33*, 240–255.

(20) Bard, A. J.; Abruiia, H. D.; Chidsey, C. E.; Faulkner, L. R.; Feldberg, S. W.; Melroy, O.; Murray, R. W.; Hill, C.; Carolina, N.; Porter, M. D.; Soriaga, M. P.; White, H. S. The Electrode/Electrolyte Interface-A status Report. *Society* **1993**, *97*, 7147–7173.

(21) Xu, S.; Barrozo, A.; Tender, L. M.; Krylov, A. I.; El-Naggar, M. Y. Multiheme Cytochrome Mediated Redox Conduction through Shewanella oneidensis MR-1 Cells. *Journal of the American Chemical Society* **2018**, *140* (32), 10085–10089.

(22) Blauch, D. N.; Savéant, J. M. Dynamics of Electron Hopping in Assemblies of Redox Centers. Percolation and Diffusion. *Journal of the American Chemical Society* **1992**, *114* (9), 3323–3332.

(23) Ing, N. L.; Spencer, R. K.; Luong, S. H.; Nguyen, H. D.; Hochbaum, A. I. Electronic Conductivity in Biomimetic α-Helical Peptide Nanofibers and Gels. *ACS Nano* **2018**, *12* (3), 2652–2661.

(24) Chen, Y. X.; Ing, N. L.; Wang, F.; Xu, D.; Sloan, N. B.; Lam, N. T.; Winter, D. L.; Egelman, E. H.; Hochbaum, A. I.; Hochbaum, A. I.; Hochbaum, A. I.; Clark, D. S.; Clark, D. S.; Glover, D. J. Structural Determination of a Filamentous Chaperone to Fabricate Electronically Conductive Metalloprotein Nanowires. *ACS Nano* **2020**, *14* (6), 6559–6569.

(25) Overproduction of the *Bradyrhizobium japonicum c*-Type Cytochrome Subunits of the cbb3Oxidase in *Escherichia coli*. *Biochemical and Biophysical Research Communications* **1998**, *251* (3), 744–747.

(26) Pechsrichuang, P.; Songsiriritthigul, C.; Haltrich, D.; Roytrakul, S.; Namvijtr, P.; Bonaparte, N.; Yamabhai, M. OmpA signal peptide leads to heterogenous secretion of B. subtilis chitosanase enzyme from E. coli expression system. *SpringerPlus* **2016**, *5* (1).

(27) Studier, F. W.; Moffat, B. A. Selective expression of cloned genes directed by T7 RNA polymerase. *J. Mol. Biol.* **1986**, *189*, 113–130.

Chapter 4

4. Spin Selectivity in the Bacterial Multiheme Cytochromes of Extracellular Electron Transfer

Christina Niman[1,⁑], Nir Sukenik,[1,⁑] Tram Dang,[2] Justus Nwachukwu,[3] Anne Jones,[3] Ron Naaman,[4] Kakali Santra,[4] Tapan Kumar Das,[4] Yossi Paltiel,[5] *Lech Tomasz Baczewski,[6] Mohamed Y. El-Naggar[1,2,7,*]*

[1]Department of Physics and Astronomy, University of Southern California, Los Angeles, California 90089, United States

[2]Department of Biological Sciences, University of Southern California, Los Angeles, California 91030, United States

[3]School of Molecular Sciences, Arizona State University, Tempe, Arizona 85287, United States

[4]Department of Chemical and Biological Physics, Weizmann Institute of Science, Rehovot 76100, Israel

[5]Institute of Applied Physics, The Hebrew University of Jerusalem, Jerusalem 9190401, Israel

[6]Institute of Physics, Polish Academy of Sciences, Warsaw 02668, Poland

[7]Department of Chemistry, University of Southern California, Los Angeles, California 90089, United States

4.1 Abstract

Metal-reducing bacteria have adapted the ability to respire extracellular solid surfaces instead of soluble oxidants. This process requires an electron transport pathway that spans from the inner membrane, across the periplasm, through the outer membrane, and to an external surface. Specialized proteins, known as multiheme cytochromes, are the primary machinery for moving electrons through this pathway. Recent studies show that the chiral induced spin selectivity (CISS) effect is observable in some of these proteins extracted from the model metal-reducing bacteria, *Shewanella oneidensis* MR-1. It was hypothesized that the CISS effect facilitates efficient electron transport in these proteins by coupling electron velocity to spin, therefore reducing the probability of backscattering. However, these studies focused exclusively on outer membrane conduits, and thus CISS has not been investigated in transmembrane proteins such as MtrA, or periplasmic proteins such as STC. Using conductive probe atomic force microscopy measurements of protein monolayers adsorbed onto ferromagnetic substrates, we show that electron transport is spin selective in both MtrA and STC. Moreover, we have determined the spin polarization of MtrA to be ~75% and STC to be ~30%. This disparity in spin polarizations could indicate that spin selectivity is length dependent in heme proteins, given that MtrA is approximately 2.5 times longer than STC. Most significantly, our study indicates that spin-dependent interactions affect the entire electron transport pathway.

Key Words: multiheme cytochrome, extracellular electron transfer, spin, chirality induced spin selectivity, conductive AFM, protein film

4.2 Introduction

All biological energy generation strategies, including photosynthesis and respiration, require electron flow. In respiration, cells route electron flow from low potential electron donors to higher potential electron acceptors, scavenging free energy in the process. While oxygen is an energetically favorable and soluble electron acceptor that can diffuse inside cells to interact with intracellular electron transfer (ET) components, many microorganisms have adapted to thrive in anaerobic environments by using alternative electron acceptors for respiration, including insoluble redox-active minerals outside the cells[1,2]. Metal-reducing bacteria transport electrons across the cell envelope, a strategy called extracellular electron transfer (EET), to gain energy from the respiration of abiotic metal-oxide minerals[3].

In the model metal-reducing bacterium *Shewanella oneidensis*, EET is achieved through a series of iron-containing proteins called multiheme cytochromes (Figure 1A), which localize to the inner membrane, periplasm, outer membrane, and along bacterial nanowires[4], collectively forming an EET pathway from the interior of cells to extracellular surfaces[5].

EET was initially observed and studied in the context of reducing environmental minerals, but it has since been shown that EET-capable microorganisms can use electrodes as terminal electron acceptors[6]. As such, these electrochemically-active microorganisms present a unique model system for investigating the biotic-abiotic interface, and for developing hybrid 'living electronics' that combine the properties of cells and biomolecules with solid-state electronics[7]. Studies exploring the applications of EET have led to the extensive development of technologies such as microbial fuel cells[8–

[10], bioelectrochemical wastewater treatment[11,12], bioelectronic sensors[13,14], and microbial electrosynthesis[15–17], while newer research indicates that biological systems have unique properties[18] which could facilitate the development of bio-spintronic devices[19].

A recent study of MtrF and OmcA, two *S. oneidensis* cell surface decaheme cytochromes which function as outermost conduits for EET to surfaces, demonstrated that electron transport in both these molecules is spin selective[20]. These results are attributed to the chiral induced spin selectivity (CISS) effect[21,22], where electron transport through chiral molecules, including proteins, has shown a correlation between the electrons' linear momentum and spin, resulting in preferential transport of certain spin. The CISS effect has been demonstrated experimentally for many types of molecules ranging from single amino acids[23] to polypeptides[24], long alpha-helix proteins and DNA[25], and biological protein complexes used for electron transport such as photosystem 1[26]. The natural abundance of chiral biological structures gives rise to the possibility of an important role of the CISS effect in biological systems. For example, CISS could improve the efficiency of electron transport in non-conductive organic structures. However, by demonstrating CISS in biomolecular electron conduits that evolved to naturally interface with abiotic surfaces, the MtrF and OmcA results raise the intriguing possibility that spin filtering plays a role in extracellular respiration and may be exploited at biotic-abiotic interfaces.

Spin polarization induced by the CISS effect has been shown to be length dependent[27,28]. Spin polarization increases approximately linearly with distance, while total charge flow decreases[28]. MtrF and OmcA transport charge along similar length

scales (~5.85 nm for MtrF and ~5.75 nm for OmcA, measured as the distance between the centers of the terminal hemes), but were observed to have different spin selectivities: 63% in OmcA vs. 37% in MtrF[20]. This difference led to a hypothesis that the secondary structure helical content (percentage of residues in α-helices within the protein) affects the net spin polarization through the protein.

The relationship between CISS and EET in *S. oneidensis* has just begun to be elucidated. MtrF and OmcA are both responsible for the terminal step in an extended EET chain that starts in the inner membrane. The Mtr-Omc pathway is a subset of cytochromes in *S. oneidensis* responsible for taking electrons from the periplasm, transporting them across and along the outer membrane, and to the terminal electron acceptor[29]. MtrA (Figure 4.1A) is a periplasmic and transmembrane protein that sits inside of the MtrB porin protein with one end dangling in the periplasm and the other exposed to the cell surface[30]. Electrons enter MtrA in the periplasm, are transported along its length by redox-driven hopping along its central heme chain, and are passed off to MtrC (or OmcA or MtrF)[31]. Electron transport between the inner membrane reductases and the periplasmic end of MtrA is still an area of active study. The small tetraheme cytochrome (STC or CctA, Figure 4.1A) is theorized to act as an electron shuttle between the inner and outer membrane-bound complexes[6,32]. If these upstream proteins also exhibit spin selectivity, it could have broader implications for the role of CISS in the EET chain. Additionally, these two proteins have significantly different lengths and secondary structures from MtrF and OmcA, providing the opportunity to examine the effects of length and secondary structure on CISS in these systems. Previous studies have looked at

conduction measurements and modeling in STC[33], but these investigations focused purely on conductivity and did not attempt to probe spin filtering behaviors. To our knowledge, no similar work has been done in MtrA.

Here, we investigated the CISS effect in two key components of the EET pathway in *S. oneidensis*: the periplasmic 2.31 nm long tetraheme cytochrome STC and the transmembrane 7.48 nm long decaheme cytochrome MtrA (measured as the distance between the centers of the terminal hemes), which transmits electrons to the previously investigated Mtr/Omc proteins. The measurements show higher spin selectivity in MtrA than STC, and demonstrate that, beyond the terminal cell surface reductases, spin filtering is exhibited by multiple EET proteins that span the cell envelope.

4.3 Materials and Methods

4.3.1. Protein Monolayer Formation

To form a monolayer of MtrA, undiluted prepared protein was dropcast on the substrate of choice. The device was then incubated for one hour at 4°C in a humid environment, rinsed with buffer solution and then DI water, and dried overnight.

To prepare a monolayer of STC, the prepared protein was diluted by a factor of 100X and dropcast on the substrate of choice. The device was then incubated for four hours at 4°C in a humid environment, rinsed with first buffer solution and then DI water, and dried overnight.

4.3.2. Protein Monolayer Characterization by AFM

Protein attachment to gold was studied for both proteins using commercially available polycrystalline 100nm Au on aluminosilicate glass substrates (Sigma-Aldrich

643246-5EA) on a Cypher ES AFM (Oxford Instruments). Substrates were cleaned by sonication for 15 minutes each in acetone, isopropanol, and deionized water (in order). Substrates were immediately dried and fixed to AFM pucks.

High resolution imaging and scratching experiments were performed on each of the following conditions to determine optimal conditions for protein monolayer formation: bare gold, buffer incubated overnight, undiluted MtrA incubated for 1-hour, undiluted MtrA incubated for 16 hours, 10X diluted STC for 4 hours, 100X STC diluted for 4 hours, and 1000X STC diluted for 4 hours. Scratching experiments were performed by quickly scanning a 1x1 μm square with a tip force large enough to scratch away the protein, but insufficient to scratch the gold surface. Then, the AFM was switched to tapping mode and a 3x3 μm image was collected (Figure 4.2, 4.3A, and 4.3B). The topographic image was background corrected with a linear planefit and the cross-sections were taken as an average of 50 scan lines from the scratched sample area (Figure 4.3C and 4.3D).

4.3.3. Protein Purification

pBAD202/D-TOPO vector containing a gene encoding recombinant MtrA was introduced into *E. coli* BL21(DE3) as described previously[34] along with the pEC86 vector[35] for cytochrome *c* maturation. The recombinant MtrA contained a 4xCys/V5/6xHis tag (DDDDKAACCPGCCKGKPIPQPLLGLDSTRTGHHHHHH) at its C-terminus for purification and covalent binding to Au surfaces. Cells were grown in lysogeny broth to an OD_{600} of 0.6 before induction with 1mM L-arabinose for another 5 hours at 25˚C. Cells were harvested at 6000*g* for 15 mins at 4˚C. Lysis was completed in

Buffer A (20mM Tris-HCl, pH 8.5, 1mM TCEP, 10% glycerol, 500mM NaCl, 1 mg/mL lysozyme, 2uL/10mL benzonase, 2mM $MgCl_2$, protease inhibitor) and passed through the French press three times at 8000 lb/in^2. The lysate was spun at 15,000*g* for 30 mins at 4˚C. The supernatant containing tetra-cysteine MtrA was loaded onto a HisTrap column, equilibrated with Buffer B (20mM Tris-HCl, pH 8.5, 1mM TCEP, 10% glycerol, 500mM NaCl, protease inhibitor) and 20mM imidazole. The protein was washed and eluted with Buffer B with an imidazole gradient (0-500mM). Fractions containing tetra-cysteine-tagged MtrA were pooled and concentrated to ~1mL using a 10kDa MWCO Amicon centrifugal filter. This sample was loaded onto a HiLoad 16/600 Superdex 200pg size exclusion column twice for removal of contaminating proteins. For both times, the column was washed with 20mM Tris-HCl, pH 8.5, 10% glycerol, 1mM TCEP, and 150mM NaCl. After testing by SDS-PAGE, fractions containing pure MtrA (13.2 µM) were pooled and concentrated using a 5kDa MWCO Amicon centrifugal filter. Concentrated samples were distributed into 50uL aliquots and stored at -80˚C.

The pD431-MR vector containing a gene encoding recombinant small tetraheme cytochrome (STC) from *Shewanella oneidensis* with an S87C point exchange and a twin *strep tag* (AWSHPQFEKAWSHPQFEK) on the C-terminus together with a kanamycin resistance gene was produced by DNA 2.0 and transformed with a pEC86 vector containing a sequence encoding the *Ccm* pathway (Cytochrome *c* maturation together with chloramphenicol resistance gene), into *E. coli* using the heat shock method. Cells were grown aerobically with shaking (250 rpm, 24 h, 37 ºC) in Luria Bertani media with kanamycin and chloramphenicol added to final concentrations of 50 mg mL^{-1} and

35 mg mL^{-1}, respectively. Cells were induced at an optical density (OD_{600}) of 0.6 by addition of isopropyl β-D-1-thiogalactopyranoside (IPTG) to a final concentration of 0.2 mM. After growing approximately 18 h, the medium changes color from yellow to brown. Cells were then harvested by centrifugation at 4 °C, 16,128 x g for 1 h. Periplasmic extracts were obtained by adding lysozyme to a final concentration of 28 μM in 20 mM PBS buffer at pH 7.2 (phosphate buffered saline) with 100 mM EDTA, 0.0002 U/μL DNase I (Thermo Fisher Scientific), and 2 tablets of Pierce protease inhibitor and gently stirring for 90 min at 4 °C. The resulting extract was cleared by centrifugation (16,128 x g) for 1 h. The supernatant was kept in 20 mM PBS at pH 7.2 at 4 °C for overnight dialysis and then applied to a 40 mL diethylaminoethyl cellulose (DEAE) column in the same buffer. The column was washed with increasingly concentrated PBS (50 mM, 100 mM, 150 mM, 200 mM, 250 mM, 300 mM, 350 mM and 400 mM) with 5 column volumes of each concentration at pH 7.2. The STC eluted at 400 mM PBS. Brownish-red fractions containing STC were pooled and concentrated with amicon ultra-centrifugal filters (2 kDa molecular weight cut-off) before applying to a 30 S*trep*-Tactin column equilibrated with 20 mM PBS at pH 7.2 at room temperature and eluting ml with 5 mM desthiobiotin. Fractions containing STC were pooled, buffer-exchanged and concentrated with amicon ultra-centrifugal filters (2 kDa molecular weight cut-off) before use. Homogeneity of purified STC was confirmed via SDS-PAGE (Figure 4.4) and UV-vis spectroscopy (Figure 4.5).

Acknowledgement: The pEC86 vector encoding the Ccm pathway for cytochrome *c* maturation was a gift from David Kramer.

4.3.4. Magnetic Heterostructure Fabrication

Magnetic substrates were fabricated by an epitaxial nanostructure growth procedure by using the Molecular Beam Epitaxy (MBE PREVAC) system at the Institute of Physics of the Polish Academy of Sciences in Warsaw.

The sample configuration is: Al2O3(0001)/Pt 5 nm/Au 20 nm/Co 1.5nm/Au 5nm, the magnetization easy axis direction of the samples is out-of-plane, exhibiting perpendicular anisotropy with a coercive field of ~160G, as shown by polar magneto-optic Kerr effect (P-MOKE) measurement (Figure 4.6). The fully rectangular shape of the hysteresis loop indicates that all cobalt spins are aligned in one direction perpendicular to the film surface. The top gold layer acts both as a capping layer to prevent oxidation of the Co layer and as a surface for covalent bonding of the Cysteine tags of the protein complexes.

Substrates were washed in acetone, isopropanol and ethanol and then dried with high-pressure Nitrogen gas flow and fixed to an AFM puck prior to the protein adsorption process.

4.3.5. Magnetic Conductive AFM Experiment

AFM measurements were performed on a Cypher ES Environmental System AFM (Oxford Instruments) using conductive AFM tips (MicroMasch HQ:NSC18/Pt). Bias was applied to the sample while the AFM tip was kept grounded. The substrate was placed in a ~1000 G magnetic field with north oriented in the down direction (applied magnetic field is much higher than the ~160G coercive field of the substrate–Figure 4.6), then carefully removed from the field and placed in the AFM. For each condition tested,

a 10x10 μm tapping scan was performed to image protein coverage. After scanning, IV spectra were collected at 270 locations for the MtrA with an engage force of 45 nN and at 100 locations for the STC with an engage force of 17 nN. The sample was then removed from the AFM, placed in a magnetic field oriented in the opposite direction, and returned to the AFM for an identical set of images and IV curves.

4.3.6. Protein Electrochemical Characterization

Electrochemical experiments were performed for both proteins to verify that the constructs modified to have gold-binding tags still behave similarly to their unmodified counterparts. Experiments were conducted under nitrogen atmosphere in a glovebox using a three-electrode configuration to perform protein film cyclic voltammetry (PFV). Platinum wire was used for the counter electrode and Ag/AgCl for the reference electrode. All potentials were corrected to the standard hydrogen electrode.

For STC, the working electrode was a 0.5 mm diameter gold electrode, polished with 120 grit sand paper and alumina (5μm size followed by 0.3 μm and 0.05 μm sizes of BASi Polishing Alumina Powder) before each use. A protein film was formed by drop casting STC on the surface and incubating for 20 minutes. The electrode was then immediately dunked into the electrochemical cell containing 20 mM Phosphate buffer and 100 mM NaCl. The electrode was cycled from 0.2V to -0.4V vs. SHE with a scan rate of 25 mV/s.

For MtrA, the working electrode was a pyrolytic graphite edge electrode (BASi) polished with alumina. A protein film was formed by drop casting MtrA on the surface and incubating for 35 minutes. The electrode was then immediately dunked into the

electrochemical cell containing 100 mM HEPES + 100 mM NaCl + 100 μM polymyxin . The electrode was cycled from -0.415V to 0.235V vs. SHE with a scan rate of 20 mV/s.

4.3.7. PMIRRAS Characterization of STC

Attachment of STC to gold was verified using a 100 nm gold coated Si substrate, adsorbing protein to the surface, and characterizing with polarization modulation infrared reflection absorption spectroscopy (PMIRRAS). The measurement was performed on a Nicolet 6700 FTIR with a PEM-90 photoelastic modulator using an incidence angle of 80°.

4.3.8. Hall Device measurements

Device Preparation

Hall devices were fabricated in a class 1000 clean room using standard photolithography on GaN HEMT wafers (NTT). The wafers consist of a sapphire substrate, an 1800 nm thick GaN layer, a 20 nm thick AlGaN layer, and a 2 nm thick GaN capping layer. Six contacts were added by annealing a metallic multilayer to create a source, a drain, and two pairs of Hall probes. The exposed channel (a 0.5 mm x 0.04 mm rectangle) was coated with a 2 nm Ti adhesion layer followed by a 5 nm Au layer for protein adsorption. Before protein adsorption, the device was boiled in acetone for 15 minutes, boiled again in fresh acetone for 15 minutes, boiled in ethanol for 15 minutes, and moved to cold ethanol for storage until protein deposition. After protein adsorption, the device was glued to a chip carrier and wire bonded. Silicone glue was used to cover the bonds and contact pads, then attach a ~200 μL PDMS chamber.

Ferromagnet characterization by polar magneto-optic Kerr effect measurement

The ferromagnetic substrates were characterized using polar magneto-optic Kerr effect (P-MOKE) as a function of applied out-of-plane external magnetic field. Results are presented in Figure 4.6.

4.3.9. STM Experiment

STM measurements were performed on a Cypher ES Environmental System AFM (Oxford Instruments) operating in the STM mode using 80/20 Pt/Ir tips (ASY-STM). Bias was applied to the sample while the STM tip was kept grounded. The substrate was placed in a magnetic field of ~1000G with the north pole oriented in the down direction, then it was carefully removed from the field and placed in the AFM. A 300x300 nm scan was performed to image protein coverage with the imaging conditions: 1V bias voltage and 1 nA current setpoint. After scanning, IV spectra were collected at 150 locations with initial tip-sample distance defined by 0.2V sample bias and 0.2 nA tunneling current. The sample was then removed from the AFM, magnetized in the opposite direction, and returned to the AFM for an identical set of images and IV curves.

4.3.10. Hall Voltage Experiment

Undiluted STC was dropcast onto the Hall channel. The device was then incubated for 16 hours at 4°C in a humid environment and rinsed with buffer solution. After attachment, the PDMS chamber was filled with 100 mM HEPES (pH 7.2). A glass coverslip coated with gold was used as the top gate with the gold side facing away from the solution. A constant current of 10 μA was applied between the source and drain electrodes. Constant potential pulses were applied for 60 seconds each in steps of 10V from 0V up to 50V and then 0V down to -50V. Both the constant current and the gate

pulses were applied using separate channels of a Keithley 2636A. Throughout the experiment, the Hall voltage was collected at <1s intervals using a Keithley 2182A nanovoltmeter. All measurements were performed inside a Faraday cage.

4.4 Results and Discussion

Monolayer deposition orientation and uniformity of both MtrA and STC was examined by AFM scratching experiments of the film deposited on clean gold-covered glass (see Materials and Methods). The tapping topography of the scratched areas (Figure 3A and 3B) showed a 1X1 μm area pit reaching the gold layer. Analyzing the cross section (Figure 3C and 3D) yielded the monolayer height of ~6 nm and ~2 nm for MtrA and STC respectively. These heights correlate with the known length scales of the protein complexes from the Protein Data Bank, and as measured in previous works[36], providing evidence for the deposition of a monolayer of proteins. Further characterizations of the protein film included protein film electrochemistry (Figure 4.7)[37], and polarization modulation infrared reflection absorption spectroscopy (PMIRRAS) (Figure 4.8).

The spin selectivity of the conduction through MtrA and STC was measured by comparing the different currents through the proteins deposited on the ferromagnetic substrate (Figure 4.1B) when magnetized in the North pole facing up versus down directions.

Figure 4.9A shows all data collected from 270 different points on the sample with MtrA proteins and Figure 4.9B shows the same for 100 points on a sample with STC. Insets in Figure 4.9 show the mean current vs. voltage of all curves as solid lines and the standard deviation as shaded error bars. It is apparent that the currents going through the

proteins when the substrate is magnetized in the up direction are larger than when the substrate is magnetized in the down direction for both MtrA and STC. However, the difference is much more significant for the MtrA proteins. This becomes even clearer when calculating the spin polarization of the current, calculated as $\left[\left(I_{up} - I_{down}\right)/\left(I_{up} + I_{down}\right)\right] \times 100$, and plotting it as a function of applied voltage (Figure 4.10). The calculated spin polarization for the MtrA is roughly 75% whereas for the STC it is around 30%. Due to the lower spin polarization and higher noise measured in STC using this method, additional spin polarization characterization methods were used to corroborate these results. Scanning tunneling microscopy IV-spectroscopy measurements yielded much cleaner results due to the different physical mechanism of operation, while presenting similar spin polarization values (Figure 4.11). Furthermore, 2D electron gas gated hall device measurements[20] in liquid also confirmed the presence of spin selectivity in STC, showing it is not limited to dry conditions (Figure 4.12).

The presented results show that spin polarization of charge is not unique for the outer membrane cytochromes (MtrF and OmcA),[20] but is prominent in both the transmembrane MtrA and the periplasmic STC. Therefore, it seems that components throughout the entire EET chain are spin selective. Moreover, all the molecules which have been measured exhibit the same spin-momentum coupling preference. This fact raises the intriguing possibility that the spin polarization from the CISS effect persists across multiple molecules in the electron transport chain. It has been recently proposed that spin selectivity promotes efficient ET in biomolecules, due to reduced backscattering caused by the fact that a change in the charge direction of motion (momentum) must

correspond with a spin flip[38]. It is possible that in multi-molecule electron transport systems, cooperative CISS facilitates hopping from one molecule to another by suppressing backscattering between molecules.

In the previous work comparing MtrF and OmcA, a significant difference in spin selectivity was observed between the two proteins, in spite of them being similar in size, length and heme arrangement. Differences in helical secondary structure content (18% for OmcA vs. 11% for MtrF) were hypothesized to be the cause of the significant difference between the spin polarizations. This hypothesis holds when comparing these two molecules to MtrA, which has a 28% helical secondary structure and higher spin polarization than either molecule. However, our results show a much lower spin polarization through STC despite having a high concentration (~44%) of helical secondary structure compared to MtrA[39,40].

Unlike the comparison between MtrF and OmcA, STC and MtrA differ dramatically in length and structure. It has been shown that the spin polarization driven by the CISS effect is directly proportional to the length of DNA and oligopeptides[28]. Therefore, due to the difference in length, it is impossible to compare the effects of helical secondary structure between these two systems. Length seems to have a larger effect on spin polarization than helical secondary structure concentration, creating small spin polarization through the highly helical STC as compared to the longer but less helical MtrA. But a true study of the effect of secondary structure would require comparing pairs of molecules where secondary structure is the primary difference. The key benefit to comparing STC and MtrA is that it allows investigation of the effects of

length dependence on CISS in cytochromes for the first time. We find that MtrA, which is approximately 2.5 times as long as STC, exhibits approximately 2.5 times larger spin polarization. The strong dependence of charge transport on spin direction in the longer MtrA, suggests that coupling the electron's velocity to its spin enacts a significant penalty on backscattering of electrons of the preferred spin. Thus, CISS may enhance the efficiency of EET through cytochromes.

4.4.1. Conclusion

Presented results show that the periplasmic STC and transmembrane MtrA both possess spin polarization properties due to the CISS effect. MtrA exhibited much higher spin selectivity at ~75% when compared to STC at ~30%. We attribute this discrepancy to the difference in length scale (2.5 times larger for MtrA), rather than the difference in protein secondary structure as was suggested previously for the outer membrane MtrF and OmcA. This is the first-time length dependence effects on CISS are reported for multiheme cytochromes, and the relationship seems similar to what has previously been reported for length dependence in DNA and polypeptides.

Another important consequence from presented results is that spin selectivity has now been measured for both extracellular, transmembrane, and periplasmic cytochromes. The results raise the possibility that CISS is present through all parts of the EET pathway and might possess an important role in the efficiency of the process.

4.5 Figures

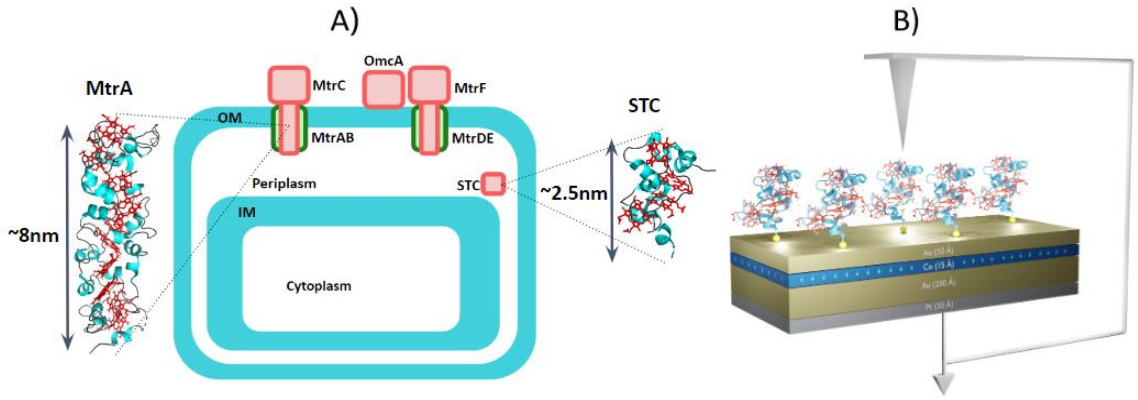

Figure 4.1. Schematic representation of the system of study and measurement. (a) Shows a cartoon of an *S.oneidensis* cell, with emphasis placed on the relative locations of key cytochromes. Full structures of the MtrA and STC, with length scale bars, are provided for reference. (b) Schematic of the experimental setup of the magnetic conductive AFM measurements.

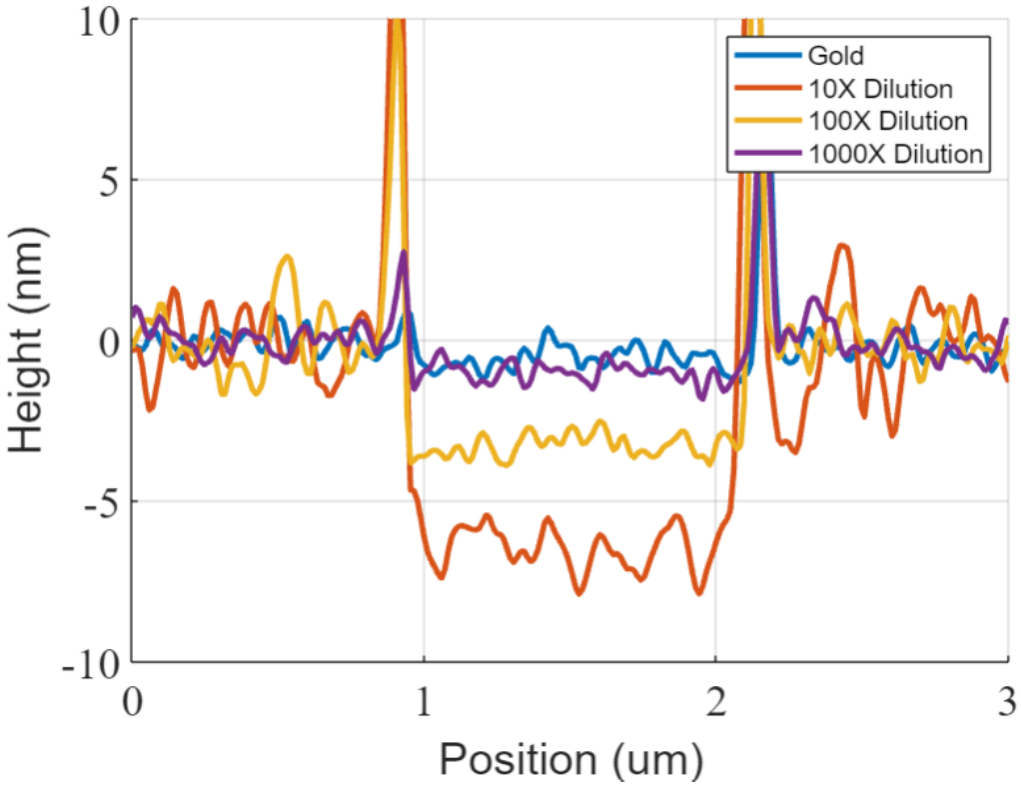

Figure 4.2. Depth profiles of STC coated gold samples after scratching experiment. In each case, the depth profile represents an average of 50 background-corrected (linear planefit) scan lines. The forces used were not sufficient to scratch the gold (blue) substrate. The depth profile generated by scratching away a layer created by 100X dilution (yellow) was in agreement with the previously recorded dimensions of STC.

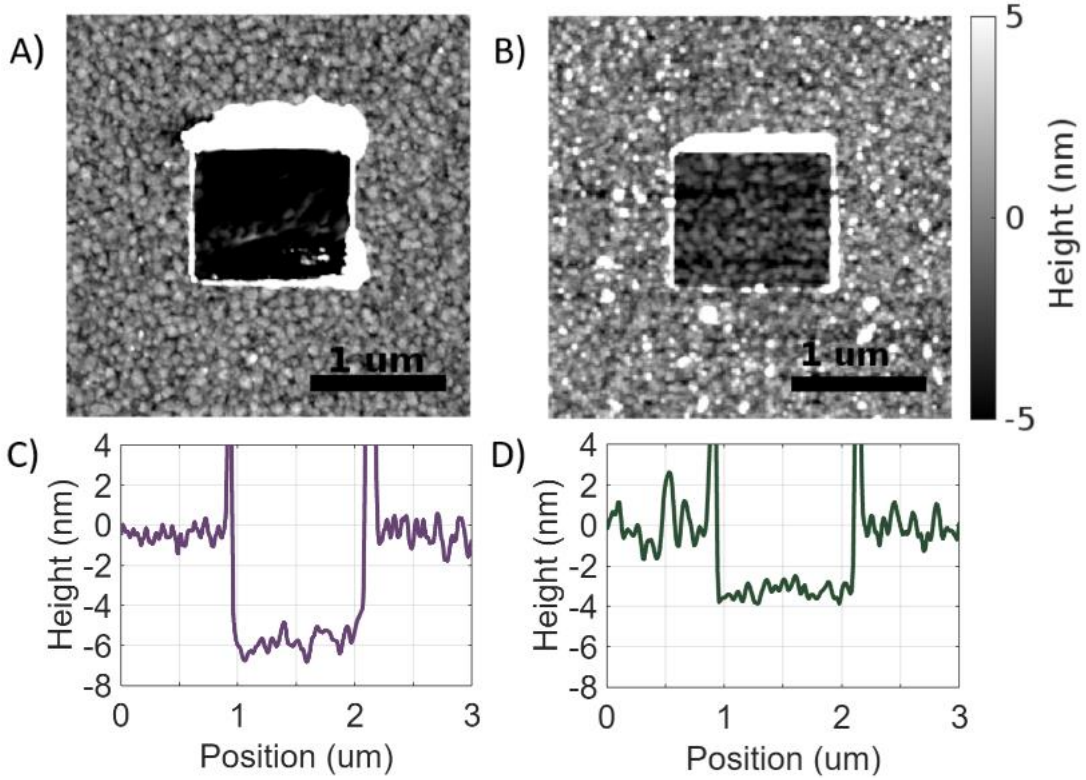

Figure 4.3. Protein adsorption test using AFM, showing the MtrA (A&C) and STC (B&D) monolayers created by the final selected adsorption conditions. (A&B) Show tapping AFM topography images collected immediately after high-force contact scanning. Forces were selected to be sufficient to remove the protein from the surface, but small enough to prevent scratching the gold substrate. (C&D) Show averaged cross sections of the scratched regions, indicating that the depth of the wells left behind are as expected for a monolayer of these molecules.

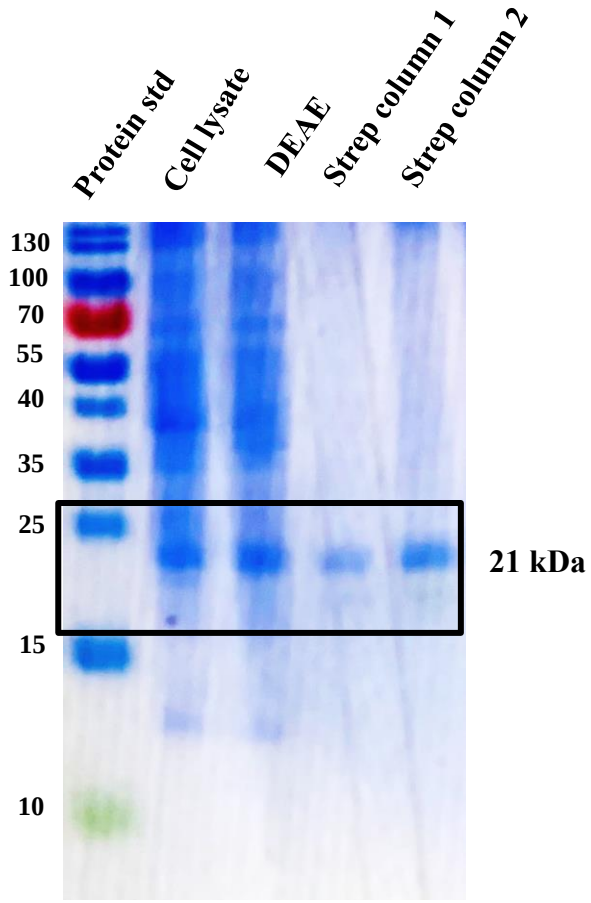

Figure 4.4. SDS-PAGE gel visualized with Coomassie blue staining of various stages of STC purification. Lane 1: protein standard (10 to 180 kDa); Lane 2: crude cell lysate; Lane 3: eluate from ion exchange chromatography; Lane 4: eluate from *Strep*tactin Column; Lane 5: purified STC from *Strep*tactin column. STC is present as a prominent 21 kDa band in all lanes as shown in the black box. In each lane, 10 µl (600 µg/ml) of the designated sample was applied to the gel.

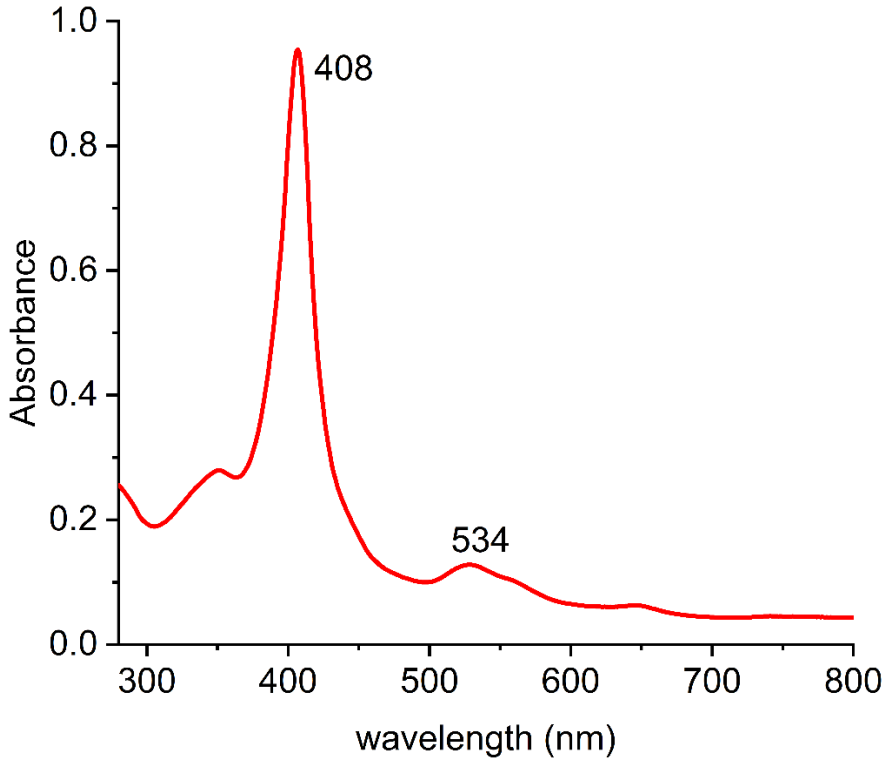

Figure 4.5. UV-vis spectrum of purified STC featuring a Soret peak at 408 nm and a broad β-band peak at 534 nm characteristic of multiheme cytochromes.

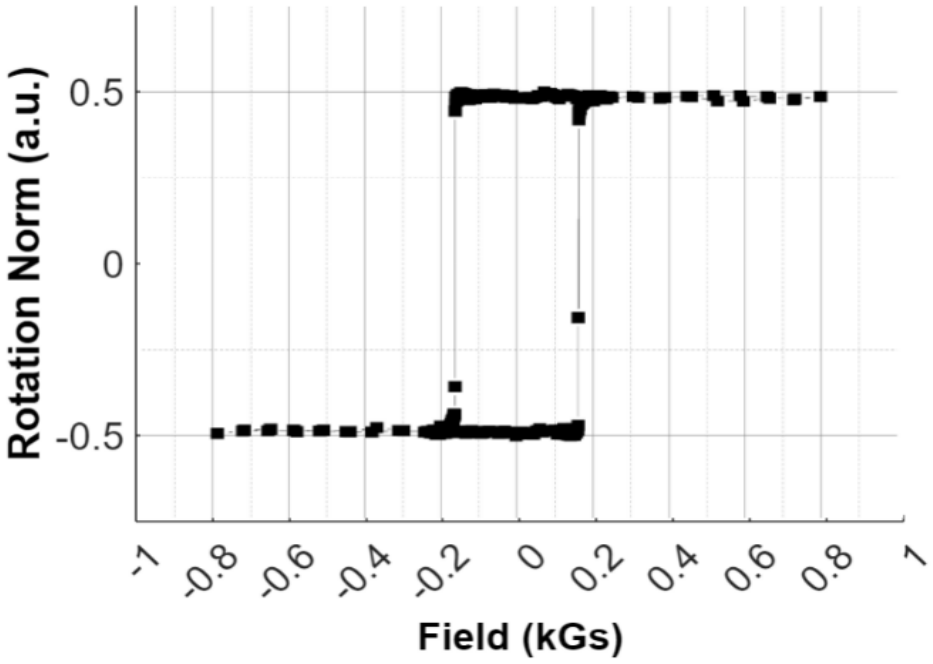

Figure 4.6. Polar magneto-optic Kerr effect measurements on the ferromagnetic substrates used in this work. The square hysteresis is a sign of the out-of-plane anisotropy and the coercive field is 162G.

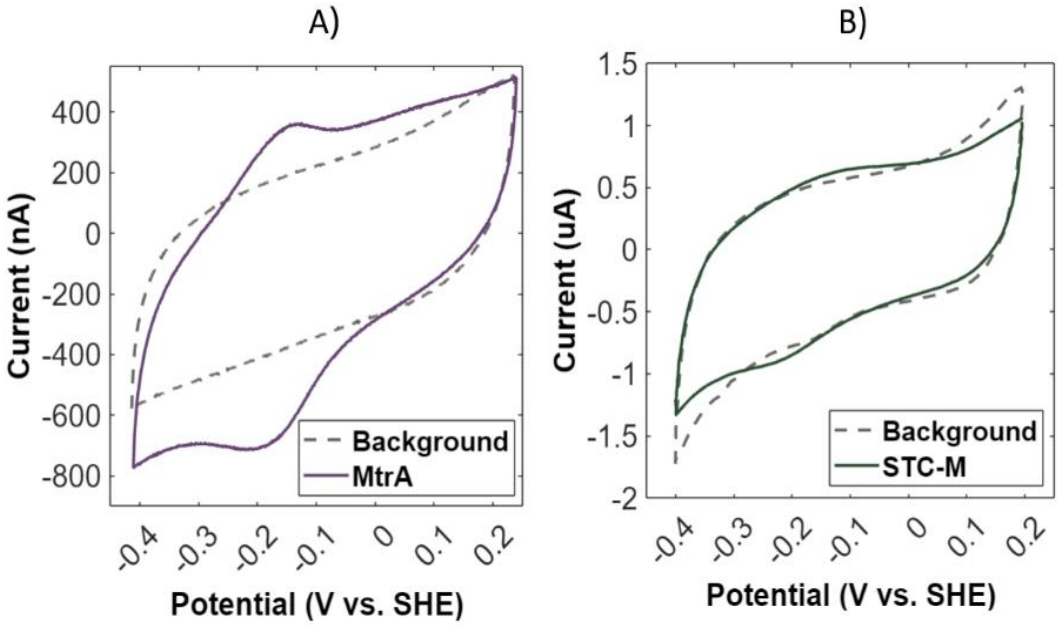

Figure 4.7. Electrochemical measurements of modified proteins. In both cases, the observed midpoint potential was in agreement with what has been previously reported.

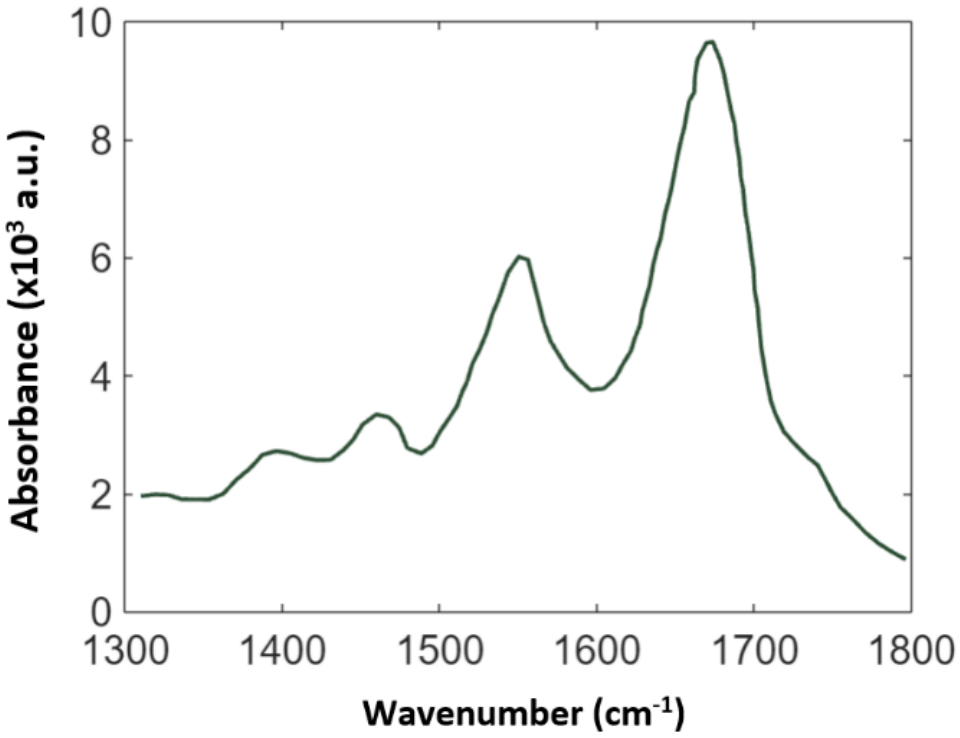

Figure 4.8. PMIRRAS spectrum of STC monolayer on a gold surface.

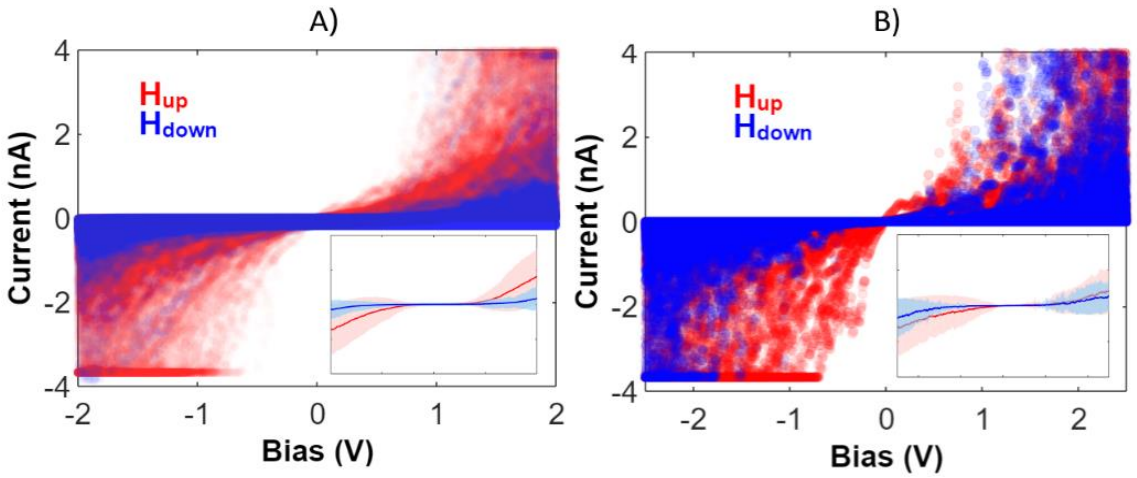

Figure 4.9. Spin dependent conduction of MtrA and STC by CAFM IV-spectroscopy for protein adsorbed onto magnetizable substrates. Insets show mean as solid lines and standard deviation as shaded error bars. (A) IV curves collected for the sample with MtrA. Data was collected at 270 different positions for each magnet orientation. (B) IV curves collected for the sample with STC. Data was collected at 100 positions for each magnet orientation.

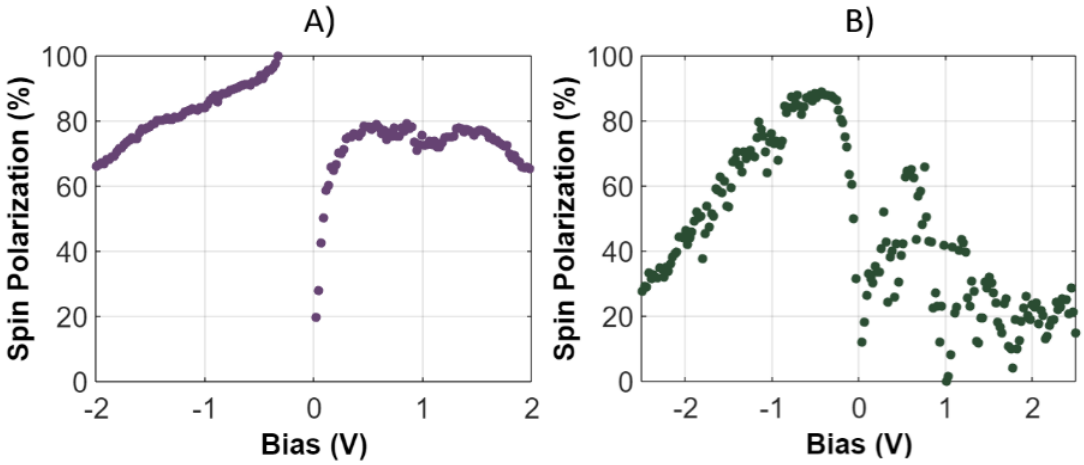

Figure 4.10. Percentage of spin polarization of MtrA and STC. Percentage of Spin polarization $\left[\left(I_{up} - I_{down}\right)/\left(I_{up} + I_{down}\right)\right] \times 100$ of (A) MtrA and (B) STC. Here, I_{up} and I_{down} are the mean currents with the substrate magnetized in the north pole up and down, respectively.

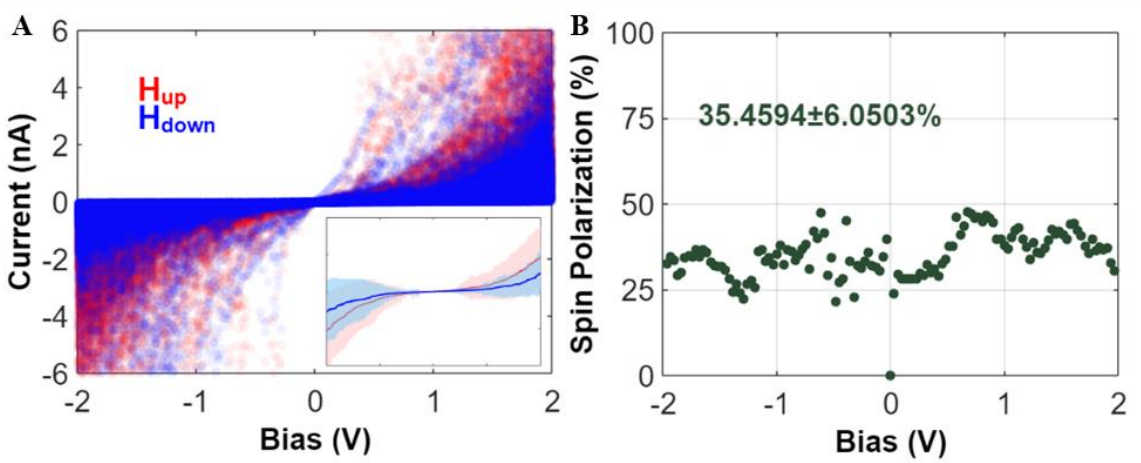

Figure 4.11. (A) Spin dependent conduction of STC by STM IV-spectroscopy for protein adsorbed onto a magnetizable substrate. Inset shows mean as solid lines and standard deviation as shaded error bars. Data was collected at 100 positions for each magnet orientation. (B) The corresponding percentage of spin polarization $\left[\left(I_{up} - I_{down}\right)/\left(I_{up} + I_{down}\right)\right] \times 100$ of STC. Here, I_{up} and I_{down} are the mean currents with the substrate magnetized in the north pole up and down, respectively. Spin polarization of 35% ± 6% is given as a mean of non-zero data points with standard deviation as the error.

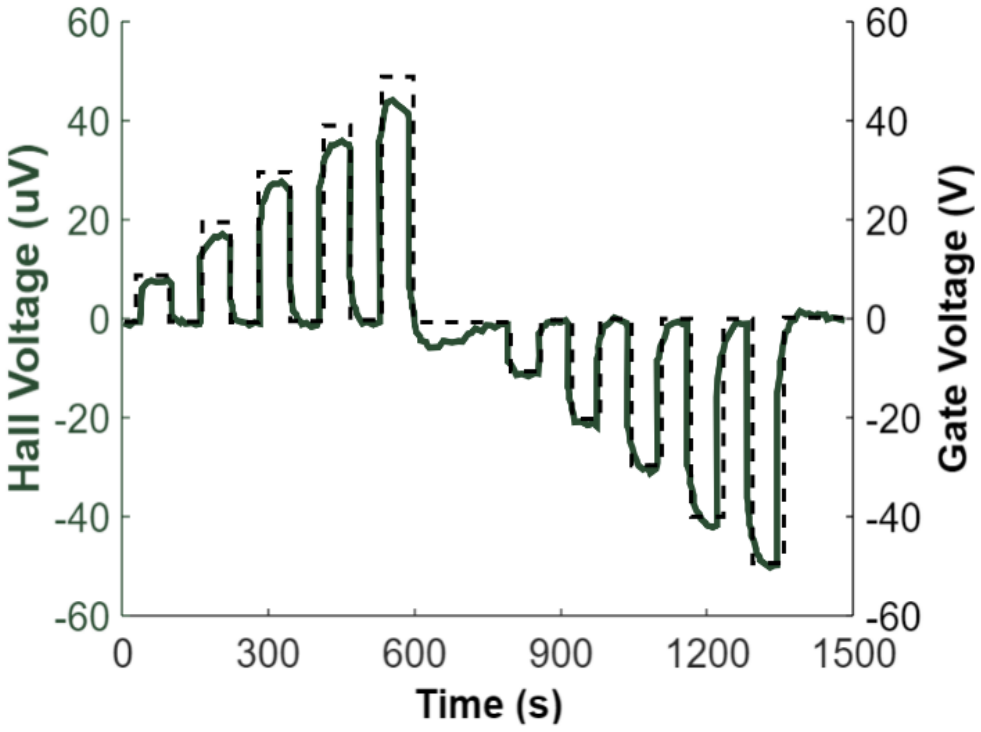

Figure 4.12. Hall polarization data for STC. Hall voltage (dark green) is measured as a function of the potential applied to the gold top gate (dotted black line).

4.6 References

(1) Lovley, D.R.; Stolz, J.F.; Nord, G.L.; Phillips, E.J.P. Anaerobic production of magnetite by a dissimilatory iron-reducing microorganism," *Nature* **1987**, *330*(V), 2–4.

(2) Myers, C.R.; Nealson, K.H. Bacterial Manganese Reduction and Growth with Manganese Oxide as the Sole Electron Acceptor. *Science* **1988**, *240*(4857), 1319–1321.

(3) Shi, L.; Dong, H.; Reguera, G.; Beyenal, H.; Lu, A.; Liu, J.; Yu, H.Q.; Fredrickson, J.K. Extracellular electron transfer mechanisms between microorganisms and minerals. *Nature Reviews Microbiology* **2016**, *14*(10), 651–662.

(4) El-Naggar, M.Y.; Wanger, G.; Leung, K.M.; Yuzvinsky, T.D.; Southam, G.; Yang, J.; Lau, W.M.; Nealson, K.H.; Gorby, Y.A. Electrical transport along bacterial nanowires from *Shewanella oneidensis* MR-1. *Proceedings of the National Academy of Science of the United States of America* **2010**, *107*(42), 18127–18131.

(5) Pirbadian, S.; Barchinger, S.E.; Leung, K.M.; Byun, H.S.; Jangir, Y. Bouhenni, R.A.; Reed, S.B.; Romine, M.F.; Saffarini, D.A.; Shi, L.; Gorby, Y.A.; Golbeck, J.H.; El-Naggar, M.Y. *Shewanella oneidensis* MR-1 nanowires are outer membrane and periplasmic extensions of the extracellular electron transport components. *Proceedings of the National Academy of Science of the United States of America* **2014**, *111*(35), 12883–12888.

(6) Bretschger, O.; Obraztsova, A.; Sturm, C.A.; Chang, I.S.; Gorby, Y.A.; Reed, S.B.; Culley, D.E.; Reardon, C.L.; Barua, S.; Romine, M.F.; Zhou, J.; Beliaev, A.S; Bouhenni, R.; Saffarini, D.; Mansfeld, F.; Kim, B.-H.; Fredrickson, J.K.; Nealson, K.H. Current Production and Metal Oxide Reduction by *Shewanella oneidensis* MR-1 Wild Type and Mutants. *Applied and Environmental Microbiology* **2007**, *73*(21), 7003–7012.

(7) Atkinson, J.T., Chavez, M.S.; Niman, C.M.; El-Naggar, M.Y. Living electronics: A catalogue of engineered living electronic components. *Microbial Biotechnology* **2023**, *16*(3), 507–533.

(8) Chaudhuri, S.K.; Lovley, D.R. Electricity generation by direct oxidation of glucose in mediatorless microbial fuel cells. *Nature Biotechnology* **2003**, *21*(10), 1229–1232.

(9) Zhang, X.; Cheng, S.; Wang, X.; Huang, X.; Logan, B.E. Separator Characteristics for Increasing Performance of Microbial Fuel Cells. *Environmental Science and Technololgy* **2009**, *43*(21), 8456–8461.

(10) Watson, V.J.; Logan, B.E. Power production in MFCs inoculated with *Shewanella oneidensis* MR-1 or mixed cultures. *Biotechnology and Bioengineering* **2010**, *105*(3), 489–498.

(11) Gorby, Y.A.; Lovley, D.R. Enzymic uranium precipitation. *Environmental Science and Technololgy* **1992**, *26*(1), 205–207.

(12) Hsu, L.; Arias-Thode, M.; Salvacion, M.; Benavidez, Z.; Mirhosseini, A.; Babanova, S.; Chen, S.; Bretschger, O. Demonstration of an Energy-Neutral, Off-Grid Microbial Fuel Cell System for Decentralized Wastewater Treatment. *ECS Transactions* **2017**, *75*(46), 19–29.

(13) Del Valle, I.; Fulk, E.M.; Kalvapalle, P.; Silberg, J.J.; Masiello, C.A.; Stadler, L.B. Translating New Synthetic Biology Advances for Biosensing Into the Earth and Environmental Sciences. *Frontiers of Microbiology* **2021**, *11*, 618373.

(14) Wan, X.; Saltepe, B.; Yu, L.; Wang, B. Programming living sensors for environment, health and biomanufacturing. *Microbial Biotechnology* **2021**, *14*(6), 2334–2342.

(15) Cheng, S.; Logan, B.E. Sustainable and efficient biohydrogen production via electrohydrogenesis. *Proceedings of the National Academy of Science of the United States of America* **2007**, *104*(47), 18871–18873.

(16) Cheng, S.; Xing, D.; Call, D.F.; Logan, B.E. Direct Biological Conversion of Electrical Current into Methane by Electromethanogenesis. *Environmental Science and Technololgy* **2009** *43*(10), 3953–3958.

(17) Rozendal, R.A.; Leone, E.; Keller, J.; Rabaey, K. Efficient hydrogen peroxide generation from organic matter in a bioelectrochemical system. *Electrochemistry Communications* **2009**, *11*(9), 1752–1755.

(18) Naaman, R.; Waldeck, D.H. Spintronics and Chirality: Spin Selectivity in Electron Transport Through Chiral Molecules. *Annual Review of Physical Chemistry* **2015**, *66*(1), 263–281.

(19) Al-Bustami, H.; Bloom, B.P.; Ziv, A.; Goldring, S.; Yochelis, S.; Naaman, R. Waldeck, D.H.; Paltiel, Y. Optical Multilevel Spin Bit Device Using Chiral Quantum Dots. *Nano Letters* **2020**, *20*(12), 8675–868.

(20) Mishra, S.; Pirbadian, S.; Mondal, A.K.; El-Naggar, M.Y.; Naaman, R. Spin-Dependent Electron Transport through Bacterial Cell Surface Multiheme Electron Conduits. *Journal of American Chemical Society* **2019**, *141*(49), 19198–19202.

(21) Naaman,R.; Waldeck, D.H. Chiral-Induced Spin Selectivity Effect. *The Journal of Physical Chemistry Letters* **2012**, *3*(16), 2178–2187.

(22) Naaman, R.; Paltiel, Y.; Waldeck, D.H. Chiral Molecules and the Spin Selectivity Effect. *The Journal of Physical Chemistry Letters* **2020**, *11*(9), 3660–3666.

(23) Naaman, R.; Sanche, L. Low-Energy Electron Transmission through Thin-Film Molecular and Biomolecular Solids. *Chemical Reviews* **2007**, 107(5), 1553–1579.

(24) Kiran, V.; Cohen, S.R.; Naaman, R. Structure dependent spin selectivity in

electron transport through oligopeptides. *Journal of Chemical Physics* **2017**, *146*(9).

(25) Göhler, B.; Hamelbeck, V.; Markus, T.Z.; Kettner, M.; Hanne, G.F.; Vager, Z. Naaman, R.; Zacharias, H. Spin selectivity in electron transmission through self-assembled monolayers of double-stranded DNA. *Science* **2011**, *331*(6019), 894–897.

(26) Carmeli, I.; Kumar, K.S.; Heifler, O.; Carmeli, C.; Naaman, R.Spin Selectivity in Electron Transfer in Photosystem I. *Angewandte Chemie International Edition* **2014**, *53*(34), 8953–8958.

(27) Xie, Z.; Markus, T.Z.; Cohen, S.R.; Vager, Z.; Gutierrez, R.; Naaman, R. Spin Specific Electron Conduction through DNA Oligomers. *Nano Letters* **2011**, *11*(11), 4652–4655.

(28) Mishra, S.; Mondal, A.K.; Pal, S.; Das, T.K.; Smolinsky, E.Z.B.; Siligardi, G.; Naaman, R. Length-Dependent Electron Spin Polarization in Oligopeptides and DNA. *Journal of Physical Chemistry C* **2020,** *124*(19), 10776–10782.

(29) Breuer, M.; Rosso, K.M.; Blumberger, J.; Butt, J.N. Multi-haem cytochromes in *Shewanella oneidensis* MR-1: Structures, functions and opportunities. *Journal of the Royal Society Interface* **2015,** *12*(102).

(30) Hartshorne, R.S.; Reardon, C.L.; Ross, D.; Nuester, J.; Clarke, T.A.; Gates, A.J.; Mills, P.C.; Fredrickson, J.K.; Zachara, J.M.; Shi, L.; Beliaev, A.S.; Marshall, M.J.; Tien, M.; Brantley, S.; Butt, J.N.; Richardson, D.J. Characterization of an electron conduit between bacteria and the extracellular environment. *Proceedings of the National Academy of Science of the United States of America* **2009**, *106*(52), 22169–22174.

(31) White, G.F.; Shi, Z.; Shi, L.; Wang, Z.; Dohnalkova, A.C.; Marshall, M.J.; Fredrickson, J.K.; Zachara, J.M.; Butt, J.N.; Richardson, D.J.; Clarke, T.A. Rapid electron exchange between surface-exposed bacterial cytochromes and Fe(III) minerals. *Proceedings of the National Academy of Science of the United States of America* **2013**, *110*(16), 6346–6351.

(32) Leys, D.; Meyer, T.E.; Tsapin, A.S.; Nealson, A.S.; Cusanovich, M.A.; Van Beeumen, J.J. Crystal structures at atomic resolution reveal the novel concept of ‘electron-harvesting’ as a role for the small tetraheme cytochrome c. *Journal of Biological Chemistry* **2002**, *277*(38), 35703–35711.

(33) Garg, K.; Ghosh, M.; Eliash, T.; Van Wonderen, B. S.; Butt, J.N.; Shi, L.; Jiang, X.; Zdenek, F.; Blumberger, J.; Pecht, I.; Sheves, M.; D. Cahen. Direct evidence for heme-assisted solid-state electronic conduction in multi-heme: c -type cytochromes. *Chemical Science* **2018,** *9*(37), 7304–7310.

(34) Shi, L.; Lin, J.-T.; Markillie, L.M.; Squier, T.C.; Hooker, B.S. Overexpression of multi-heme c-type cytochromes. *BioTechniques* **2005,** *38*(2), 297–299.

(35) Thöny-Meyer, L.; Fischer, F.; Künzler,P.; Ritz, D.; Hennecke, H. *Escherichia coli* genes required for cytochrome c maturation. *Journal of Bacteriology* **1995**, *177*(15), 4321–4326.

(36) Garg, K.; Ghosh, M.; Eliash, T.; Van Wonderen, J. H.; Butt, J. N.; Shi, L.; Jiang, X.; Zdenek, F.; Blumberger, J.; Pecht, I.; Sheves,M.; Cahen, D. Direct evidence for heme-assisted solid-state electronic conduction in multi-heme c -type cytochromes. *Chemical Science* **2018,** *9*(37), 7304–7310.

(37) Firer-Sherwood, M.; Pulcu, G.S.; Elliott, S.J. Electrochemical interrogations of the Mtr cytochromes from *Shewanella*: Opening a potential window. *Journal of Biological Inorganic Chemistry* **2008**, *13*(6), 849–854.

(38) Naaman, R.; Paltiel, Y.; Waldeck, D.H. Chiral Induced Spin Selectivity and Its Implications for Biological Functions. *Annual Review of Biophysics* **2022**, *51*(1), 99–114.

(39) Touw, W.G.; Baakman, C.; Black, J.; Te Beek, T.A.H.; Krieger, E.; Joosten, R.P. Vriend, G. A series of PDB-related databanks for everyday needs. *Nucleic Acids Research* **2015**, *43*(D1), D364–D368.

(40) Kabsch, W.; Sander C. Dictionary of protein secondary structure: Pattern recognition of hydrogen-bonded and geometrical features. *Biopolymers* **1983**, *22* (12), 2577–2637.

Chapter 5

5. Conclusion

J. N. Nwachukwu[1]

[1]School of Molecular Sciences, Arizona State University, Tempe, AZ, USA

This dissertation is focused on the physical understudy of the mechanisms of long-range electron transport along microbial nanowires with an emphasis on the construction of synthetic protein fibers; it also focuses on the possibility of chiral induced spin selectivity in small tetraheme cytochrome as an added property supporting fast, long-range electron transport.

Chapter 2 describes the first functional synthetic model comprised of a *c*-type cytochrome assembled into a fiber. Electrochemical gating shows the fibers are conductive with voltage and temperature dependence. This suggests that the most probable mechanism is cytochrome-mediated electron transport by electron hopping between redox-active centers.

Chapter 3 employs an alternative, more constrained, assembly system to construct a second fiber containing *c*-type cytrochrome. The fibers are still conductive and likely rely on a cytochrome-mediated mechanism of electron transport. Ideally, this construct will prove tunable, allowing us to evaluate the effect of inter-protein distance on conductivity across long distances.

Chapter 4 demonstrates that the small tetraheme cytochrome from *Shewanella oneidensis* transports electrons in a spin-selective fashion. Since little is known about the spin selectivity of proteins in exoelectrogens, this is important information that may be functionally relevant. In the future, it may be possible to explore whether spin selectivity of proteins in exoelectrogens is important for efficient extracellular electron transfer. This study provides an improved understanding of electron transport physics in biomolecules

and sheds light on this intriguing phenomenon in which biology may exploit electron spin and charge for interaction with abiotic surfaces.

In conclusion, this dissertation lays the groundwork for synthetic materials capable of long-range electron transport, an essential component underpinning living and self-repairing electronics.

REFERENCES

(1) Ragan, C. I.; Reed, J. S. Regulation of electron transfer by the quinone pool. *Journal of Bioenergetics and Biomembranes* **1986**, *18* (5), 403–418.

(2) Feist, A. M.; Nagarajan, H.; Rotaru, A. E.; Tremblay, P. L.; Zhang, T.; Nevin, K. P.; Lovley, D. R.; Zengler, K. Constraint-Based Modeling of Carbon Fixation and the Energetics of Electron Transfer in Geobacter metallireducens. *PLoS Computational Biology* **2014**, *10* (4), 1–10.

(3) Logan, B. E. Exoelectrogenic bacteria that power microbial fuel cells. *Nature Reviews Microbiology* **2009**, *7* (5), 375–381.

(4) Kumar, R.; Singh, L.; Zularisam, A. W. Exoelectrogens: Recent Advances in Molecular Driver Involved in Extracellular Electron Transfer and Strategies used to Improve it for Microbial Fuel Cell Applications. *Renewable and Sustainable Energy Reviews* **2016**, *56* (18), 1322–1336.

(5) Reguera, G. Harnessing the power of microbial nanowires. *Microbial Biotechnology* **2018**, *11* (6), 979–994.

(6) Lovley, D. R.; Walker, D. J. F. Geobacter Protein Nanowires. *Frontiers in Microbiology* **2019**, *10* (September).

(7) Cui, Y.; Lai, B.; Tang, X. Microbial Fuel Cell-Based Biosensors. *Biosensors* **2019**, *9* (3), 92.

(8) Lovley, D. R.; Yao, J. Intrinsically Conductive Microbial Nanowires for 'Green' Electronics with Novel Functions. *Trends in Biotechnology* **2021**, *39* (9), 940–952.

(9) Shi, M.; Jiang, Y.; Shi, L. Electromicrobiology and biotechnological applications of the exoelectrogens Geobacter and Shewanella spp. *Science China Technological Sciences* **2019**, *62* (10), 1670–1678.

(10) Newsome, L.; Morris, K.; Lloyd, J. R. The biogeochemistry and bioremediation of uranium and other priority radionuclides. *Chemical Geology* **2014**, *363*, 164–184.

(11) Logan, B. E. Extracting Hydrogen. *Environmental Science and Technology* **2004**, No. January 2004.

(12) Mehanna, M.; Kiely, P. D.; Call, D. F.; Logan, B. E. Microbial electrodialysis cell for simultaneous water desalination and hydrogen gas production. *Environmental Science and Technology* **2010**, *44* (24), 9578–9583.

(13) Clarke, T. A.; Edwards, M. J.; Gates, A. J.; Hall, A.; White, G. F.; Bradley, J.; Reardon, C. L.; Shi, L.; Beliaev, A. S.; Marshall, M. J.; Wang, Z.; Watmough, N. J.; Fredrickson, J. K.; Zachara, J. M.; Butt, J. N.; Richardson, D. J. Structure of a bacterial cell surface decaheme electron conduit. *Proceedings of the National Academy of Sciences of the United States of America* **2011**, *108* (23), 9384–9389.

(14) Gross, B. J.; El-Naggar, M. Y. A combined electrochemical and optical trapping platform for measuring single cell respiration rates at electrode interfaces. *Review of Scientific Instruments* **2015**, *86* (064301), 1–8.

(15) El-Naggar, M. Y.; Wanger, G.; Leung, K. M.; Yuzvinsky, T. D.; Southam, G.; Yang, J.; Lau, W. M.; Nealson, K. H.; Gorby, Y. A. Electrical transport along bacterial nanowires from Shewanella oneidensis MR-1. *Proceedings of the National Academy of Sciences of the United States of America* **2010**, *107* (42), 18127–18131.

(16) Gilbert Gatty, M.; Kahnt, A.; Esdaile, L. J.; Hutin, M.; Anderson, H. L.; Albinsson, B. Hopping versus Tunneling Mechanism for Long-Range Electron Transfer in Porphyrin Oligomer Bridged Donor-Acceptor Systems. *Journal of Physical Chemistry B* **2015**, *119* (24), 7598–7611.

(17) Creasey, R. C. G.; Mostert, A. B.; Nguyen, T. A. H.; Virdis, B.; Freguia, S.; Laycock, B. Microbial nanowires – Electron transport and the role of synthetic analogues. *Acta Biomaterialia* **2018**, *69*, 1–30.

(18) Lovley, D. R. Electrically conductive pili: Biological function and potential applications in electronics. *Current Opinion in Electrochemistry* **2017**, *4* (1), 190–198.

(19) Subramanian, P.; Pirbadian, S.; El-Naggar, M. Y.; Jensen, G. J. Ultrastructure of *Shewanella oneidensis* MR-1 nanowires revealed by electron cryotomography. *Proceedings of the National Academy of Sciences of the United States of America* **2018**, *115* (14), E3246–E3255.

(20) Malvankar, N. S.; Tuominen, M. T.; Lovley, D. R. Lack of cytochrome involvement in long-range electron transport through conductive biofilms and nanowires of *Geobacter sulfurreducens*. *Energy and Environmental Science* **2012**, *5* (9), 8651–8659.

(21) Wang, F.; Gu, Y.; O'Brien, J. P.; Yi, S. M.; Yalcin, S. E.; Srikanth, V.; Shen, C.; Vu, D.; Ing, N. L.; Hochbaum, A. I.; Egelman, E. H.; Malvankar, N. S. Structure of Microbial Nanowires Reveals Stacked Hemes that Transport Electrons over Micrometers. *Cell.* **2019**, *177*, 361–369.

(22) Filman, D. J.; Marino, S. F.; Ward, J. E.; Yang, L.; Mester, Z.; Bullitt, E.; Lovley, D. R.; Strauss, M. Cryo-EM reveals the structural basis of long-range electron transport in a cytochrome-based bacterial nanowire. *Communications Biology* **2019**, *2* (1), 19–24.

(23) Gu, Y.; Srikanth, V.; Salazar-Morales, A. I.; Jain, R.; O'Brien, J. P.; Yi, S. M.; Soni, R. K.; Samatey, F. A.; Yalcin, S. E.; Malvankar, N. S. Structure of Geobacter pili reveals secretory rather than nanowire behaviour. *Nature* **2021**, *597* (7876), 430–434.

(24) Yalcin, S. E.; O'Brien, J. P.; Gu, Y.; Reiss, K.; Yi, S. M.; Jain, R.; Srikanth, V.; Dahl, P. J.; Huynh, W.; Vu, D.; Acharya, A.; Chaudhuri, S.; Varga, T.; Batista, V. S.; Malvankar, N. S. Electric field stimulates production of highly conductive microbial OmcZ nanowires. *Nature Chemical Biology* **2020**, *16* (10), 1136–1142.

(25) Thirumurthy, M. A.; Jones, A. K. Geobacter cytochrome OmcZs binds riboflavin: Implications for extracellular electron transfer. *Nanotechnology* **2020**, *31* (12).

(26) Lovley, D. R. Untangling Geobacter sulfurreducens Nanowires. *mBio* **2022**, No. June, 1–3.

(27) Giri, K.; Bhattacharyya, N. P.; Basak, S. pH-dependent self-assembly of polyalanine peptides. *Biophysical Journal* **2007**, *92* (1), 293–302.

(28) Hendricks, M. P.; Sato, K.; Palmer, L. C.; Stupp, S. I. Supramolecular Assembly of Peptide Amphiphiles. *Accounts of Chemical Research* **2017**, *50* (10), 2440–2448.

(29) Restuccia, A.; Seroski, D. T.; Kelley, K. L.; O'Bryan, C. S.; Kurian, J. J.; Knox, K. R.; Farhadi, S. A.; Angelini, T. E.; Hudalla, G. A. Hierarchical self-assembly and emergent function of densely glycosylated peptide nanofibers. *Communications Chemistry* **2019**, *2* (1).

(30) Creasey, R. C. G.; Mostert, A. B.; Solemanifar, A.; Nguyen, T. A. H.; Virdis, B.; Freguia, S.; Laycock, B. Biomimetic Peptide Nanowires Designed for Conductivity. *ACS Omega* **2019**, *4* (1), 1748–1756.

(31) Xu, H.; Das, A. K.; Horie, M.; Shaik, M. S.; Smith, A. M.; Luo, Y.; Lu, X.; Collins, R.; Liem, S. Y.; Song, A.; Popelier, P. L. A.; Turner, M. L.; Xiao, P.; Kinloch, I. A.; Ulijn, R. V. An investigation of the conductivity of peptide nanotube networks prepared by enzyme-triggered self-assembly. *Nanoscale* **2010**, *2* (6), 960–966.

(32) Ing, N. L.; Spencer, R. K.; Luong, S. H.; Nguyen, H. D.; Hochbaum, A. I. Electronic Conductivity in Biomimetic α-Helical Peptide Nanofibers and Gels. *ACS Nano* **2018**, *12* (3), 2652–2661.

(33) Cosert, K. M.; Castro-Forero, A.; Steidl, R. J.; Worden, R. M.; Reguera, G. Bottom-up fabrication of protein nanowires via controlled self-assembly of recombinant *Geobacter* pilins. *mBio* **2019**, *10* (6), 1–15.

(34) Altamura, L.; Horvath, C.; Rengaraj, S.; Rongier, A.; Elouarzaki, K.; Gondran, C.; Maçon, A. L. B.; Vendrely, C.; Bouchiat, V.; Fontecave, M.; Mariolle, D.; Rannou, P.; Le Goff, A.; Duraffourg, N.; Holzinger, M.; Forge, V. A synthetic redox biofilm made from metalloprotein-prion domain chimera nanowires. *Nature Chemistry* **2017**, *9* (2), 157–163.

(35) Chen, Y. X.; Ing, N. L.; Wang, F.; Xu, D.; Sloan, N. B.; Lam, N. T.; Winter, D. L.; Egelman, E. H.; Hochbaum, A. I.; Hochbaum, A. I.; Hochbaum, A. I.; Clark, D. S.; Clark, D. S.; Glover, D. J. Structural Determination of a Filamentous Chaperone to Fabricate Electronically Conductive Metalloprotein Nanowires. *ACS Nano* **2020**, *14* (6), 6559–6569.

(36) Naaman, R.; Waldeck, D. H. Chiral-Induced Spin Selectivity Effect. *The Journal of Physical Chemistry* **2012**, *1021* (3), 2178–2187.

(37) Naaman, R.; Paltiel, Y.; Waldeck, D. H. Chiral Induced Spin Selectivity and Its Implications for Biological Functions. *Annual Review of Biophysics* **2022**, *51* (1).

(38) Xu, S.; Barrozo, A.; Tender, L. M.; Krylov, A. I.; El-Naggar, M. Y. Multiheme

Cytochrome Mediated Redox Conduction through Shewanella oneidensis MR-1 Cells. *Journal of the American Chemical Society* **2018**, *140* (32), 10085–10089.

(39) El-Naggar, M. Y.; Wanger, G.; Leung, K. M.; Yuzvinsky, T. D.; Southam, G.; Yang, J.; Lau, W. M.; Nealson, K. H.; Gorby, Y. A. Electrical transport along bacterial nanowires from *Shewanella oneidensis* MR-1. *Proceedings of the National Academy of Sciences of the United States of America* **2010**, *107* (42), 18127–18131.

(40) Malvankar, N. S.; Lovley, D. R. Microbial nanowires: A new paradigm for biological electron transfer and bioelectronics. *ChemSusChem* **2012**, *5* (6), 1039–1046.

(41) Terao, T. Hopping electron model with geometrical frustration: Kinetic Monte Carlo simulations. *European Physical Journal B* **2016**, *89* (10), 209–216.

(42) Otter, R.; Besenius, P. Supramolecular assembly of functional peptide–polymer conjugates. *Organic & Biomolecular Chemistry* **2019**, *17* (28), 6719–6734.

(43) Hudalla, G. A.; Sun, T.; Gasiorowski, J. Z.; Han, H.; Tian, Y. F.; Chong, A. S.; Collier, J. H. Gradated assembly of multiple proteins into supramolecular nanomaterials. *Nature Materials* **2014**, *13* (8), 829–836.

(44) Bradford, M. M. A rapid and sensitive method for the quantitation of microgram quantities of protein utilizing the principle of protein-dye binding. *Analytical Biochemistry* **1976**, *72*, 248–254.

(45) Chantell, C. A.; Onaiyekan, M. A.; Menakuru, M. Fast conventional Fmoc solid-phase peptide synthesis: A comparative study of different activators. *Journal of Peptide Science* **2012**, *18* (2), 88–91.

(46) Amblard, M.; Fehrentz, J.; Martinez, J.; Subra, G. Modern Solid Phase Peptide Synthesis: Methods and Protocols of Modern Solid Phase Peptide Synthesis. *Molecular Biotechnology* **2006**, *33*, 240–255.

(47) Bard, A. J.; Abruiia, H. D.; Chidsey, C. E.; Faulkner, L. R.; Feldberg, S. W.; Melroy, O.; Murray, R. W.; Hill, C.; Carolina, N.; Porter, M. D.; Soriaga, M. P.; White, H. S. The Electrode/Electrolyte Interface-A status Report. *Society* **1993**, *97*, 7147–7173.

(48) Tsapin, A. I.; Nealson, K. H.; Meyers, T.; Cusanovich, M. A.; Van Beuumen, J.; Crosby, L. D.; Feinberg, B. A.; Zhang, C. Purification and properties of a low-redox-potential tetraheme cytochrome c3 from Shewanella putrefaciens. *Journal of Bacteriology* **1996**, *178* (21), 6386–6388.

(49) Wada, K.; Hase, T.; Tokunaga, H.; Matsubara, H. Amino Acid Sequence of *Spirulina platensis* Ferredoxin: A Far Divergency of Blue-Green Algal Ferredoxins. *FEBS Letters* **1975**, *55* (1), 102–104.

(50) Blauch, D. N.; Savéant, J. M. Dynamics of Electron Hopping in Assemblies of Redox Centers. Percolation and Diffusion. *Journal of the American Chemical Society* **1992**, *114* (9), 3323–3332.

(51) Sun, Y. L.; Montz, B. J.; Selhorst, R.; Tang, H. Y.; Zhu, J.; Nevin, K. P.; Woodard, T. L.; Ribbe, A. E.; Russell, T. P.; Nonnenmann, S. S.; Lovley, D. R.; Emrick, T.; Russell, T. P. Solvent-Induced Assembly of Microbial Protein Nanowires into Superstructured Bundles. *Biomacromolecules* **2021**, *22* (3), 1305–1311.

(52) Dahl, P. J.; Yi, S. M.; Gu, Y.; Acharya, A.; Shipps, C.; Neu, J.; Patrick O'Brien, J.; Morzan, U. N.; Chaudhuri, S.; Guberman-Pfeffer, M. J.; Vu, D.; Yalcin, S. E.; Batista, V. S.; Malvankar, N. S. A 300-fold conductivity increase in microbial cytochrome nanowires due to temperature-induced restructuring of hydrogen bonding networks. *Science Advances* **2022**, *8* (19).

(53) Amdursky, N.; Wang, X.; Meredith, P.; Riley, D. J.; Payne, D. J.; Bradley, D. D. C.; Stevens, M. M. Electron Hopping Across Hemin-Doped Serum Albumin Mats on Centimeter-Length Scales. *Advanced Materials* **2017**, *29* (27).

(54) Arslan, E.; Schulz, H.; Zufferey, R.; Künzler, P.; Thöny-Meyer, L. Overproduction of the Bradyrhizobium japonicum c-type cytochrome subunits of the cbb3 oxidase in Escherichia coli. *Biochemical and Biophysical Research Communications* **1998**, *251* (3), 744–747.

(55) Pechsrichuang, P.; Songsiriritthigul, C.; Haltrich, D.; Roytrakul, S.; Namvijtr, P.; Bonaparte, N.; Yamabhai, M. OmpA signal peptide leads to heterogenous secretion of B. subtilis chitosanase enzyme from E. coli expression system. *SpringerPlus* **2016**, *5* (1).

(56) Studier, F. W.; Moffat, B. A. Selective expression of cloned genes directed by T7 RNA polymerase. *J. Mol. Biol.* **1986**, *189*, 113–130.

(57) Creasey, R. C. G.; Shingaya, Y.; Nakayama, T. Improved electrical conductance through self-assembly of bioinspired peptides into nanoscale fibers. *Materials Chemistry and Physics* **2015**, *158*, 52–59.

(58) Hosseinzadeh, P.; Lu, Y. Design and fine-tuning redox potentials of metalloproteins involved in electron transfer in bioenergetics. *Biochimica et Biophysica Acta - Bioenergetics* **2016**, *1857* (5), 557–581.

(59) Seroski, D. T.; Restuccia, A.; Sorrentino, A. D.; Knox, K. R.; Hagen, S. J.; Hudalla, G. A. Co-Assembly Tags Based on Charge Complementarity (CATCH) for Installing Functional Protein Ligands into Supramolecular Biomaterials. *Cellular and Molecular Bioengineering* **2016**, *9* (3), 335–350.

(60) Tsapin, A. I.; Vandenberghe, I.; Nealson, K. H.; Scott, J. H.; Meyer, T. E.; Cusanovich, M. A.; Harada, E.; Kaizu, T.; Akutsu, H.; Leys, D.; Van Beeumen, J. J. Identification of a Small Tetraheme Cytochrome *c* and a Flavocytochrome *c* as Two of the Principal Soluble Cytochromes *c* in *Shewanella oneidensis* Strain MR1. *Applied and Environmental Microbiology* **2001**, *67* (7), 3236–3244.

(61) Simpósio, X. I. I.; Enzimática, D. E. H.; Rinaldi, B. G.; Santos, M. M.; Mello, C. M.; Marteleto, N. B.; Marques, T. O.; Linhares, D. C.; Piccoli, R. A. M.; Léo, P.; Rodrigues, F. A. Evaluation of Plasmid Stability in *E. coli* Cultivation in High Cell

Density. *journal of bioprocessing* **2017**, *6*, 1–4.

(62) Bergmans, H.; Van, D.; Hoekstra, P. Transformation in *Escherichia coli*: Stages in the Process. *J. Bacteriol.* **1981**, *146* (2), 564–570.

(63) Thomas, P. E.; Ryan, D.; Levin, W. An improved staining procedure for the detection of the peroxidase activity of cytochrome P-450 on sodium dodecyl sulfate polyacrylamide gels. *Analytical Biochemistry* **1976**, *75* (1), 168–176.

(64) Overproduction of the *Bradyrhizobium japonicum c*-Type Cytochrome Subunits of the cbb3Oxidase in *Escherichia coli*. *Biochemical and Biophysical Research Communications* **1998**, *251* (3), 744–747.

(65) Lovley, D.R.; Stolz, J.F.; Nord, G.L.; Phillips, E.J.P. Anaerobic production of magnetite by a dissimilatory iron-reducing microorganism," *Nature* **1987**, *330*(V), 2–4.

(66) Myers, C.R.; Nealson, K.H. Bacterial Manganese Reduction and Growth with Manganese Oxide as the Sole Electron Acceptor. *Science* **1988**, *240*(4857), 1319–1321.

(67) Shi, L.; Dong, H.; Reguera, G.; Beyenal, H.; Lu, A.; Liu, J.; Yu, H.Q.; Fredrickson, J.K. Extracellular electron transfer mechanisms between microorganisms and minerals. *Nature Reviews Microbiology* **2016**, *14*(10), 651–662.

(68) El-Naggar, M.Y.; Wanger, G.; Leung, K.M.; Yuzvinsky, T.D.; Southam, G.; Yang, J.; Lau, W.M.; Nealson, K.H.; Gorby, Y.A. Electrical transport along bacterial nanowires from *Shewanella oneidensis* MR-1. *Proceedings of the National Academy of Science of the United States of America* **2010**, *107*(42), 18127–18131.

(69) Pirbadian, S.; Barchinger, S.E.; Leung, K.M.; Byun, H.S.; Jangir, Y. Bouhenni, R.A.; Reed, S.B.; Romine, M.F.; Saffarini, D.A.; Shi, L.; Gorby, Y.A.; Golbeck, J.H.; El-Naggar, M.Y. *Shewanella oneidensis* MR-1 nanowires are outer membrane and periplasmic extensions of the extracellular electron transport components. *Proceedings of the National Academy of Science of the United States of America* **2014**, *111*(35), 12883–12888.

(70) Bretschger, O.; Obraztsova, A.; Sturm, C.A.; Chang, I.S.; Gorby, Y.A.; Reed, S.B.; Culley, D.E.; Reardon, C.L.; Barua, S.; Romine, M.F.; Zhou, J.; Beliaev, A.S; Bouhenni, R.; Saffarini, D.; Mansfeld, F.; Kim, B.-H.; Fredrickson, J.K.; Nealson, K.H. Current Production and Metal Oxide Reduction by *Shewanella oneidensis* MR-1 Wild Type and Mutants. *Applied and Environmental Microbiology* **2007**, *73*(21), 7003–7012.

(71) Atkinson, J.T., Chavez, M.S.; Niman, C.M.; El-Naggar, M.Y. Living electronics: A catalogue of engineered living electronic components. *Microbial Biotechnology* **2023**, *16*(3), 507–533.

(72) Chaudhuri, S.K.; Lovley, D.R. Electricity generation by direct oxidation of glucose

in mediatorless microbial fuel cells. *Nature Biotechnology* **2003**, *21*(10), 1229–1232.

(73) Zhang, X.; Cheng, S.; Wang, X.; Huang, X.; Logan, B.E. Separator Characteristics for Increasing Performance of Microbial Fuel Cells. *Environmental Science and Technololgy* **2009**, *43*(21), 8456–8461.

(74) Watson, V.J.; Logan, B.E. Power production in MFCs inoculated with *Shewanella oneidensis* MR-1 or mixed cultures. *Biotechnology and Bioengineering* **2010**, *105*(3), 489–498.

(75) Gorby, Y.A.; Lovley, D.R. Enzymic uranium precipitation. *Environmental Science and Technololgy* **1992**, *26*(1), 205–207.

(76) Hsu, L.; Arias-Thode, M.; Salvacion, M.; Benavidez, Z.; Mirhosseini, A.; Babanova, S.; Chen, S.; Bretschger, O. Demonstration of an Energy-Neutral, Off-Grid Microbial Fuel Cell System for Decentralized Wastewater Treatment. *ECS Transactions* **2017**, *75*(46), 19–29.

(77) Del Valle, I.; Fulk, E.M.; Kalvapalle, P.; Silberg, J.J.; Masiello, C.A.; Stadler, L.B. Translating New Synthetic Biology Advances for Biosensing Into the Earth and Environmental Sciences. *Frontiers of Microbiology* **2021**, *11*, 618373.

(78) Wan, X.; Saltepe, B.; Yu, L.; Wang, B. Programming living sensors for environment, health and biomanufacturing. *Microbial Biotechnology* **2021**, *14*(6), 2334–2342.

(79) Cheng, S.; Logan, B.E. Sustainable and efficient biohydrogen production via electrohydrogenesis. *Proceedings of the National Academy of Science of the United States of America* **2007**, *104*(47), 18871–18873.

(80) Cheng, S.; Xing, D.; Call, D.F.; Logan, B.E. Direct Biological Conversion of Electrical Current into Methane by Electromethanogenesis. *Environmental Science and Technololgy* **2009** *43*(10), 3953–3958.

(81) Rozendal, R.A.; Leone, E.; Keller, J.; Rabaey, K. Efficient hydrogen peroxide generation from organic matter in a bioelectrochemical system. *Electrochemistry Communications* **2009**, *11*(9), 1752–1755.

(82) Naaman, R.; Waldeck, D.H. Spintronics and Chirality: Spin Selectivity in Electron Transport Through Chiral Molecules. *Annual Review of Physical Chemistry* **2015**, *66*(1), 263–281.

(83) Al-Bustami, H.; Bloom, B.P.; Ziv, A.; Goldring, S.; Yochelis, S.; Naaman, R. Waldeck, D.H.; Paltiel, Y. Optical Multilevel Spin Bit Device Using Chiral Quantum Dots. *Nano Letters* **2020**, *20*(12), 8675–868.

(84) Mishra, S.; Pirbadian, S.; Mondal, A.K.; El-Naggar, M.Y.; Naaman, R. Spin-Dependent Electron Transport through Bacterial Cell Surface Multiheme Electron Conduits. *Journal of American Chemical Society* **2019**, *141*(49), 19198–19202.

(85) Naaman,R.; Waldeck, D.H. Chiral-Induced Spin Selectivity Effect. *The Journal of Physical Chemistry Letters* **2012**, *3*(16), 2178–2187.

(86) Naaman, R.; Paltiel, Y.; Waldeck, D.H. Chiral Molecules and the Spin Selectivity Effect. *The Journal of Physical Chemistry Letters* **2020**, *11*(9), 3660–3666.

(87) Naaman, R.; Sanche, L. Low-Energy Electron Transmission through Thin-Film Molecular and Biomolecular Solids. *Chemical Reviews* **2007**, 107(5), 1553–1579.

(88) Kiran, V.; Cohen, S.R.; Naaman, R. Structure dependent spin selectivity in electron transport through oligopeptides. *Journal of Chemical Physics* **2017**, *146*(9).

(89) Göhler, B.; Hamelbeck, V.; Markus, T.Z.; Kettner, M.; Hanne, G.F.; Vager, Z. Naaman, R.; Zacharias, H. Spin selectivity in electron transmission through self-assembled monolayers of double-stranded DNA. *Science* **2011**, *331*(6019), 894–897.

(90) Carmeli, I.; Kumar, K.S.; Heifler, O.; Carmeli, C.; Naaman, R.Spin Selectivity in Electron Transfer in Photosystem I. *Angewandte Chemie International Edition* **2014**, *53*(34), 8953–8958.

(91) Xie, Z.; Markus, T.Z.; Cohen, S.R.; Vager, Z.; Gutierrez, R.; Naaman, R. Spin Specific Electron Conduction through DNA Oligomers. *Nano Letters* **2011**, *11*(11), 4652–4655.

(92) Mishra, S.; Mondal, A.K.; Pal, S.; Das, T.K.; Smolinsky, E.Z.B.; Siligardi, G.; Naaman, R. Length-Dependent Electron Spin Polarization in Oligopeptides and DNA. *Journal of Physical Chemistry C* **2020,** *124*(19), 10776–10782.

(93) Breuer, M.; Rosso, K.M.; Blumberger, J.; Butt, J.N. Multi-haem cytochromes in *Shewanella oneidensis* MR-1: Structures, functions and opportunities. *Journal of the Royal Society Interface* **2015,** *12*(102).

(94) Hartshorne, R.S.; Reardon, C.L.; Ross, D.; Nuester, J.; Clarke, T.A.; Gates, A.J.; Mills, P.C.; Fredrickson, J.K.; Zachara, J.M.; Shi, L.; Beliaev, A.S.; Marshall, M.J.; Tien, M.; Brantley, S.; Butt, J.N.; Richardson, D.J. Characterization of an electron conduit between bacteria and the extracellular environment. *Proceedings of the National Academy of Science of the United States of America* **2009**, *106*(52), 22169–22174.

(95) White, G.F.; Shi, Z.; Shi, L.; Wang, Z.; Dohnalkova, A.C.; Marshall, M.J.; Fredrickson, J.K.; Zachara, J.M.; Butt, J.N.; Richardson, D.J.; Clarke, T.A. Rapid electron exchange between surface-exposed bacterial cytochromes and Fe(III) minerals. *Proceedings of the National Academy of Science of the United States of America* **2013**, *110*(16), 6346–6351.

(96) Leys, D.; Meyer, T.E.; Tsapin, A.S.; Nealson, A.S.; Cusanovich, M.A.; Van Beeumen, J.J. Crystal structures at atomic resolution reveal the novel concept of

'electron-harvesting' as a role for the small tetraheme cytochrome c. *Journal of Biological Chemistry* **2002**, *277*(38), 35703–35711.

(97) Garg, K.; Ghosh, M.; Eliash, T.; Van Wonderen, B. S.; Butt, J.N.; Shi, L.; Jiang, X.; Zdenek, F.; Blumberger, J.; Pecht, I.; Sheves, M.; D. Cahen. Direct evidence for heme-assisted solid-state electronic conduction in multi-heme: c -type cytochromes. *Chemical Science* **2018,** *9*(37), 7304–7310.

(98) Shi, L.; Lin, J.-T.; Markillie, L.M.; Squier, T.C.; Hooker, B.S. Overexpression of multi-heme c-type cytochromes. *BioTechniques* **2005,** *38*(2), 297–299.

(99) Thöny-Meyer, L.; Fischer, F.; Künzler,P.; Ritz, D.; Hennecke, H. *Escherichia coli* genes required for cytochrome c maturation. *Journal of Bacteriology* **1995**, *177*(15), 4321–4326.

(100) Garg, K.; Ghosh, M.; Eliash, T.; Van Wonderen, J. H.; Butt, J. N.; Shi, L.; Jiang, X.; Zdenek, F.; Blumberger, J.; Pecht, I.; Sheves,M.; Cahen, D. Direct evidence for heme-assisted solid-state electronic conduction in multi-heme c -type cytochromes. *Chemical Science* **2018,** *9*(37), 7304–7310.

(101) Firer-Sherwood, M.; Pulcu, G.S.; Elliott, S.J. Electrochemical interrogations of the Mtr cytochromes from *Shewanella*: Opening a potential window. *Journal of Biological Inorganic Chemistry* **2008**, *13*(6), 849–854.

(102) Naaman, R.; Paltiel, Y.; Waldeck, D.H. Chiral Induced Spin Selectivity and Its Implications for Biological Functions. *Annual Review of Biophysics* **2022**, *51*(1), 99–114.

(103) Touw, W.G.; Baakman, C.; Black, J.; Te Beek, T.A.H.; Krieger, E.; Joosten, R.P. Vriend, G. A series of PDB-related databanks for everyday needs. *Nucleic Acids Research* **2015**, *43*(D1), D364–D368.

(104) Kabsch, W.; Sander C. Dictionary of protein secondary structure: Pattern recognition of hydrogen-bonded and geometrical features. *Biopolymers* **1983**, *22* (12), 2577–2637.

APPENDIX

APPENDIX A

A PLASMID MAP OF PD431 (BETA-TAIL STC FROM DNA 2.0)

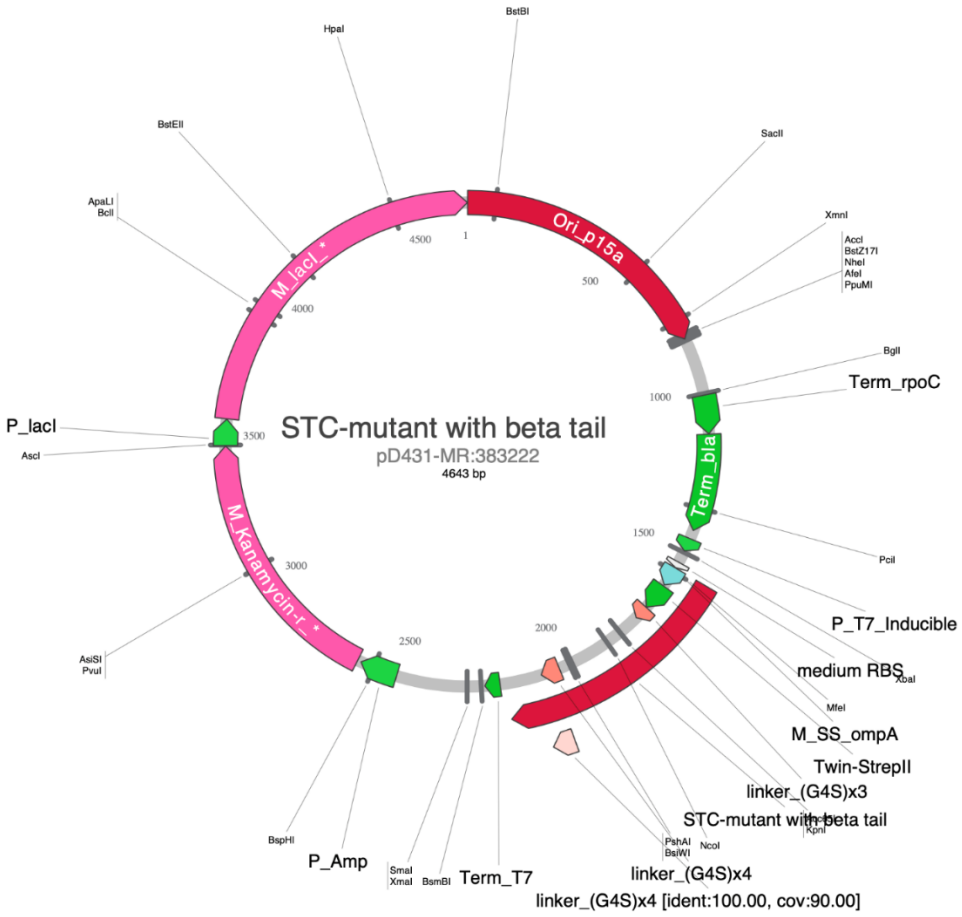
STC-mutant with beta tail
pD431-MR:383222
4643 bp
1
500
1000
1500
2000
2500
3000
3500
4000
4500
Ori_p15a
Term_rpoC
Term_bla
P_T7_Inducible
medium RBS
M_SS_ompA
Twin-StrepII
linker_(G4S)x3
STC-mutant with beta tail
linker_(G4S)x4
linker_(G4S)x4 [ident:100.00, cov:90.00]
Term_T7
P_Amp
M_kanamycin-r_*
P_lacI
M_lacI_*
HpaI
BstBI
SacII
XmnI
AccI
BstZ17I
NheI
AflII
PpuMI
BglII
PciI
XbaI
MfeI
PshAI
BsiWI
NcoI
KpnI
SmaI
XmaI
BsmBI
BspHI
AsiSI
PvuI
AscI
ApaLI
BclI
BstEII

APPENDIX B

B PLASMID MAP OF PD434 (STC-CATCH FROM DNA 2.0)

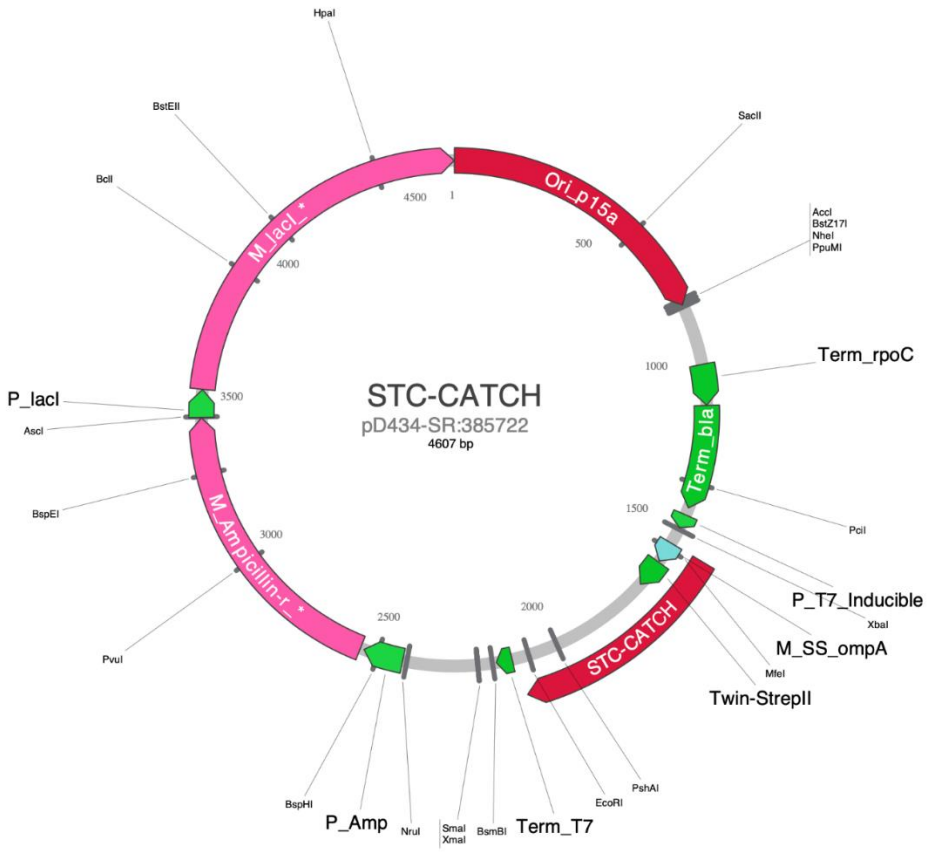
STC-CATCH
pD434-SR:385722
4607 bp
Ori_p15a
M_lacI_*
M_Ampicillin-r_*
Term_rpoC
Term_bla
P_T7_Inducible
M_SS_ompA
Twin-StrepII
STC-CATCH
Term_T7
P_Amp
P_lacI
HpaI
BstEII
BclI
AscI
BspEI
PvuI
BspHI
NruI
SmaI
XmaI
BsmBI
EcoRI
PshAI
MfeI
XbaI
PciI
SacII
AccI
BstZ17I
NheI
PpuMI
1
500
1000
1500
2000
2500
3000
3500
4000
4500

APPENDIX C

C PLASMID MAP OF PD431 **(**STC FROM DNA 2.0)

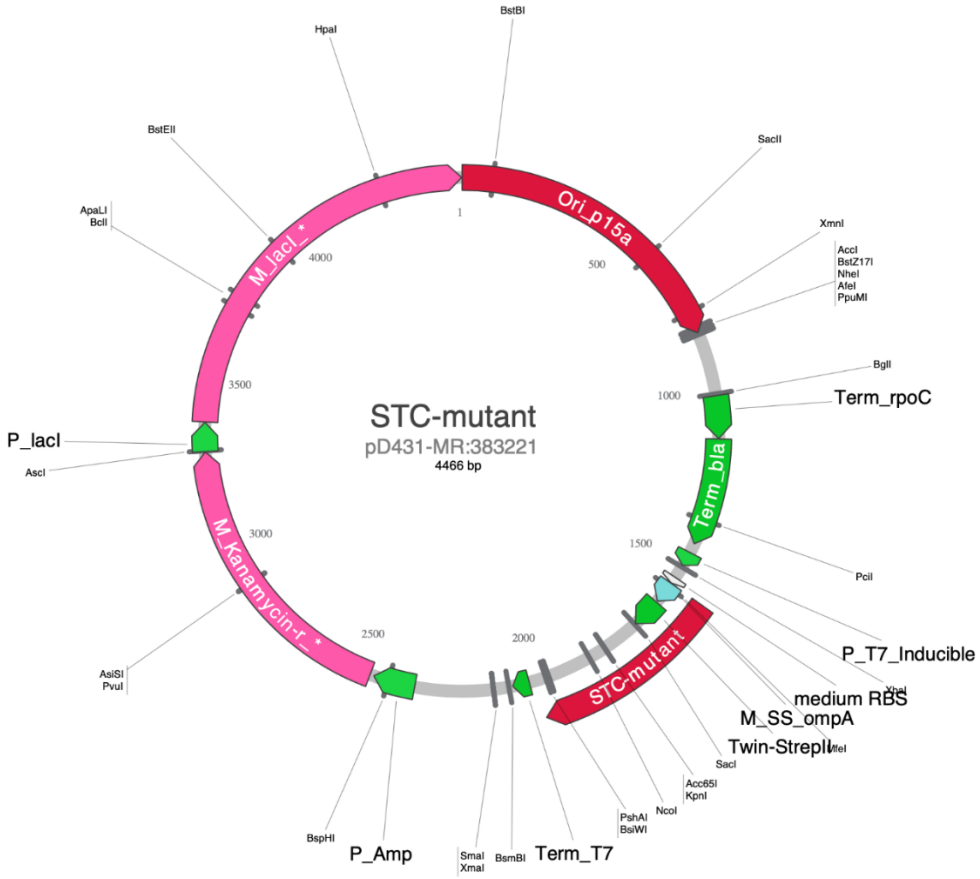
STC-mutant
pD431-MR:383221
4466 bp
BstBI
HpaI
SacII
XmnI
AccI
BstZ17I
NheI
AfeI
PpuMI
BglII
Term_rpoC
Term_bla
PciI
P_T7_Inducible
medium RBS
M_SS_ompA
Twin-StrepII
SacI
Acc65I
KpnI
NcoI
PshAI
BsiWI
Term_T7
SmaI
XmaI
BsmBI
P_Amp
BspHI
AsiSI
PvuI
M_Kanamycin-r_*
P_lacI
AscI
M_lacI_*
ApaLI
BclI
BstEII
Ori_p15a
1
500
1000
1500
2000
2500
3000
3500
4000

APPENDIX D

D STATEMENT OF PERMISSION BY ALL CO-AUTHORS

I hereby confirm that all co-authors involved in the submission of the manuscript described in Chapter 4 have granted their permission for its report in this thesis.

Justus Nmaduka Nwachukwu

APPENDIX E

E AUTHOR CONTRIBUTIONS

Chapter 2

Justus Nwachukwu. Designed research. Performed research. Contributed new reagents or analytical tools. Analyzed Data. Wrote the Paper.

Muyuki Abirami Thirmurthy. Designed research. Performed research. Contributed new reagents or analytical tools. Analyzed Data.

Joshua T. Atkinson. Performed research. Contributed new reagents or analytical tools. Analyzed Data. Wrote Paper.

Mohammed El-naggar. Designed research.

Anne K. Jones. Designed research. Contributed new reagents or analytical tools. Wrote Paper.

Chapter 3

Justus Nwachukwu. Designed research. Performed research. Contributed new reagents or analytical tools. Analyzed Data. Wrote the Paper.

Muyuki Abirami Thirmurthy. Designed research.

Gaurav Galiyan. Performed research. Contributed new reagents or analytical tools.

Joshua T. Atkinson. Performed research. Contributed new reagents or analytical tools. Analyzed Data. Wrote Paper.

Mohammed El-naggar. Designed research. Contributed new reagents or analytical tools.

Anne K. Jones. Designed research. Contributed new reagents or analytical tools. Wrote Paper.

Chapter 4

Christina Niman. Designed research. Performed research. Contributed new reagents or analytical tools. Analyzed Data. Wrote the Paper.

Nir Sukenik. Designed research. Performed research. Contributed new reagents or analytical tools. Analyzed Data. Wrote the Paper.

Tram Dang. Performed research. Contributed new reagents or analytical tools. Analyzed Data. Wrote the Paper.

Justus Nwachukwu. Performed research. Contributed new reagents or analytical tools. Analyzed Data. Wrote the Paper.

Anne Jones. Designed research. Contributed new reagents or analytical tools. Analyzed Data. Wrote the Paper.

Ron Naaman. Designed research. Contributed new reagents or analytical tools. Analyzed Data. Wrote the Paper.

Kakali Santra. Analyzed Data. Wrote the Paper.

Tapan Kumar Das. Analyzed Data. Contributed new reagents or analytical tools. Analyzed Data. Wrote the Paper.

Yossi Paltiel. Analyzed Data. Wrote the Paper.

Lech Tomasz Baczewski. Designed research. Contributed new reagents or analytical tools. Analyzed Data.

Mohamed Y. El-Naggar. Designed research. Performed research. Contributed new reagents or analytical tools. Analyzed Data. Wrote the Paper.